OBSERVATION AND MODELING OF

PARAMAGNETIC PARTICLE ENTRAPMENT

IN A MAGNETIC FIELD

by

DAVID ANDREW HIMMELBLAU

Submitted in Partial Fulfillment

of the Requirements for the

Degree of Master of Science

at the

MASSACHUSETTS INSTITUTE OF TECHNOLOGY

September, 1973

Signature of author: _____
                     Department of Chemical Engineering
                     June 25, 1973

Certified by: _____
                     Thesis Supervisor

Accepted by: _____
                     Chairman,
                     Departmental Committee on Graduate Theses

ABSTRACT

OBSERVATION AND MODELING OF PARAMAGNETIC

PARTICLE ENTRAPMENT IN A MAGNETIC FIELD

by

David Andrew Himmelblau

Submitted to the Department of Chemical Engineering

on June 25, 1973, in partial fulfillment of the

requirements for the degree of Master of Science.

A magnetic force may be extended to paramagnetic materials by production of a high magnetic field gradient. The gradient is produced by perturbing a uniform field in a solenoid with ferromagnetic packing, normally stainless steel wool. Paramagnetic particles can be filtered using the resulting magnetic force.

To determine how particles are trapped and how system variables of a magnetic filter affect efficiency, a mathematical model was developed for a single strand of packing material. Concurrently, an experimental program was designed to observe trapping at a single strand. The experimental results and the mathematical model produce a correlation between the variables at a constant particle size, R. The correlation expresses y/R as a function of KHH/pVV and Reynolds number based on strand diameter where y is an effective trapping length, K is the susceptibility of the particle, H is the applied field strength, p is the fluid density, and V is the fluid velocity.

Applying the correlation results to actual filter data, the model predicts that all filtering occurs in a small zone. However, the model does not account for particles already trapped. The experimental results showed a small maximum trapping volume per strand. Future work should incorporate this result, and magnetic separators or filters should be treated as adsorbers.

Thesis Supervisor: Gary J. Powers
Title: Assistant Professor of Chemical Engineering

Department of Chemical Engineering
Massachusetts Institute of Technology
Cambridge, Massachusetts   02139
June 25, 1973

Professor David B. Ralston
Secretary of the Faculty
Massachusetts Institute of Technology
Cambridge, Massachusetts   02139

Dear Professor Ralston:

In accordance with the regulations of the Faculty, I
herewith submit a thesis, entitled "Observation and Modeling
of Paramagnetic Particle Entrapment in a Magnetic Field,"
in partial fulfillment of the requirements for the degree
of Master of Science in Chemical Engineering at the Massachusetts
Institute of Technology.

Respectfully submitted,

David Andrew Himmelblau

Acknowledgements

Table of Contents

page

List of Figures

SUMMARY

Although paramagnetic particles when placed in a magnetic field may be only slightly magnetized, one can produce a useable attractive force on a paramagnetic particle, since the force per unit volume is equal to the magnetization multiplied by the field gradient.

$$\overline{F}_{Mag} = K\overline{H} \cdot \nabla \overline{H} \qquad (S-1)$$

where $K\overline{H}$ is the magnetization of the paramagnetic material. K is the susceptibility of the material and is much less than one. $\overline{H}$ is the applied field. The high gradients are produced by placing a ferromagnetic material in a uniform field, causing perturbations in the field in the vicinity of the ferromagnetic object. Common stainless steel wool is often used.

With a magnetic force applicable to ordinary nonferromagnetic materials, one can use an electromagnet filled with stainless steel wool as a filter to remove a material from a fluid stream where a conventional filter is inapplicable. Some practical possibilities include water purification and ore benefication.

To date, studies of magnetic separators have been based on material balances around a pilot machine or mathematical models based on incomplete or inaccurate descriptions. The purpose of this work was to develop an accurate description of particle entrapment onto a single strand of steel wool wire and visually confirm the model.

Particle entrapment is dependent on two forces other than gravity, magnetic force and fluid drag force. Gravitational force is dependent on volume, i.e., particle radius R and particle density $\rho*$. The magnetic force is a function of applied field H, field gradient, particle volume, and susceptibility K. The drag force depends on the relative velocity and particle surface area. The local magnetic field description depends on the shape of the ferromagnetic material placed in the applied field; fluid velocity also depends on the shape of the trapping material.

An infinitely long ferromagnetic cylinder of radius a was used to describe the steel wool strand. Potential flow was used to describe the fluid velocity, since the Reynolds numbers of interest are too low to directly use boundary layer theory and too high for the viscous flow approximation. The magnetic field was originally modeled as a line of point dipoles. However, this gave erroneous results because of self-demagnetization of the cylinder. An assumption of constant permeability was used to adopt an analytic solution which deals with demagnetization through the boundary conditions (Stratton, 1941). The resulting magnetic force was

$$\overline{F}_M = \frac{-2\beta KHH}{r^3}s\left[\left(\frac{\beta'}{r^2} + \cos 2\theta\right)\hat{r} - \sin 2\theta \hat{\phi}\right] \qquad \text{(S-2)}$$

where

$$\beta = \frac{\mu_s - 1}{\mu_s + 1}a^2 \qquad \text{(S-3)}$$

$$\beta' = \beta \qquad H \le H_s \qquad (S-4)$$

$$\beta' = \beta H_s/H \qquad H > H_s \qquad (S-5)$$

H_s is the applied field necessary for apparent saturation of the cylinder, μ_s is the intrinsic permeability of the ferromagnetic cylinder at saturation, θ is the angle measured from the second quadrant (upstream side), r is the radial distance from the center of the cylinder along the major axis, and a is the radius of the cylinder. The force is on a volume basis.

The three forces were placed into a vector equation of Newton's second law which produced four simultaneous scalar first order differential equations. These were integrated numerically by the fourth order Runge-Kutta method, given initial particle velocity V_∞ and starting position. The imaginary particles were started at a constant upstream x distance and at variable y values above the x axis. For given conditions of $K,H,H_s,\rho*$ (particle density), R (particle radius), and a, the maximum y at which particles could be trapped by the cylinder was determined.

The trajectories produced by the computer program corresponded well with the regions in which particles were trapped experimentally. Most particles (real or imaginary) trapped on the front or upstream side near the induced pole of the cylinder (figure S1).
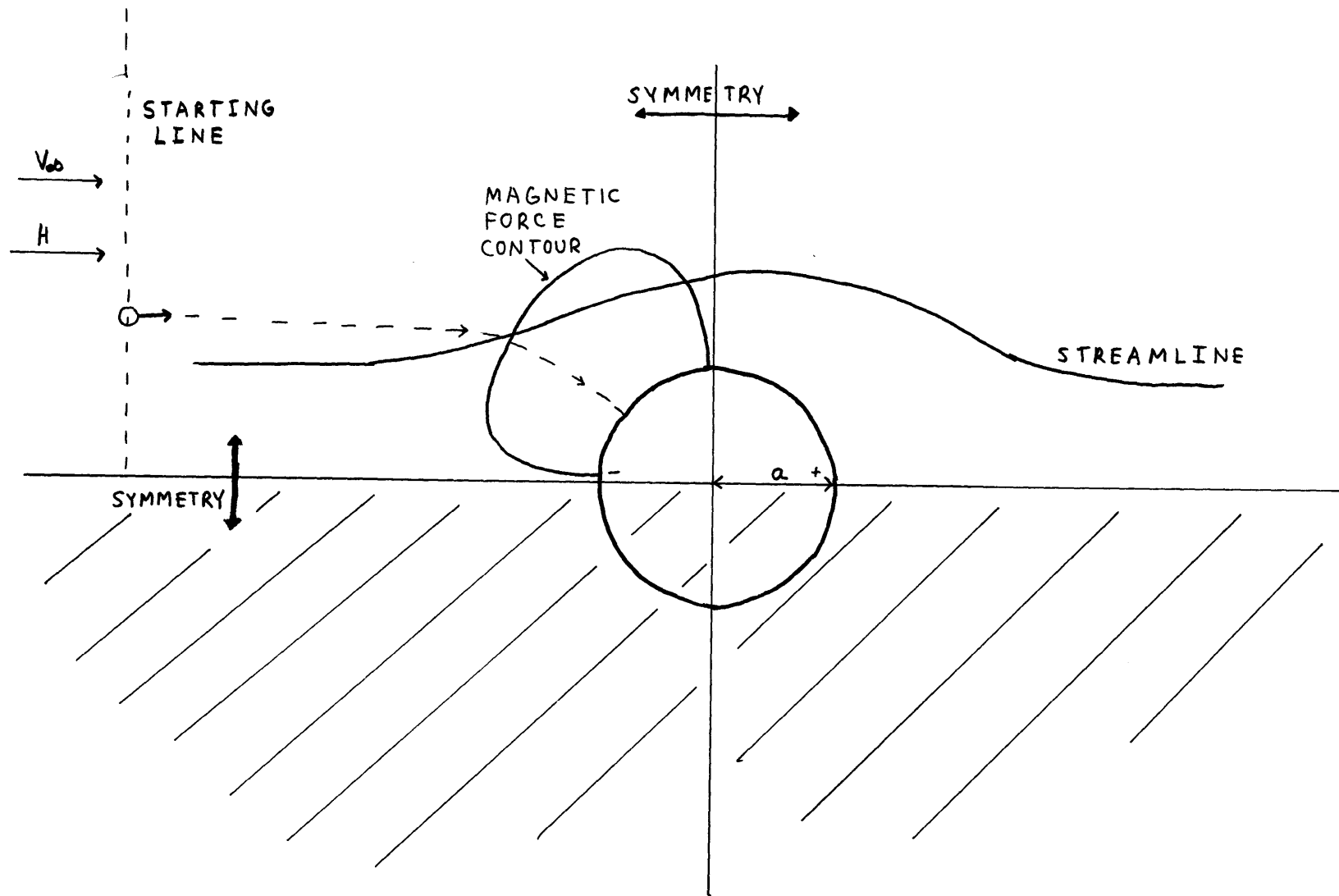
Figure S1 Computer Trajectory

A high value of H_s (20,000 gauss) caused a temporary
drop in y with increasing H above H_s. This was due to the
H_s/H term in equation (S-2) decreasing rapidly when H first
rises above H_s. The drop in H_s/H causes the region of
attractive force to decrease. A value of H_s (10,000 gauss)
was used in most cases to avoid this phenomenon. A lower
H_s value allowed the H_s/H changes to occur at a much smaller
magnitude of magnetic force and without any noticeable
effect on y.

The effect of particle density on trapping length y
was found to be negligible. A dimensionless correlation
between all the remaining variables except particle size R
was found and is shown in Figure S-2. The plot is at constant
R. The results demonstrated that free stream velocity V_∞
and cylinder radius a could be paired, since changes in a
affected the velocity field and drag force much more than
it affected the magnetic force. Only at low fluid velocities
did the a effects in magnetic force appear. The group
on the abscissa relates the magnetic potential KH^2 of a
particle to the kinetic energy of the fluid $\rho_f V_\infty^2$ that
must be overcome, if the particle is to be trapped.

The functionality of y with R was found to be complex
since the magnetic force is dependent on R^3 while the drag
force is dependent on R or R^2. A plot of dimensionless
R/R_o was used to correlate R with the other variables

The mathematical model broke down at low values of R or
H at certain velocities. A test particle would colloid
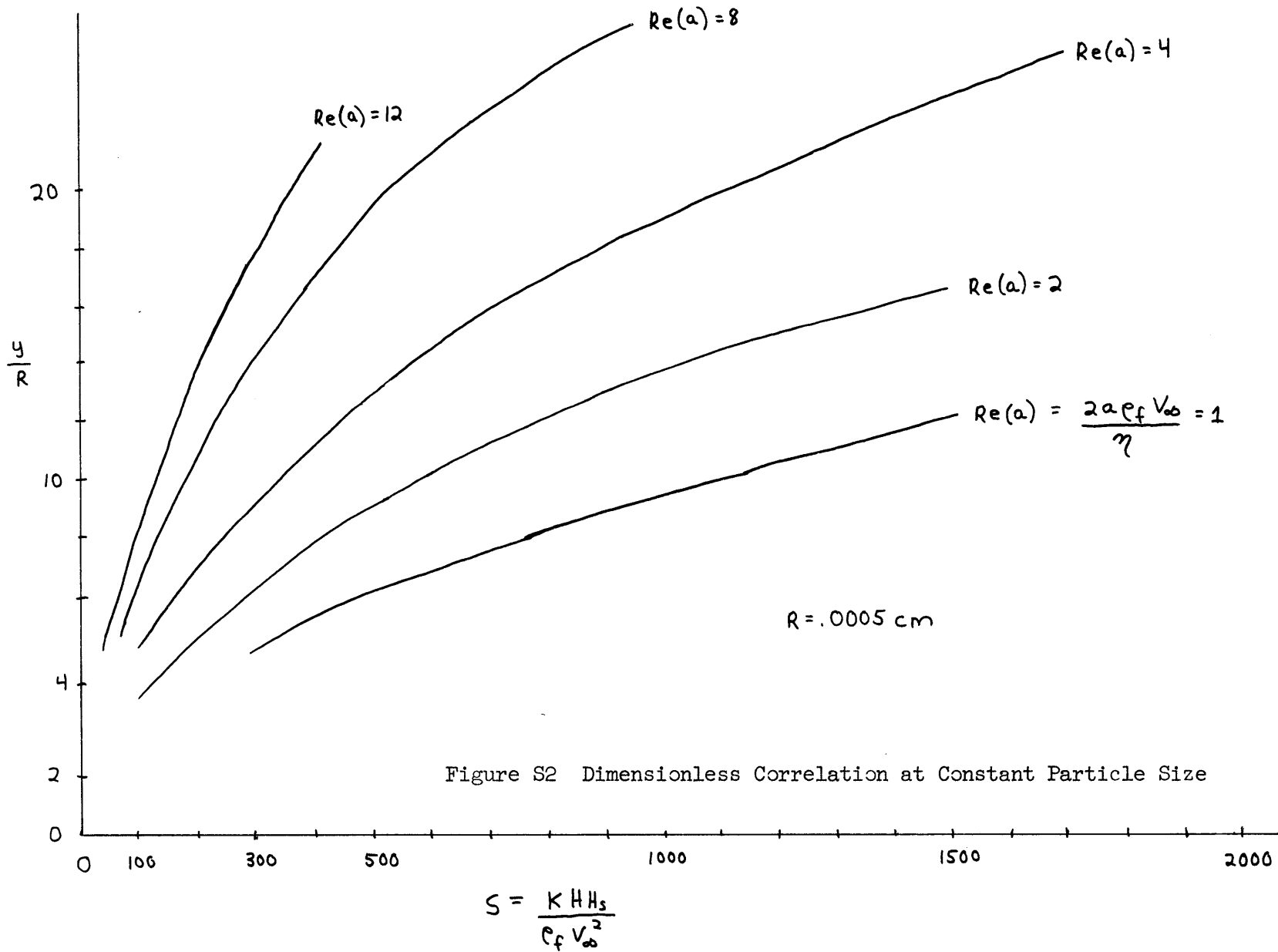
Figure S2 Dimensionless Correlation at Constant Particle Size

$Re(a) = 8$

$Re(a) = 4$

$Re(a) = 12$

$Re(a) = 2$

$Re(a) = \dfrac{2a\rho_f V_\infty}{\eta} = 1$

$R = .0005 \, cm$

$\dfrac{y}{R}$

$S = \dfrac{K H H_s}{\rho_f V_\infty^2}$

with the cylinder, but with a positive y velocity due to
the slip condition at the surface of the cylinder produced
by the potential flow description. A boundary layer is
necessary to get an accurate description.

The useable experimental data were confined to a single
material because of the range in particle sizes between
materials. $CO_3(PO_4)_2 \cdot 2H_2O$ gave good visual results, al-
though poor reproducibility which was probably due to
small particle size variations between samples. The
averaged experimental data, assuming constant R, could
be placed in a dimensionless correlation of the same form
and curve shape as the mathematical results.

The results of the mathematical model were extended
to a bed composed of cylinders. Assuming separation dis-
tances (perpendicular to the axes) between cylinders of
e and f, the trapping ability of a bed of cylinders of
length L could be expressed as

$$N = N_o (1 - \exp[-2y\gamma L/ef])$$ (S-6)

where y is the trapping length and γ is the probability
that the particle is initially perpendicular to the wire
and parallel to the field. For actual separation data
(Oberteuffer, 1971), and $\gamma = 1$, the required length neces-
sary to perform a real separation was found to be a bed
about two cylinders deep. This suggested that the bed

should be analyzed as an adsorber column and that in reality
a maximum wedge or total volume trapped occurs.

The single cylinder model always assumed that the wire
was clean. Including a better description of the fluid
mechanics that includes a boundary layer, a model that
retains and accounts for all trapped material should be
developed to get a value for the maximum trapping volume
at given operating conditions. Alternatively, one could
try to obtain visual evidence or use breakthrough analysis.

1. Magnetic Separation

1.1. Conventional Magnetic Separators

Magnetic separation is the practice of separating one solid material from another by using a magnetic force. Most applications to date remove ferromagnetic materials, mainly iron and iron compounds, from essentially neutral paramagnetic or diamagnetic streams, using permanent magnets or electromagnets. The stream to be processed is passed by the magnet which retains the magnetic impurity. Typical industrial magnetic separators are magnetic grates or screens (for cleaning grain), magnetic pulleys (for materials transported on conveyer belts), and wet drum separators (for ore benefication) which have magnets in the rotating drum (Perry, 1963).

1.2. High Gradient Techniques

1.2.1. Magnetic Properties of Materials

Most current magnetic separations have been limited to large sized ferromagnetic materials because of their favorable magnetic properties. Any material when placed in an external magnetic field will be affected or magnetized by the field to some extent. The phenomena is best explained atomically by quantum mechanics (Purcell, 1965). However, materials can be classified according to their macroscopic behavior in an external field at a given temperature. When the magnetization of a material is a nonlinear function of the intensity of the field and a residual magnetization (hysteris effect) remains if the external field is removed, the material is considered ferromagnetic. The total field around the material is equal to the superpositioning of

the external field and the induced magnetization, both vectors.

$$\bar{B} = \bar{H} + \bar{M} \tag{1}$$

The proportionality between the applied field and the total field is called the permeability.

$$\mu = B/H = f(H) \tag{2}$$

and is a function of the applied external field for ferromagnetic materials. Generally, the permeability of a ferromagnetic material has a high initial value which rises to a maximum and then falls off (Fig. 1). At a certain point called the saturation magnetization, the material will saturate (no further increase in magnetization) and $dB/dH = 1$. Note that the magnetization reaches a large value for a small applied field. Since the magnetic force on a material in the vicinity of a nonuniform field is given by

$$\bar{F} = \bar{M} \cdot \nabla \bar{H} \tag{3}$$

the force on a ferromagnetic material generally depends only on the field gradient. With a large magnetization there is not a critical need for a large gradient.

The magnetization of a paramagnetic material is a linear function of the applied field; the permeability is a constant at constant temperature and there is no hysteris effect. Generally, the permeabilities are only slightly greater than 1 (the permeability of a vacuum). Another unit, susceptibility, is generally used to describe paramagnetic magnetization.

$$K = M/H \tag{4}$$

Figure 1. Permeability as a Function of Applied Field for a
Ferromagnetic Material
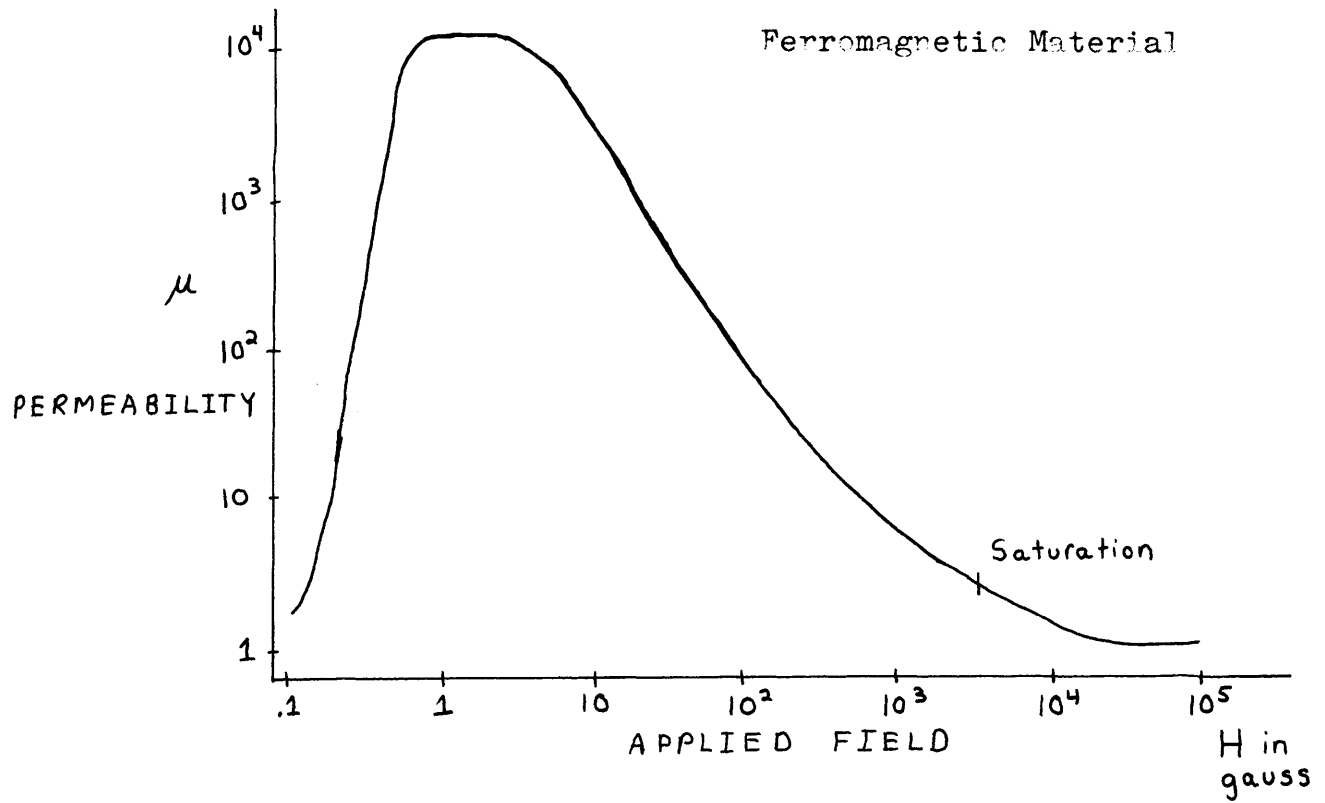
Permeability as a Function of Total Field for a
Ferromagnetic Material
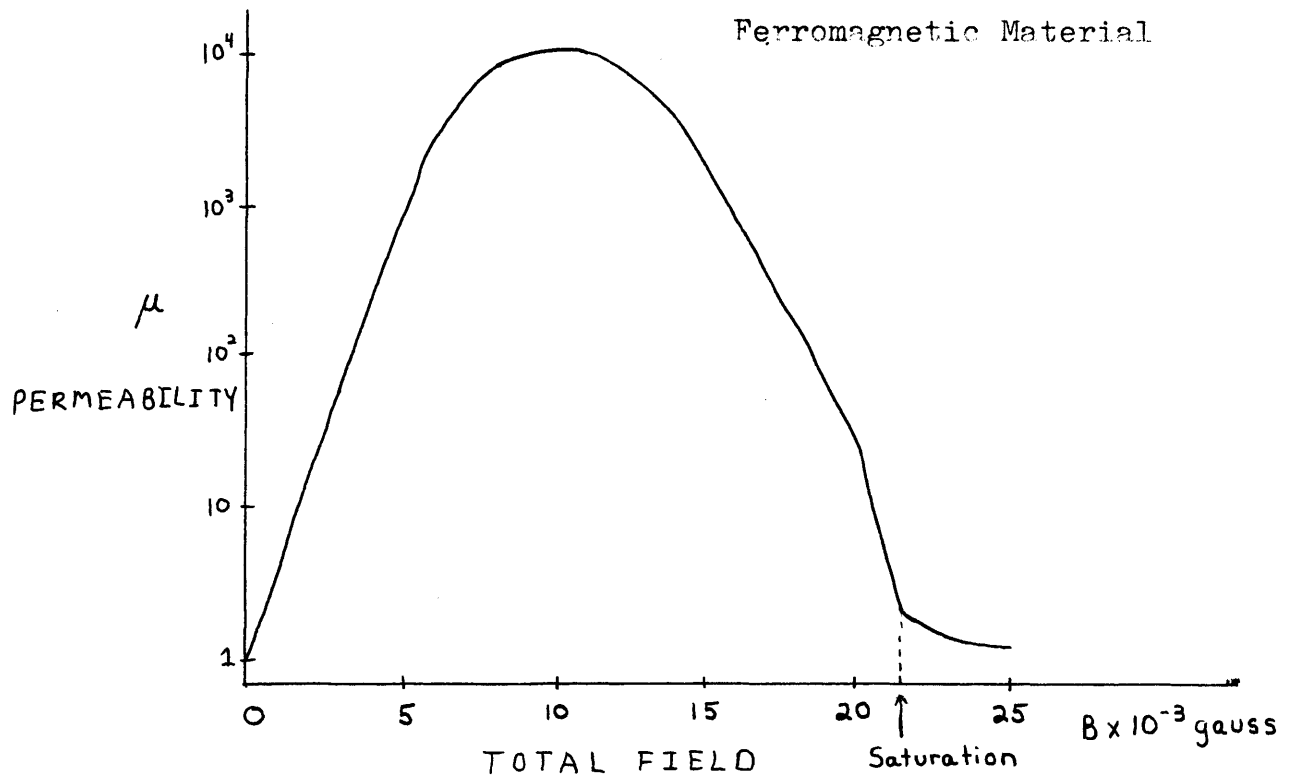
The susceptibility is often given on a molar basis, χ_M

$$\chi_M = \frac{Km}{\rho} \tag{5}$$

where m = molecular weight.

The molar susceptibility is normally in the range of 10^{-6} to 10^{-2}. The magnetization is then

$$\bar{M} = \frac{\rho \chi_M \bar{H}}{m} \tag{6}$$

The magnetization of diamagnetic materials is oriented opposite to $\bar{H}$, i.e. $\chi_M < 0$. The magnetic force on a paramagnetic particle in a magnetic field is given by

$$\bar{F} = K\bar{H} \cdot \nabla\bar{H} = \frac{\chi_M \rho}{m} \bar{H} \cdot \nabla\bar{H} \tag{7}$$

$\bar{F}$ has units dynes/cm^3 when $\bar{H}$ is expressed in gauss (oersteds) and ρ and m are in cgs units. To produce a force on a paramagnetic particle, equivalent to the force needed to retain an equally sized ferromagnetic particle, a higher field is necessary. Since there is a very low upper limit on the amount of magnetization practically producible, roughly $\chi_M \rho/m$ times 100 kilogauss, one needs to produce high gradients.

1.2.2. Production of High Gradients

A high gradient can be produced by placing a ferromagnetic object in a uniform field, increasing and distorting the field in the vicinity of the object. The maximum gradient achievable is limited by the saturation magnetization of the ferromagnetic material and by the rate at which the total field of the object falls off to the applied field, i.e. the geometry of the object. The ideal object would be a point dipole from which the field will fall off as r^3, r being the distance from the point.

However, the amount of trapping or retaining area would be infinitely small. Kolm, et al. (1971) have used stainless steel wool as the gradient producing material. A strand of wool is similar to a line of dipoles when magnetized and the field falls off roughly with r^2. Stainless steel is not ordinarily ferromagnetic, but when it is cold worked, it becomes ferromagnetic (Kinzel and Franks, 1940). Kaiser, et al. (1971) have used carbon steel screening, iron powder, cobalt powder, and a composite mixture. Gardini, Perona, and Sesini (1967) used a metal "comb" with pin shaped teeth.

1.2.3. Applications

The generation of high gradients is relatively new. The only current industrial use outside of more efficient removal of small, unwanted iron particles is the removal of impurities which discolor clay. Many possible applications are now under investigation. Oil can be removed from water by attaching an oil-soluble, strongly paramagnetic ferrofluid to the oil droplets, forming a paramagnetic droplet which can be collected when passed through a separator (Kaiser, et al. 1971). By a similar process, oil may be ferromagnetically tagged for pinpointing culpability for oil spills; the tagging material is removed with a magnetic separator when the cargo has reached its destination (Bean, 1971). Boiler scale which is ferromagnetic, but only about one micron in size may be removed from boiler water at the high boiler water temperatures (Gardini, Perona, and Sesini, 1967). Bacteria and suspended solids can be removed from water by adding Fe_3O_4 to the flocculant and then removing

the floc magnetically (de Latour, 1973; Kelland et al., 1972).
A study has been made of the feasibility of removing ash and
pyritic sulfur from coal (Trindade, 1973). Finally, benefica-
tion of semi-taconite iron ores is under study at the National
Magnet Laboratory at the Massachusetts Institute of Technology.
Semi-taconite ores contain weakly magnetic iron particles
which when liberated by grinding are too small to be separated
by a conventional magnetic separator (Kelland, et al., 1972;
Kelland, 1973).

1.2.4. A Typical Separator

A typical high gradient magnetic separator (Fig. 2) is
operated as a batch operation analagously to a filter. The feed
to be separated is introduced into the bore of the magnet which
contains the ferromagnetic packing or matrix. The feed is
passed through the packing (filter) while the
magnet is on. When the packing is filled to capacity, the feed
is stopped, and the magnet is turned off, eliminating any
hysteresis effect in the matrix. The filter is then backwashed,
washing the trapped material out of the packing. The procedure
is then repeated. If the amount of material to be retained is
small relative to the volume processed, a large amount can be
dealt with between each backwashing. However, if the retained
material is a large fraction of the total stream, the down time
for backwashing will be considerable, possibly necessitating
one or more back up separators. To overcome this problem which
is inherent to batch operations, a continuous process with a
moving matrix is being developed at the National Magnet
Laboratory for benefication of taconite ores in which the iron

Figure 2. A Typical Magnetic Separator

FEED
IN

RETAINED
FEED
OUT

MAGNET
COIL

MAGNET
COIL

APPLIED
FIELD

STAINLESS
STEEL WOOL
MATRIX

FILTERED
LIQUID
OUT

BACKWASH
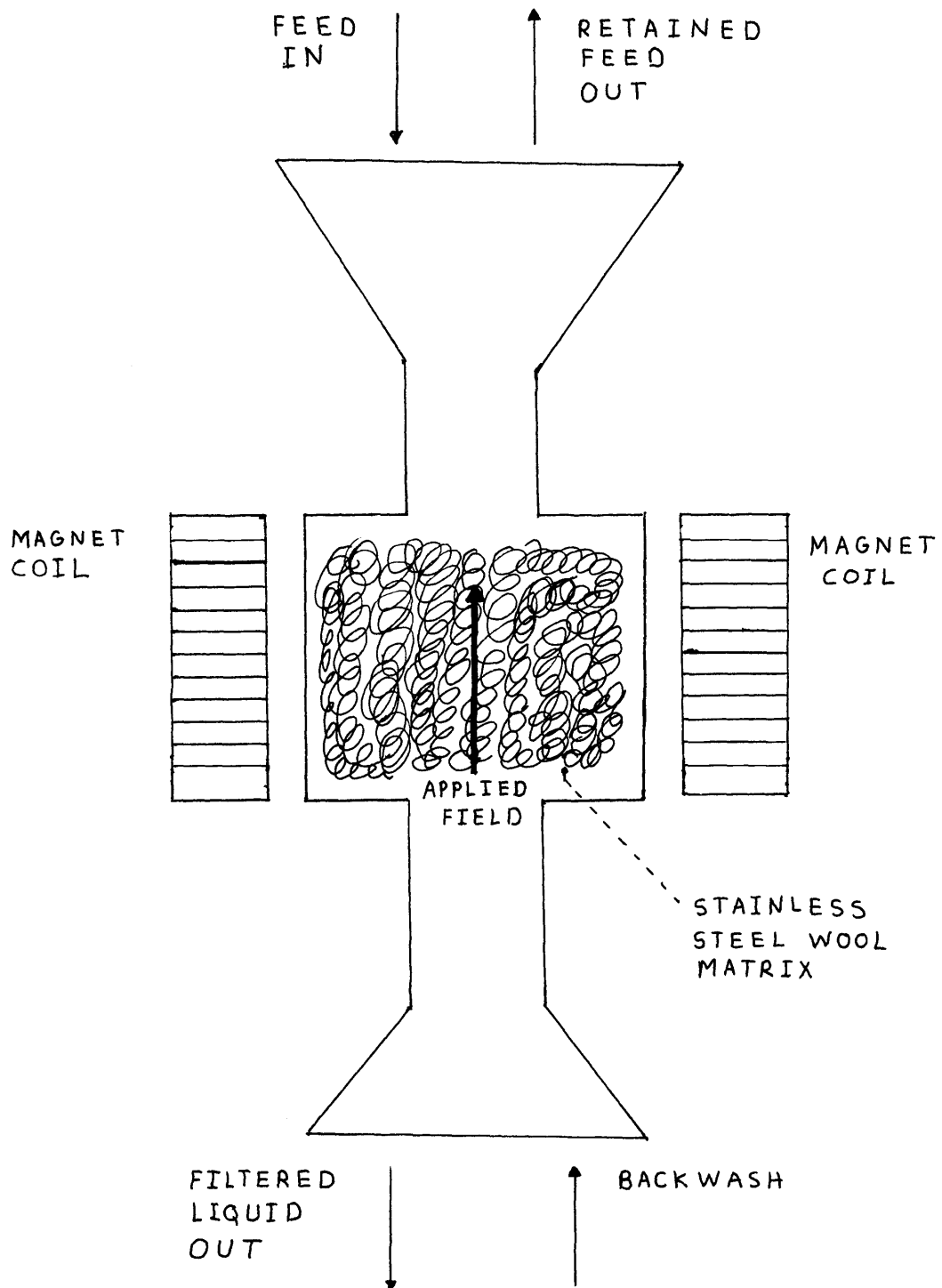
ore fraction which is to be retained is about 30-35% of the feed (Kelland et al., 1972, Kelland, 1973).

1.2.5. Forces Involved in Separators

The entrapment of particles in a magnetic separator depends on the forces acting on individual particles. There are three forces to consider in describing the behavior of a particle in the vicinity of a high gradient-producing object. Unless the particle is very much smaller than the collecting object, London or Van der Waal forces which are extremely short ranged need not be considered. The primary force is the magnetic force. Its characteristics depend on the trapping material used, the particle's susceptibility, and the intensity of the external field. The magnetic field gradient around the material which is responsible for the magnetic force depends on the size and shape of the material and its orientation relative to the field. The external field intensity determines the magnetization of the trapping material and the particle to be trapped, given the susceptibility of the particle. There will be a fluid drag force on the particle. The magnitude and direction of the drag force are functions of the particle size and velocity as well as the fluid velocity field around the trapping material. The viscosity and density of the fluid must also be considered. Finally, depending on the relative densities of the fluid and particle, there will be a gravitational or bouyant force.

The net force on the particle will produce an acceleration of the particle, changing its velocity and position in the force fields.

1.2.6. Need for Microscopic Analysis

Before the macroscopic behavior of a magnetic separator can be well understood, a description of the basic phenomena must be available. A macroscopic model based on the material balances made around a particular "black box" or separator cannot be automatically extended to any other separator system without some basic understanding about the principles which govern the trapping of individual particles inside the magnetic separator. While a direct correlation between the microscopic phenomena and macroscopic behavior of a separator might be unreasonably complex, a macroscopic model should reflect the microscopic phenomena.

The purpose of this work is to develop mathematical models for the trapping of individual paramagnetic particles on particular geometries of high magnetic gradient sources. Concurrently, an experimental program will be designed to test the validity of the models and to make general observations of the trapping phenomena which may be enlightening to a macroscopic treatment of magnetic separation.

2. Prior Development of Paramagnetic Trapping Models

2.1. Magnetic Force Model of Gill and Malone

Gill and Malone (1963), while looking into the production of high gradients for paramagnetic susceptibility measurements, investigated the magnetic field of a ferromagnetic material when placed in a uniform external field. As a model, they used Stratton's (1941) analytic solution of the total magnetic field $\bar{B}$ surrounding an infinite circular cylinder of radius a perpendicular to the external field H.

$$\bar{B} = (1 + Aa^2/r^2)H\cos\phi\,\hat{r} + (-1 + Aa^2/r^2)H\sin\phi\,\hat{\theta} \qquad (8)$$

where $A = (\mu_1 - \mu_2)/(\mu_1 + \mu_2)$ \qquad (8a)

and r is the radial distance from the center of the cylinder, μ_1 and μ_2 are the permeabilities of the cylinder and the media, respectively, ϕ is the position angle measured from the first quadrant, and $\hat{r}$ and $\hat{\theta}$ are polar unit vectors. They then calculated the force field that results in taking the gradient of the total magnetic field ($\bar{B}$ replacing $\bar{H}$ in equation [7]) for the case of $A = 1$ ($\mu_1 \gg \mu_2$).

$$\bar{F}_M = \frac{2K'Ha^2}{r^3}\left[\left(\frac{a^2}{r^2} + \cos2\phi\right)\hat{r} + \sin2\phi\,\hat{\theta}\right] \qquad (9)$$

where K' is the relative susceptibility between the particle and the media. Tracing the motion of polystyrene particles in the vicinity of an iron cylinder, they experimentally determined the force "lines of flow." Their data was more or less in agreement with the analytic solution. However, in the derivation of the analytic solution, the permeability μ_1 of the cylinder was assumed constant to make the problem linear. Unfortunately,

ferromagnetic materials have varying permeabilities and the solution is invalid near or beyond saturation when μ_1 tends to one (and A tends to zero). Well below saturation, A is approximately one only for materials of high and constant permeability, since in the derivation of the model, μ_1 is the intrinsic permeability of the cylinder.

2.2. Trapping Design of Gardini, Perona, and Sesini

To remove solid particles from boiler feed water at temperatures above those permitted by conventional methods, Gardini, Perona, and Sesini (1967) developed a magnetic filter utilizing banks of ferromagnetic pins. They calculated equal force (magnetic and fluid drag) surfaces for different pin geometries, fluid velocities, and particle sizes for a given applied field. They also calculated theoretical trapping efficiencies for a given pin in terms of particle size, fluid velocity, and applied field. However, no indications were given about the assumptions of the design except that the magnetic fields were evidently calculated for conditions well below saturation of the pins. However, the plots of field strength are in the vicinity of complete saturation. Although the experimental data "confirms the trends" according to the authors, no quantitative correlation is given. Also, because of the design of their experimental filter, the collection reported experimentally could have occurred on the pin supports instead of the pins.

2.3 Filter Model of Bean

Bean (1971) developed a filter model based on a microscopic cross section of cylinders integrated over the length of the

filter, L. The resulting form is expressed in terms of rejection, R

$$R = 1 - \frac{C_{out}}{C_{in}} \tag{10}$$

where C_{out} and C_{in} are particle outlet and inlet concentrations, respectively.

$$\frac{C_{out}}{C_{in}} = \exp\left[\frac{-4/3\ M_S\ d^2 K\ H}{4\ a^2\ \eta\ V_\infty}(1 - X)X\right] \tag{10a}$$

where M_s is saturation magnetization of the cylinder, η is the viscosity of the fluid, d is the diameter of the particle, K is the volume susceptibility, a is the radius of the cylinder, H is the applied field, X is the volume fraction of packing material, and V_∞ is the fluid velocity. However, the model is based on a high Reynolds number which is suspect, considering that the model is for a packed bed. No experimental data is given.

2.4 Capture Model of Oberteuffer, et al.

Using CuO in a laboratory scale magnetic separator, Oberteuffer, et al. (1971) fit separator performance data to a mathematical model which is briefly summarized below.

Assuming the matrix of a separator can be described as a number of site absorbers per unit volume, n, each with cross section α, the retention of feed or MAGS can be described by

$$MAGS = FEED(1 - e^{-n\alpha L}) \tag{11}$$

where L is the length of the separator. To specify α, a fixed geometry of the steel wool packing was assumed such that the longer strand width parameter was parallel to the field, and so

that

$$\text{MAGS} = \text{FEED}(1 - \exp(-\lambda L/d_1 d_2)) \tag{12}$$

where d_1 and d_2 are separation distances between strands and λ is an effective impact parameter, i.e. any particle coming within λ (in the x direction) of the strand will be trapped. The criteria for capture was chosen as

$$V_{xm} = C(V_{ym} + V_\infty) \tag{13}$$

that the component of velocity induced by the magnetic force in the x direction must be some fraction C of the total y direction velocity (magnetic plus fluid) in order for the particle to reach the strand. (Far from the strand, the particle is moving in the y direction only. The applied field is also in the y direction.)

Modeling the magnetic field as a line of point charges, using Stokes law to describe the fluid drag force, and assuming the capture criteria can always be applied along a 45° line from the center of the strand.

$$\lambda = C \left(\frac{b \ K \ HM_s a}{\rho V_\infty^2} \right)^{1/2} \tag{14}$$

where b is the radius of the particle, ρ is the density of the fluid. The other variables are defined by previous usage. The constant C is a function of feed. Replacing and incorporating Equation (14) into Equation (12)

$$\text{MAGS} = \text{FEED} \left[1 - \exp \left(\frac{-CL}{d_1 d_2} \left(\frac{bKHM_s a}{eV^2} \right)^{1/2} \right) \right] \tag{15}$$

The model predicted that the exponents of H and V_f should be .5

and 1.0 respectively. A fit of the data produced exponents of
.65 and 1.0 respectively. C was found to be 7.92×10^{-3}.

The model is a three parameter model, and the fit may be
somewhat artificial. The dynamics of capture have been neg-
lected (the impact parameter may be oversimplified), and the
exponential term of the fit is not dimensionally correct.
Unfortunately, the model has not been tested on other para-
magnetic materials or packing.

2.5. Absorber Model of Kaiser, et al.

In designing a separator to remove oil from water, Kaiser,
et al. (1971) developed an absorber model to analyze the data.
However, the only parameters dealt with were packing material,
applied field intensity, and flow rate through the filter, al-
though a great deal of care was taken in the design of the
experiment.

2.6. Static Model of Trindade

In an analysis of coal purification Trindade (1973)
developed a static model of particle capture. Given a
ferromagnetic circular cylinder perpendicular to an applied
field with uniform fluid flow and gravity parallel to the mag-
netic field, Trindade calculated the net force on a stationary
particle at variable distances downstream from and angles to the
cylinder. Other variables used were particle susceptibility,
density, size, fluid velocity, and applied field intensity.
Capture was defined by a net force towards the cylinder. How-
ever, the model used the improper formulation for field strength
around the cylinder (see section 2.1) and fluid velocity was not

a function of position. The problem is not actually a static problem, nor is backside capture preferable to capture at the front.

2.7. Dynamic Models of Watson, Steckly and Tarr

Watson (1972) has developed a dynamic description of particle capture. Watson's magnetic field equations are not universally applicable. He also neglects inertial terms. However, the trajectories produced from the model seem plausible. Watson goes on to consider an absorber model and compares it with Bean's results (see section 2.3). The paper, unfortunately, is extremely brief and obtuse.

Steckly (1972) has formulated a dynamic model, again using the constant permeability assumption in calculating the magnetic field (see section 2.1). Inertial terms have been dropped. No trajectories were available.

2.8. Electrostatic Dynamic Model of Zebel

For particle capture on a cylindrical fiber in an electric field, Zebel (1965) has formulated a dynamic model. The electric field and electric forces are analagous to those of the Stratton solution and are thus not directly applicable (see section 2.1). Zebel used both potential flow and Oseen flow in the model, depending on the Reynolds number based on the cylinder. Gravity and inertia are neglected, but their omission is justified by order of magnitude analysis. Zebel goes on to describe a deposition coefficient or capture parameter and builds a macroscopic model from integration of a single fiber layer. However, except for the limiting case of a dielectric constant equal to 1 which

corresponds to a permeability of 1 ($\overline{H} \gg \overline{M}$ or $\overline{B} \simeq \overline{H}$) only a few capture coefficients were calculated.

3. Paramagnetic Particle Trapping Models to be Investigated

3.1. Factors to be Investigated

3.1.1. Trapping Visualization

The first step in the program to investigate paramagnetic particle entrapment is the creation of a flow chamber that will enable one to actually view the trapping phenomenon (through a microscope). This step is vital to assure that the mathematical models have some basis in reality, as well as to eventually test them.

Several factors must be considered for visualization. One needs to provide a clear view for observation, yet the fluid dynamics of the system should be readily describable. One must also provide for a wide range of operating conditions so that several variables may be easily adjusted. The major problem in the visual experimentation lies in the design of a flow chamber. With the exception of the trapping materials, paramagnetic particles, and field strengths available, the flow chamber will be the limiting factor in any experimental program. The design and actually experimental detail are described in section 3.2.

3.1.2. Mathematical Models

There are four basic orientations which should be considered in the development of mathematical models for the description of particle entrapment. Fluid flow may be parallel or perpendicular to the long axis of the trapping material. The applied magnetic field may also be parallel or perpendicular to the long axis of the trapping material. Any other orientations may be resolved vectorially. Spheres which obviously do not

have a long axis are not considered for several reasons. First, they would be hard to physically support in an experimental chamber without disturbing the velocity or magnetic fields. Second, they do not seem to offer any particular advantages over other packing shapes in actual magnetic separators (Kaiser, 1971). Third, in an actual bed, there would be little separation distance; thus, studying a single sphere seems rather fruitless.

Of the four possible orientations of cylindrical objects, two are of interest; magnetic field and flow direction either both parallel or perpendicular to the long axis. The other two may be neglected since magnetic field lines (and higher gradients) tend to congregate near the poles of a magnetized material. A cylindrical object parallel to the field would tend to draw particles to the ends or poles (see figure 3a). This is not conducive for creating a large trapping area if the flow is per-pendicular to the long axis, since particles crossing the long axis in the center region would be attracted to either end simultaneously and slip past. Only particles near the ends should trap, and the trapping surface is not oriented to acheive head on trapping (there is no stagnation region). If the long axis of the cylinder is perpendicular to the magnetic field and parallel to the direction of flow (see figure 3b), there will always be a considerable shear force on the particle, since there is no shielding from the fluid velocity in stagnation regions. The magnetic force can only operate perpendicular to the drag force, requiring a large magnetic force to overcome the drag force. Also, the possibility of buildup on the "sides" of the

Figure 3. Various Orientations of a Wire to Magnetic Field
and Flow Direction
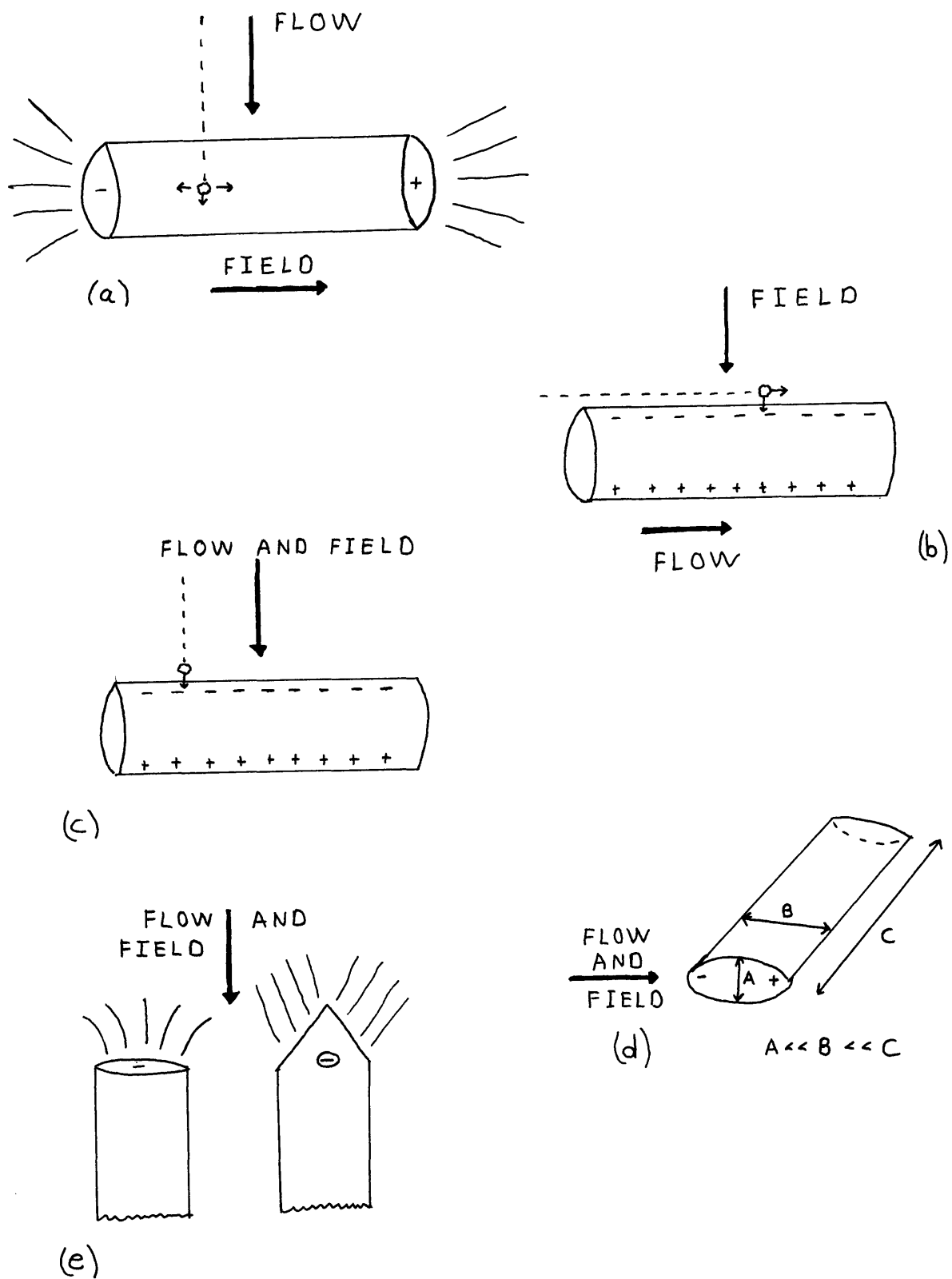
long axis would make the problem more complex because of the
particles' effect on the boundary layer. These two orientations
(magnetic field perpendicular to flow direction) will be observed
visually, but not modelled, since they are not expected to con-
tribute greatly to any actual trapping.

The most preferred orientation of strands for particle
capture in a steel wool matrix seems to be perpendicular to both
the applied magnetic field and the flow direction (Oberteuffer,
et al., 1971). The steel wool strands used to produce high
gradients will be approximated by circular cylinders (see figure
3c). The wool strands are actually ribbons or parabolic cylinders.
In the limit, there is no fundamental difference in fluid flow
around a circular or parabolic cylinder, nor is the magnetic
field greatly changed. A circular cylinder model will be explored
for the cylinder perpendicular to both the magnetic and flow
direction (see section 3.3).

If the non axial dimensions of a ribbon shaped strand are
not the same order of magnitude, the strand may be considered
parallel to the magnetic field with respect to a secondary axis,
the longer width dimension (see figure 3d). Instead of a line
of point dipoles as in figure 3c, the leading edge may be modeled
as a line of point charges. However, this is not accurate (and
will not be modeled), since the true field configuration is
ellipsoidal and quite complicated (see Stratton, 1941).

Flow and field parallel to the major axis of a strand will
not be modeled. The end of a cylinder is blunt and would be
equivalent to the end of a solenoid, magnetically (see figure 3e).
A more intriguing end shape is a wedge or cylinder with a shar-

pened tip, but the description of the induced magnetic field around a wedge or tip depends strongly on the shape of the wedge, thus a large number of models would be necessary to provide a complete description. Additionally, a wedge or blunt end only offers a small trapping area compared with a cylinder perpendicular to both field and flow.

Finally, interactions between two objects must be considered as a limiting case of macroscopic behavior. A model consisting of two circular cylinders of equal radius will be developed and tested for various spacings and compared with a single cylinder. Only the case of cylinders being in a plane perpendicular to the flow direction and applied field will be considered because of the large number of possible staggered orientations (see section 3.3.5).

3.1.3 Correlation Between the Models and Observed Phenomena

For each of the models a series of computer simulations will be run to determine a trapping length or maximum distance (perpendicular to the flow direction) at which a particle can be captured for the given conditions in the model. The results will be reduced to correlations among a set of dimensionless groups composed of the pertinent variables.

An experimental program will be undertaken to test the correlations suggested by the mathematical models. The experimental variables will be suggested by the models and the practicality of actually manipulating them. The results of the experimental program should be reducible to the same dimensionless groups and a direct graphical comparison can be made. Since the data that will be taken can only be considered semi-quantitative (see section 3.2.2), no attempt will be made to establish a rigorous comparison, and only similarities can be checked.

3.1.4. Correlation Between the Cylinder(s) Model and Macroscopic Phenomena

An attempt will be made to scale up the cylindrical model (taking into account the two cylinder model) by integrating a cross section of one-deep cylinders over a given separator length and calculating the total retention based on the correlations derived for the model. The integrated model will be compared with the parameters of previously developed macroscopic models and the retention of an actual separator (Oberteuffer, et al.,1971). An analysis of the validity of the integrated model will then be made.

3.2. Experimental Design and Methods

3.2.1. Equipment Used

The experimental equipment was basically a controlled water flow passing through a viewing chamber (described in section 3.2.2). The chamber was placed between the pole pieces of a conventional water cooled electromagnet (see figure 4). The electromagnet with coils wired in series, was powered by a controlled current d.c. power supply capable of approximately 11 amperes at 40 volts (voltage limited). A maximum applied field of 5000 gauss was attainable in the center of the gap between the pole pieces. The tubing carrying the flow passed through holes drilled in the pole pieces. A rotometer upstream of the chamber measured flow rate; the controlling valve was placed downstream of the chamber. A gravity feed was used, the reservoir having a large cross section to provide a constant head over a period of several minutes. Chlorine was added to the water in the form of NaOCl (approximately 1000 ppm) to prevent algae. Air bubbles due to dissolved air were removed by first bringing any water added to the reservoir to room temperature. Particles were added to the flow stream by syringe injection at a septum covered tee upstream of the chamber.

Viewing was done through a Bausch and Lomb Stereo Zoom microscopic capable of 20-140 power magnification. The microscope was placed directly above the flow chamber. A camera with a 4"×5" Polaroid back could be attached to the microscope, leaving one eyepiece free for viewing. The light source used was a 500 watt projector with a fiber optics tip, the tip placed next to the chamber perpendicular to the viewing direction (reflected light). The intensity of the light source was variable.

Figure 4   Experimental Equipment
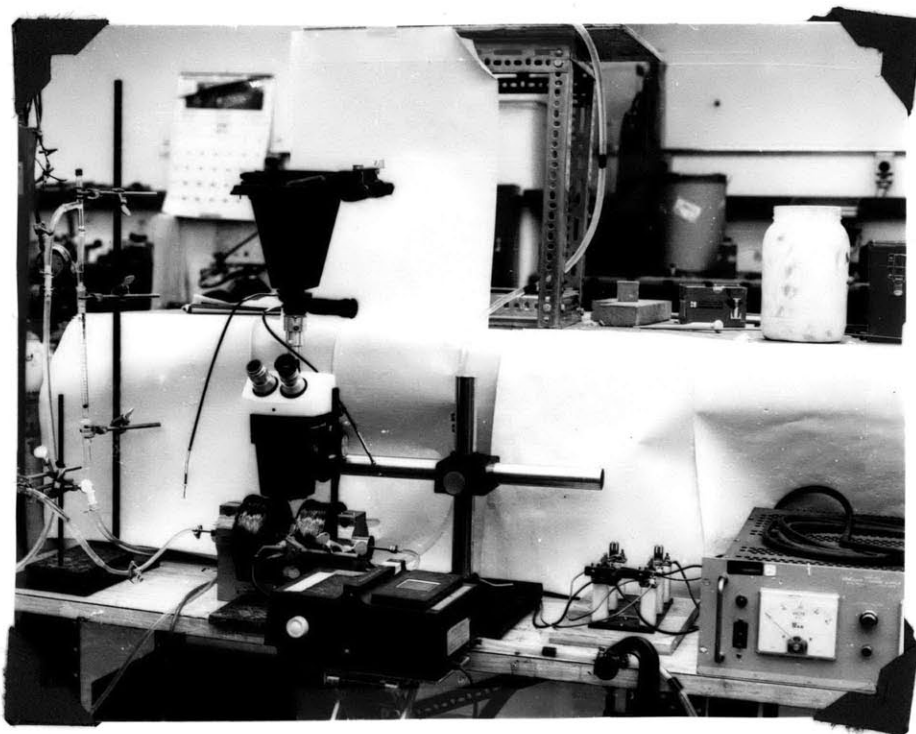
Figure 4   Experimental Equipment
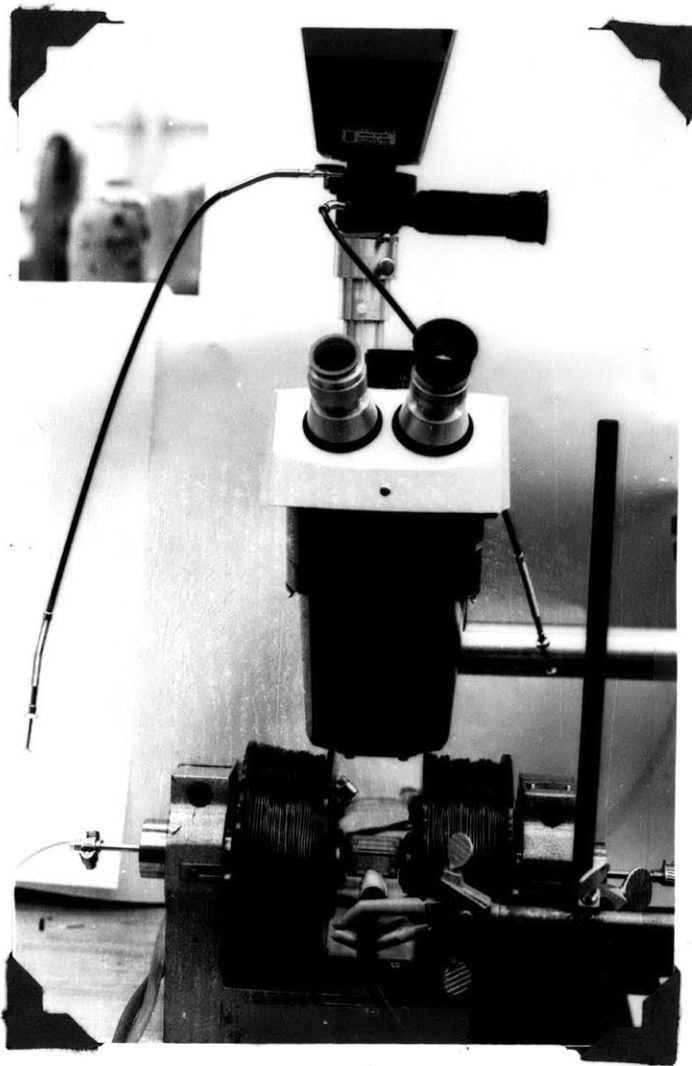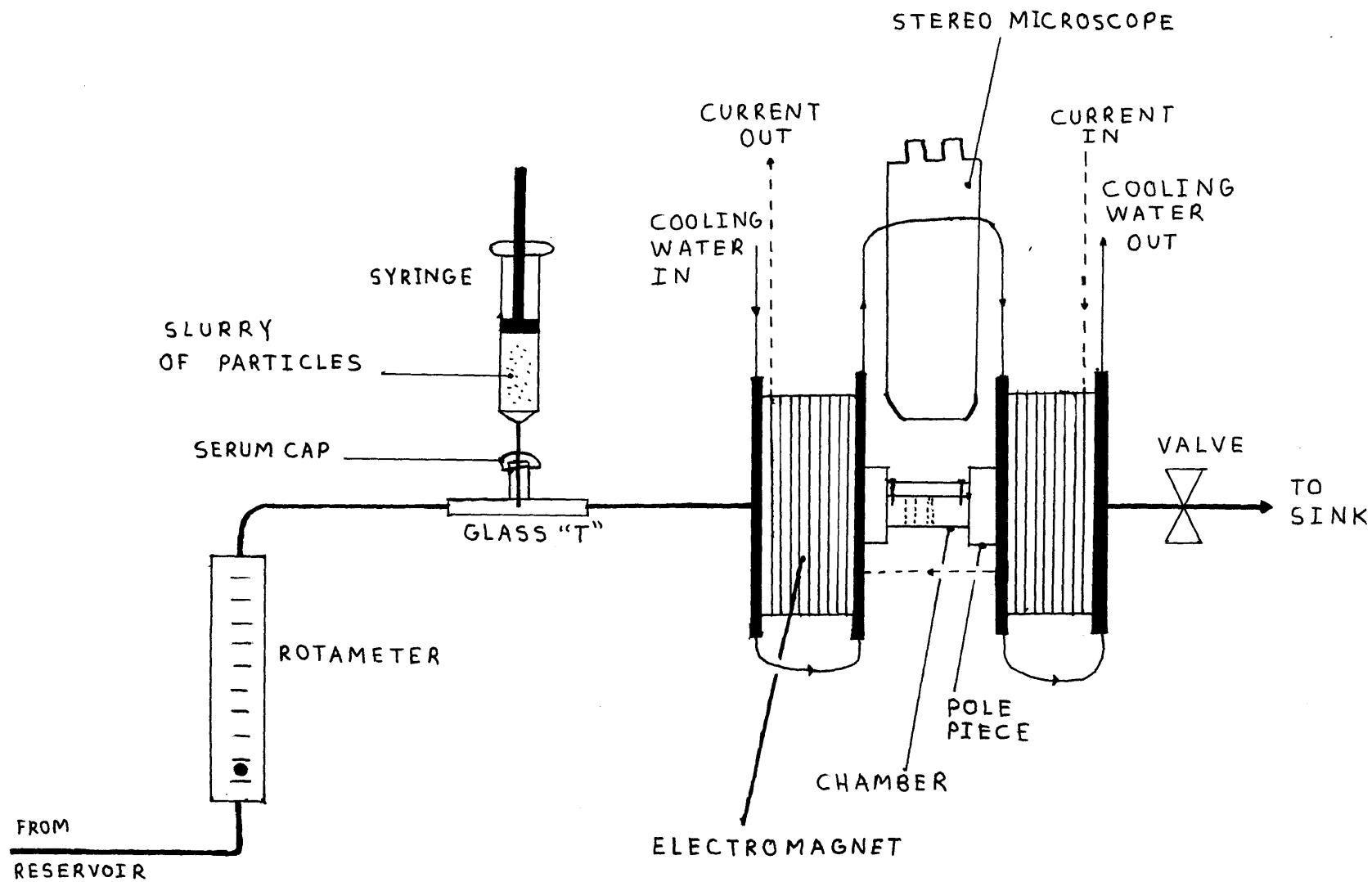
Figure 4   Experimental Equipment

Various insoluble (in water), low density, paramagnetic materials were selected to assure neutrally bouyant particles. Figure 4a gives the properties of the materials used.

Stainless steel wool and pure iron wire were used as trapping material. The steel wool was assumed to have a saturation permeability of 10. Nearly cylindrical strands of uniform diameter were selected for use from a clump of strands. The iron wire available was 500μm in diameter. The iron was spray painted with a coat of black primer to avoid the formation of $Fe(OH)_2$ and Fe_2O_3 scum which formed on the iron when it was placed in the liquid stream.

3.2.2. The Flow Chamber

Three basic concepts were incorporated into the design of the chamber, consistency of flow patterns, ease of viewing, and adaptability for different experiments. The pole pieces of the magnet were drilled to allow a piece of tubing to pass through them. The length of the entry tube to the actual chamber was designed so that at the flow rates desired, the flow on entry to the chamber proper would be laminar, regardless of the upstream orientation of connecting tubing. The criteria used was

$$\frac{L}{D_t} \geq \frac{Re}{20} \tag{16}$$

where L is the length of the entry tube, D_t is the tube diameter and Re is the Reynolds number based on the tube. Rearranging,

$$V_v \leq \frac{5\Pi L\eta}{\rho} \tag{17}$$

where V_v is the volumetric flow rate and η and ρ are the viscosity

Figure 4a Properties of Paramagnetic Materials Used

Material	$Co_3(PO_4)_2 \cdot 2H_2O$	$Cu(OH)_2$- CuO	Al	NiC_2O_4	CuO
Molecular Weight	403	$Cu(OH)_2$= 97.5	27	147	79.5
Molar Susceptibility (cgs units x 10^6)					
table	n.a.	$Cu(OH)_2$= 1170	16.5	3200	239
measured	1800	237			
Measured Density	2.6 gm/ cm^3	3.6	2.8	2.2	5.4
Color	pink	brownish-black	grey	green	black
Particle Diameter Range	8 - 15 microns	5 - 40	5 - 20	1 - 50	5 - 20

and density of the fluid, respectively. For 7½" entry tube, the maximum flow rate is about 3 cm^3/sec. This corresponds to a maximum velocity of 6 cm/sec in the chamber.

The entry of the chamber widened from the tube diameter to a square duct .7 cm in width. Aligned bronze 60 mesh screens were placed at the beginning of the duct to create a flat velocity profile (Grootenhuis, 1954), a flat profile preventing any fluid phenomena being a function of position across the chamber. A gap in the walls was designed so that various screen inserts could be tested for creation of a flat velocity profile. Another gap downstream of the screening was made for the insertion of a holder for the wire shapes to be examined. The wire insert was placed so that the flow profile would still be flat except very near the walls, i.e. well before the establishment of laminar flow.

$$L \ll \frac{D_t \text{ Re}}{20} \tag{18}$$

where D_t = .7 cm is the width of the duct. The inserts were made to fit flush with the walls of the duct. The exit was similar to the entry except without any screens. The chamber size was quite small in order to minimize the gap between the pole pieces. The entire chamber was constructed out of plexiglass with a removable top plate polished for viewing. The chamber is illustrated in figures 5 and 6.

The flow patterns produced by the screens (without a wire insert) were investigated by two methods. A red recorder ink was injected upstream at the septum. The colloidal particles of the ink reflected green when exposed to white light (projected into

Figure Five Flow Chamber
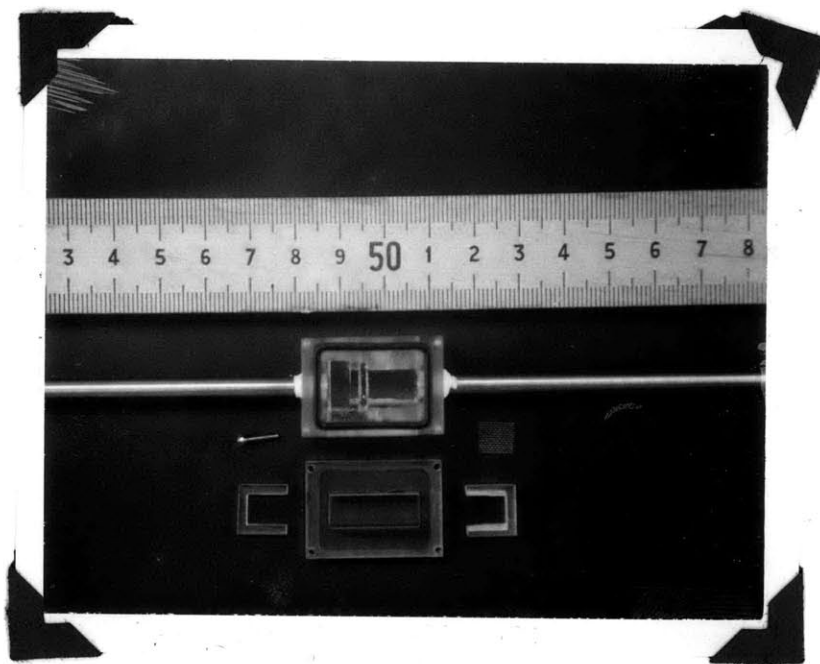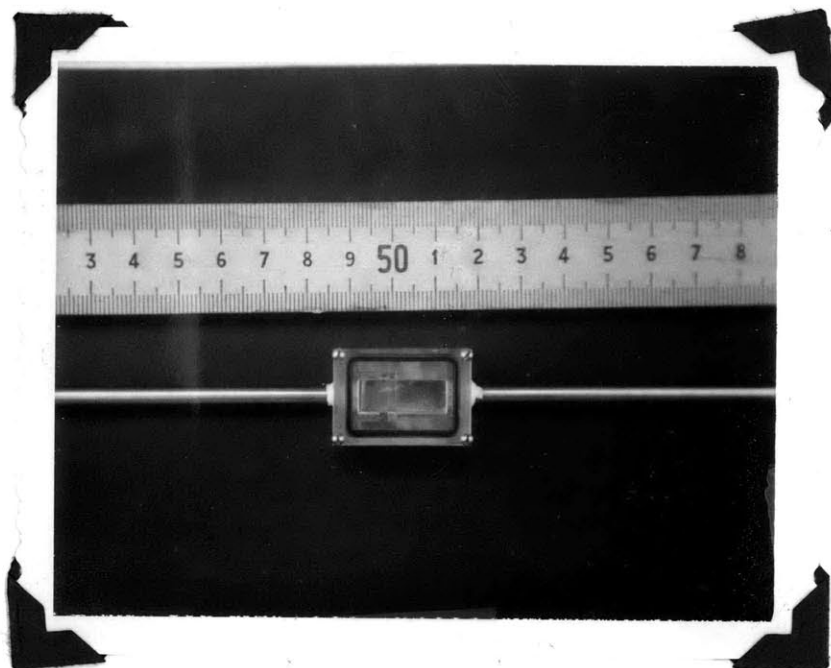
Figure 6 Dimensions of Chamber

TOP VIEW
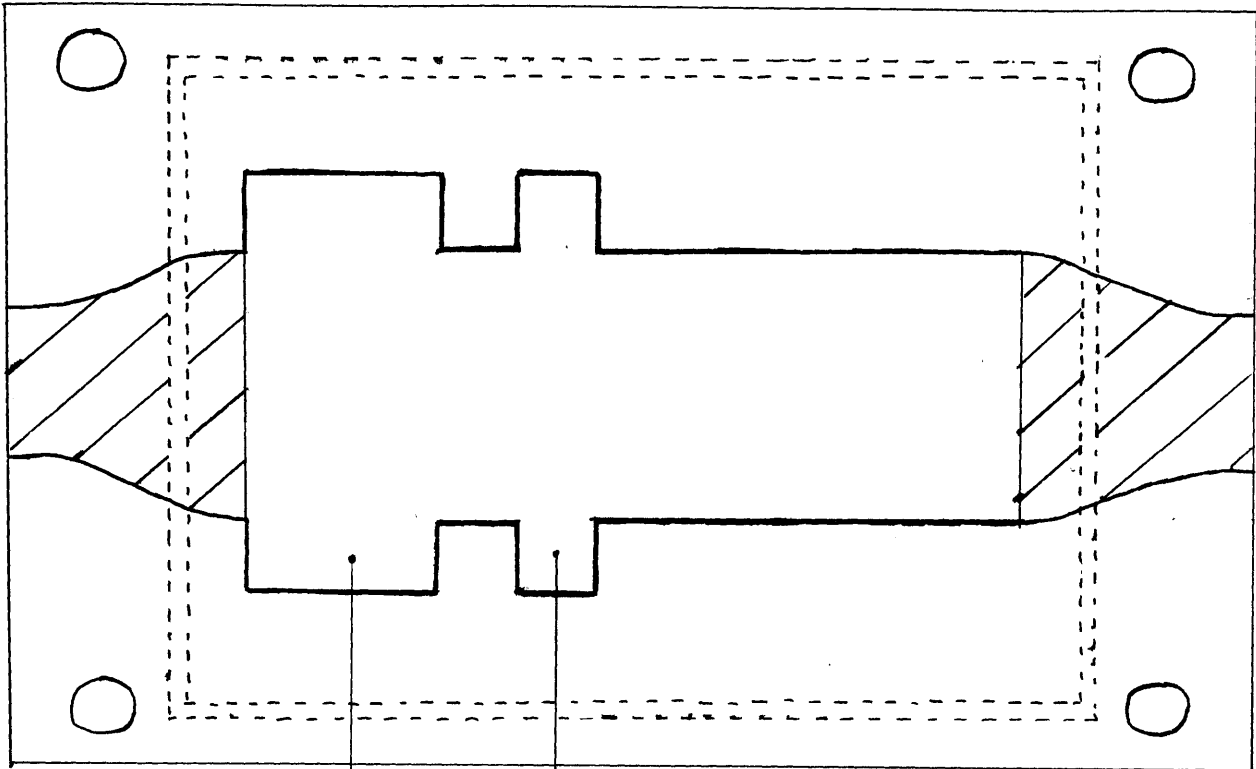
GAP FOR
SCREEN
INSERT

GAP FOR
WIRE
INSERT

SCALE

0   .5 cm

SIDE VIEW
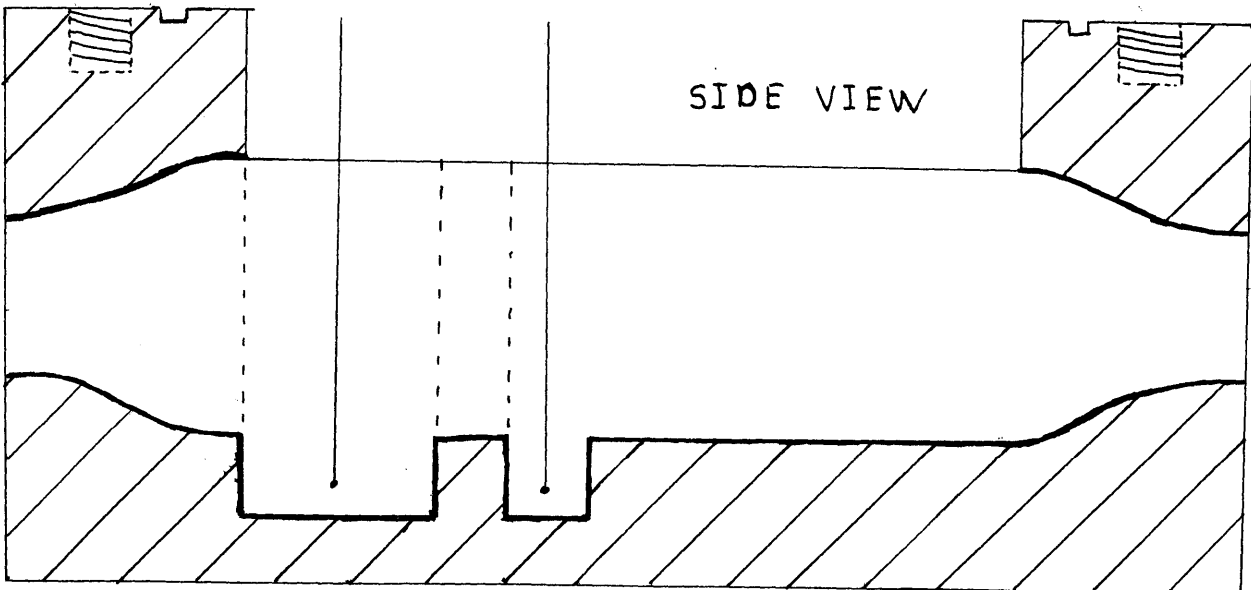
the chamber perpendicular to viewing). The screens "blocked" the
flow creating dark streamlines indicating relative absence of dye
(no reflection). Any mixing downstream of the screens would
obliterate the observed streamlines. Pictures of the streamlines
at several flow rates were taken with a 35 mm camera equiped with
a close up lens and blown up to show detail (see figure 7).
Concurrently, hydrogen bubbles (Shraub, Kline, et al., 1964) and
particles were photographed at given shutter speeds, and track
lengths across the width of the chamber were observed for
nonuniformity. Except near the walls, the velocity profile
seemed quite flat. Over any small section in the vicinity of the
wire, the flow seemed uniform at any flow rate used.

3.2.3. Experimental Methods

Originally, actual photographs of particle trajectories were
to have been a major portion of the experimental program. These
would have allowed direct comparison with the computer simulated
trajectories. However, the depth of field was lost when the particles
were photographed. Also the amount of light necessary to get a
properly exposed particle track was enormous. The only available
method that worked was triggering a flash cube at approximately
two inches from the chamber. Finally, the percentage of particles
that trapped over a period of time was small, so the photographs,
being of short time durations, were a "hit or miss" proposition,
consisting almost entirely of misses. A high powered strobe was
needed as well as better optics.

Besides general observations, the experiments finally
performed, consisted of injecting a slurry of particles into the

Figure 7 Flow Pattern in Chamber

$$V_v = 1.25 \text{ cm}^3/\text{sec}$$
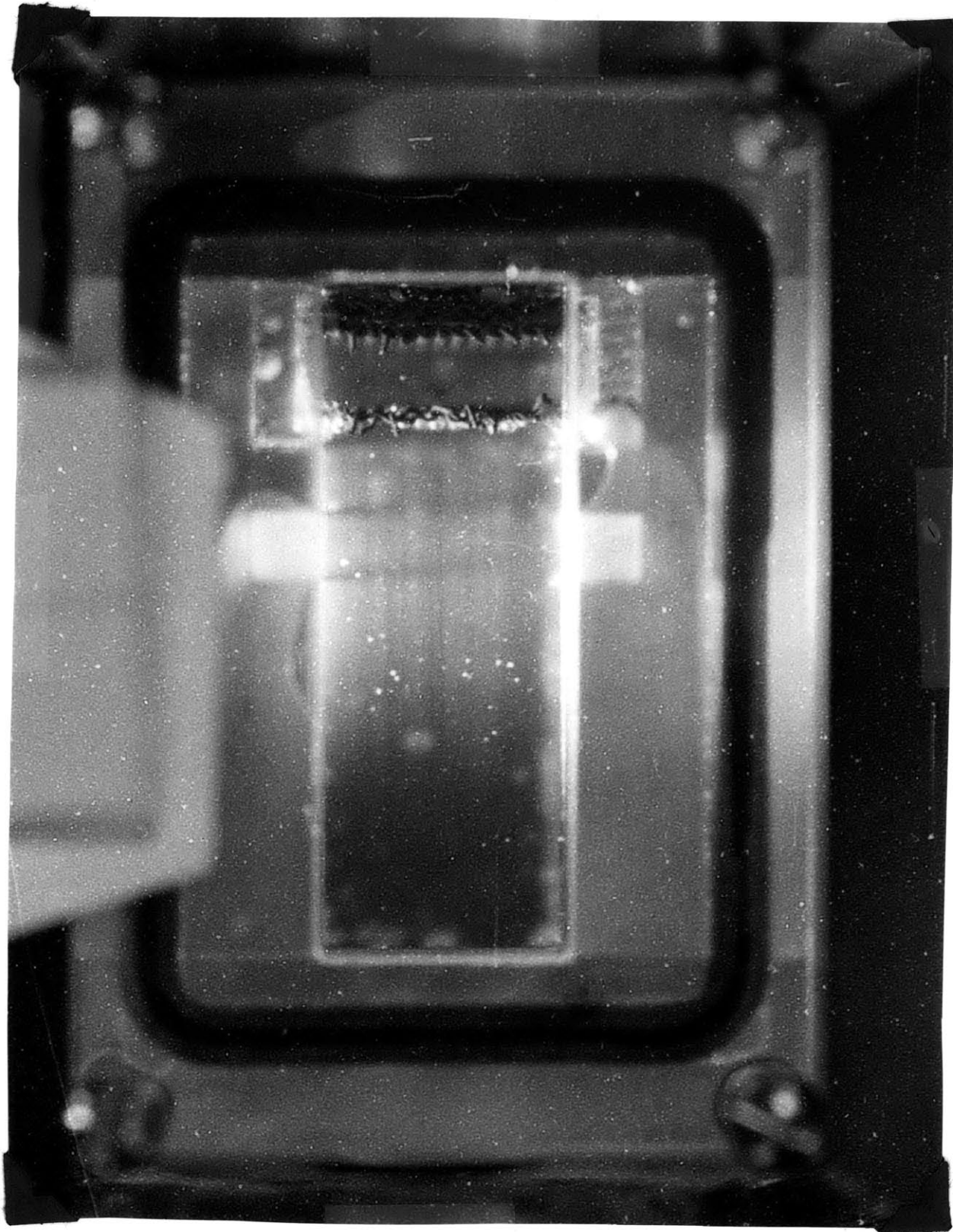
flow and photographing the layering that occured on the wire.
Pictures of this layering, for pulses large enough to allow an
equilibrium build up (no further net trapping), could be interpreted
with the aid of a projector as a thickness for a given length of
wire and considered a function of the variables of the system
similar to a capture length. However, capture length and layering
thickness are not equal. The former is based on a single particle,
the latter is based on a large number of particles and is a com-
posite result. Only if all particles in the flow system could be
described would they be equivalent.

The variables that could be altered experimentally were field
strength (current), fluid velocity, particle susceptibility, and
the geometry of the trapping object. Particle size was not
controlled. A slurry for injection was made by stirring an amount
of particles, then allowing the larger, heavier ones to settle,
leaving only those suspended which were almost neutrally bouyant.
Particle size was then mainly a function of particle density.
Particle sizes trapped could be measured from the photographs.
Generally, there was little variation in size for a given material;
most variation was due to agglomeration. Care was taken to develop
a pulse volume containing enough particles so that the layering
could fully develop, and no more particles would trap to form further
layers regardless of the number available. The time between the
pulse and the photograph was extensive enough to allow the entire
pulse to pass the trapping object. The experimental data is then
semi-quantitative since not all variables were controlled nor were
initial conditions for each particle equal.

3.3 Mathematical Models

3.3.1. Magnetic Field and Force Field about a Circular Cylinder Perpendicular to an Applied Field

Assuming an infinitely long cylinder of radius a placed perpendicular to an external field of intensity H has an induced field of intensity $B'=(\mu-1)H$ (the permeability μ may be a function of H) inside the cylinder, the vector of the external field, $\bar{B}'$, may be considered that due to a line of dipoles (see figure 8a). Letting $\bar{A}$ be the magnetic vector potential,

$$\bar{A} = \frac{\bar{m} \times \hat{r}}{r^2} \tag{19}$$

for a single magnetic dipole $\bar{m}$, where $\hat{r}$ is the unit radial vector from a point in space to the center of the dipole and r is the actual distance. An implicit assumption is that the distances r_1 and r_2 to the individual poles are approximately equal (see figure 8b). By convention, the sign of a magnetic field or dipole will be positive when from left to right (or negative to positive).

$$\bar{m} = (\mu - 1)\bar{H}\pi a^2 \tag{20}$$

(see appendix A). The contribution of a line of dipoles can be found by integration.

$$\bar{A} = \int_{r_1'}^{r_2'} \frac{\bar{m} \times \hat{r}}{(r')^2} dr' \tag{21}$$

As in figure 8c, let $r = r'\cos\phi$. Then changing the limits of integration

Figure 8   Diagrams for Magnetic Field Description

$(8a)$

$(8b)$

$r_1 \simeq r_2 \simeq r$

$(8c)$

(8d)

(8e)

(8f)
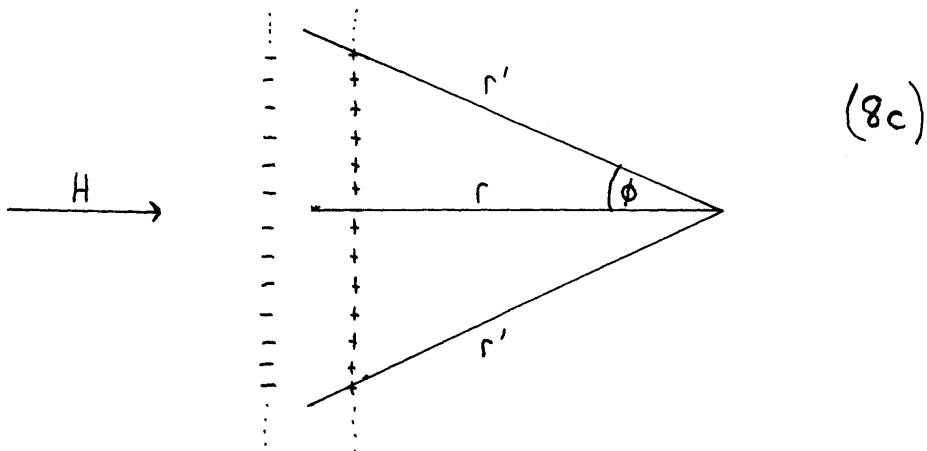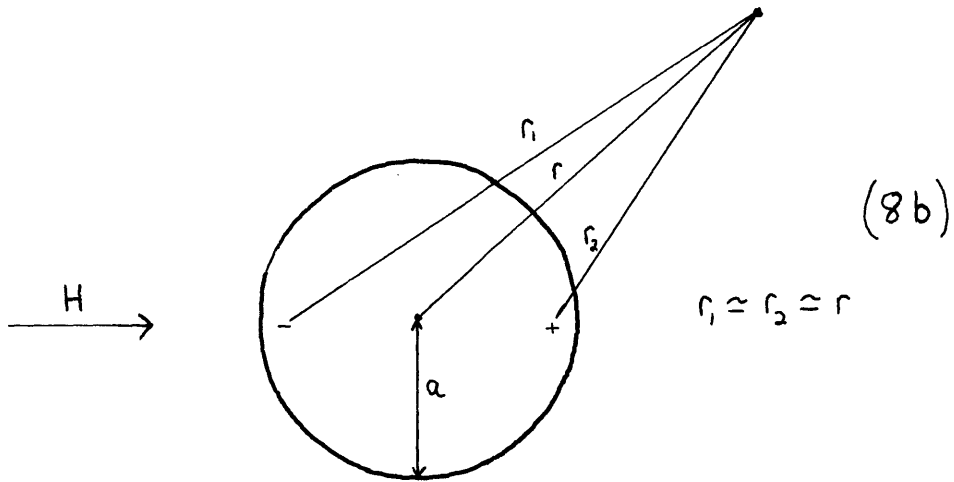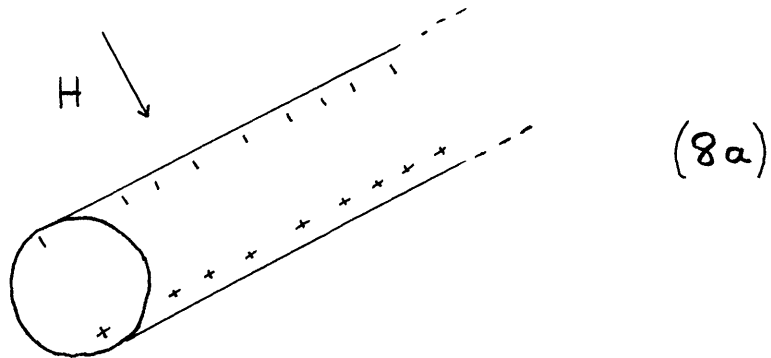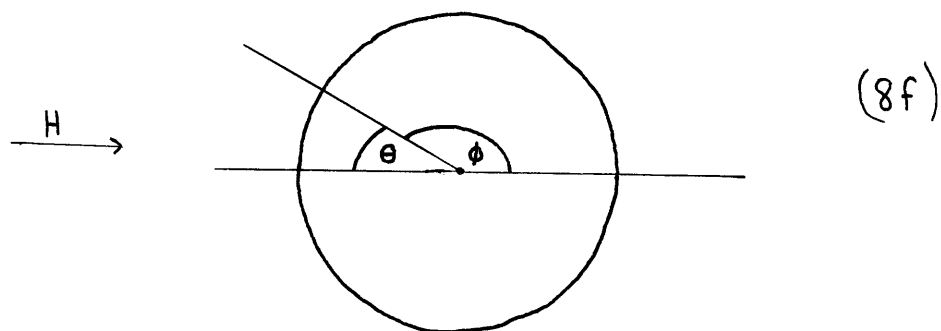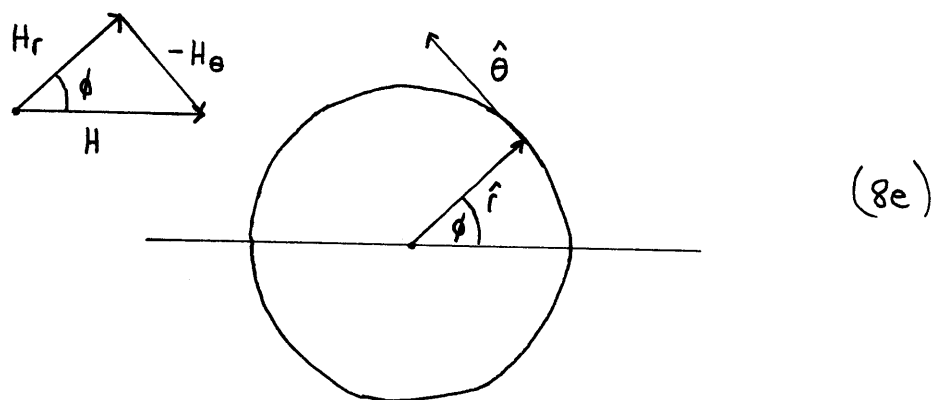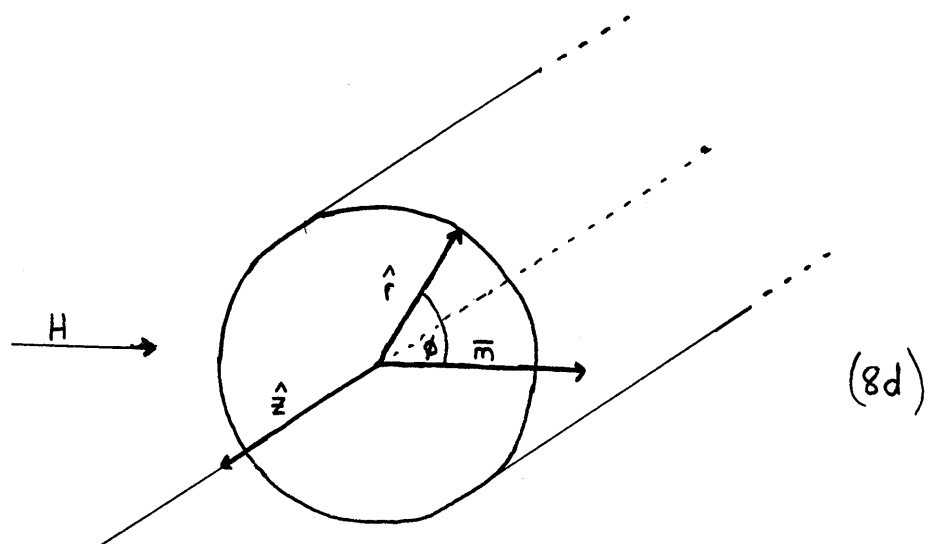
$$\bar{A} = \int_{-\pi/2}^{\pi/2} \frac{\bar{m} \times \hat{r}}{r^2} \ r \cos\phi d\phi \tag{22a}$$

$$\bar{A} = \frac{2\bar{m} \times \hat{r}}{r} \tag{22b}$$

Taking the cross product, following figure 8d.

$$\bar{A} = \frac{2|\bar{m}||\hat{r}|\sin\phi}{r} \ \hat{z} \tag{23a}$$

$$\bar{A} = \frac{2(\mu - 1)H\pi a^2 \sin\phi}{r} \ \hat{z} \tag{23b}$$

By definition $\bar{B}' = \nabla \times \bar{A}$. Then

$$\bar{B}' = \frac{2\pi a^2 (\mu - 1)H}{r^2} \left[\cos\phi \hat{r} + \sin\phi \hat{\theta}\right] \tag{24}$$

where $\hat{\theta}$ is the polar unit vector orthagonal to $\hat{r}$ and $\hat{z}$.

To the external field due solely to the magnetized object, the applied field must be superimposed. In polar coordinates, the applied field in figure 8e can be represented by

$$\bar{H} = H(\cos\phi \hat{r} - \sin\phi \hat{\theta}) \tag{25}$$

Adding equation (25) to (24), the total field is

$$\bar{B} = H\left(1 + \frac{2\pi(\mu-1)a^2}{r^2}\right) \cos\phi \hat{r} + H\left(-1 + \frac{2\pi(\mu-1)a^2}{r^2}\right) \sin\phi \hat{\theta} \tag{26}$$

For a paramagnetic material, the force per unit volume at a point due to the magnetic field is

$$\bar{F}_M = K'\bar{B} \cdot \nabla\bar{B} \tag{27}$$

where K' is the relative volume susceptibility between the

material and the media.

$$\overline{F}_M = \frac{-H^2 2\beta K'}{r^3} \left[\left(\frac{\beta}{r^2} + \cos2\phi \right) \hat{r} + \sin2\phi \hat{\theta} \right] \quad (28)$$

where $\beta = 2\pi(\mu - 1)a^2$. Transforming the angle measurement from the first quadrant to the second quadrant (figure 8f).

$$\cos\theta = -\cos(180° - \theta) = -\cos\phi \quad (29)$$

$$\overline{F}_M = \frac{-H^2 2\beta K'}{r^3} \left[\left(\frac{\beta}{r^2} + \cos2\theta \right) \hat{r} - \sin2\theta \hat{\phi} \right] \quad (30)$$

For clarity $\hat{\theta}$ has been replaced with $\hat{\phi}$. This tranformation is made to adhere to the convention of measuring fluid phenomena from the leading edge (with flow from left to right).

To get a better understanding of the magnetic force, it can be resolved into rectangular components

$$F_x = -F_r\cos\theta - F_\phi\sin\theta \quad (31a)$$

$$F_y = F_r\sin\theta - F_\phi\cos\theta \quad (31b)$$

Then

$$F_{Mx} = \frac{+H^2 2\beta K'}{r^3} \left[\left(\frac{\beta}{r^2} + \cos2\theta \right) \cos\theta - \sin2\theta\sin\theta \right] \quad (32a)$$

$$F_{My} = \frac{-H^2 2\beta K'}{r^3} \left[\left(\frac{\beta}{r^2} + \cos2\theta \right) \sin\theta + \sin2\theta\cos\theta \right] \quad (32b)$$

A typical resulting force is illustrated in figures 9, 10, and 11. One should keep in mind that the force at each point is based on a volume.

3.3.2. Flow Field and Drag Forces About a Cylinder

Before selecting a description of the velocity field around a circular cylinder perpendicular to the flow direction, one
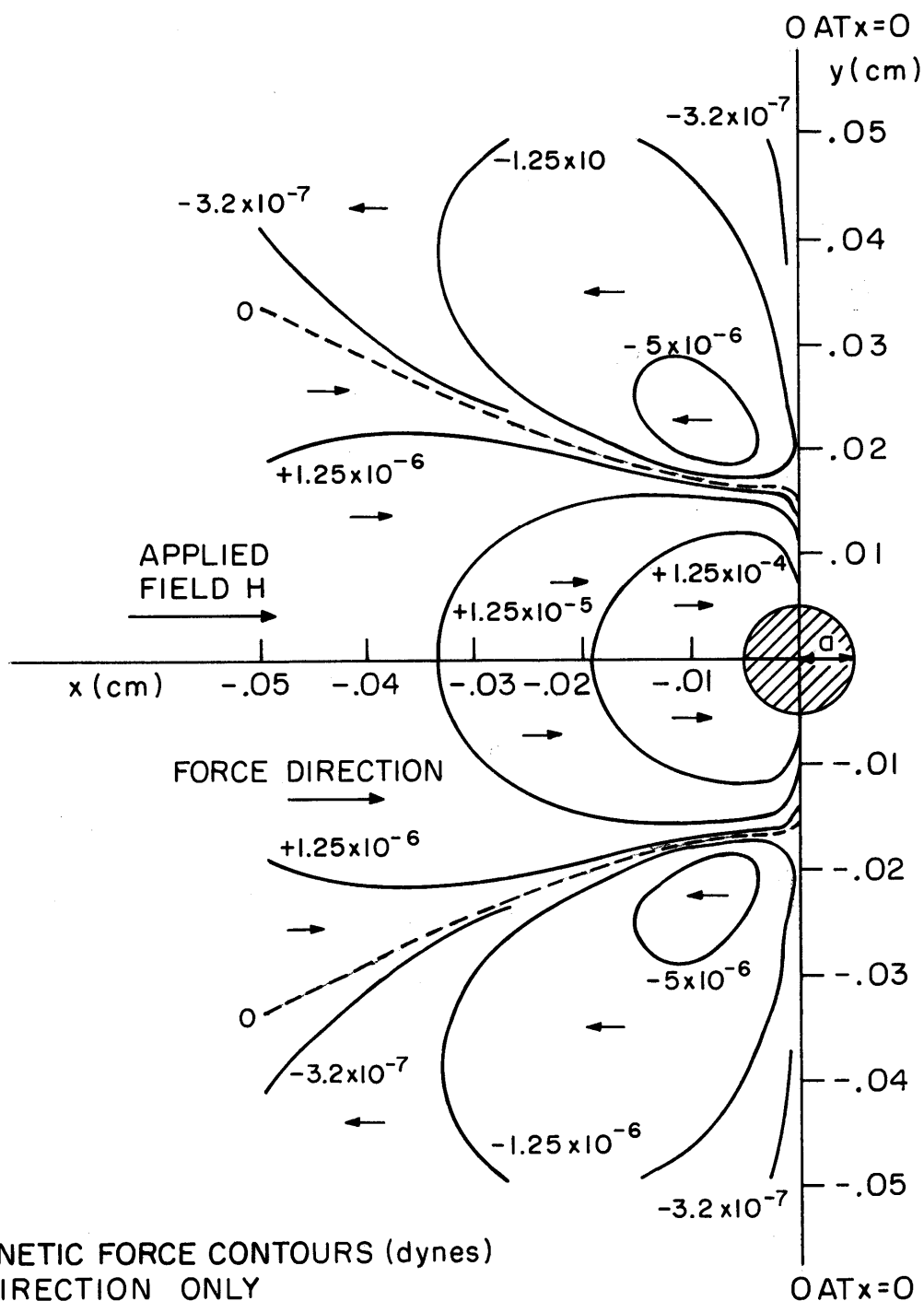
MAGNETIC FORCE CONTOURS (dynes)
x DIRECTION ONLY
BASED ON A SPHERICAL PARTICLE OF
RADIUS .0005 cm
H = 4000 GAUSS
a = .005 cm
μ = 6.4
K' = 19 x 10^{-6}
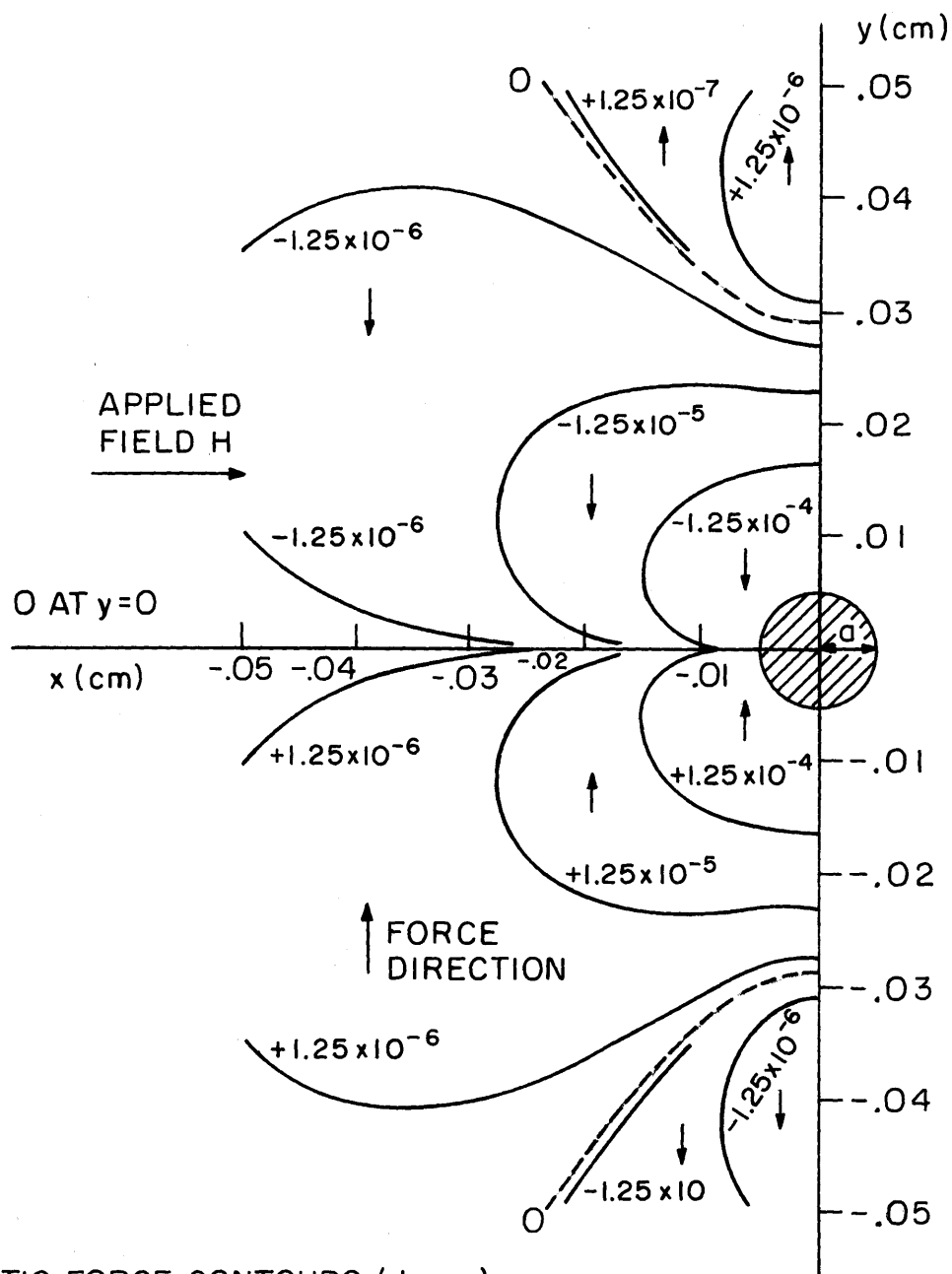
FIGURE 9

MAGNETIC FORCE CONTOURS (dynes)
y DIRECTION ONLY
BASED ON A SPHERICAL PARTICLE OF
RADIUS .0005 cm
H = 4000 GAUSS
a = .005 cm
μ = 6.4
K' = 19 x 10^{-6}

FIGURE 10

$|F_y/F_x|$ FOR MAGNETIC FORCES

H = 4000 GAUSS

a = 0.005 cm

μ = 6.4

$K' = 19 \times 10^{-6}$

BASED ON SPHERICAL PARTICLE OF

RADIUS = 0.0005 cm

>10 ON AXIS

y (cm)

$F_y = 0$

0.05

.5-1.0   1-5   >10

.1-.5   5-10

.1-.5   0.04

.5-1.0

$F_x = 0$

1-5   0.03

5-10

>10

.5-10   0.02

APPLIED
FIELD H

FORCE
DIRECTION   1-5

.5-1.0   0.01

.1-.5

O ON
AXIS

<.1   a

0.05   0.04   0.03   0.02   0.01

x (cm)
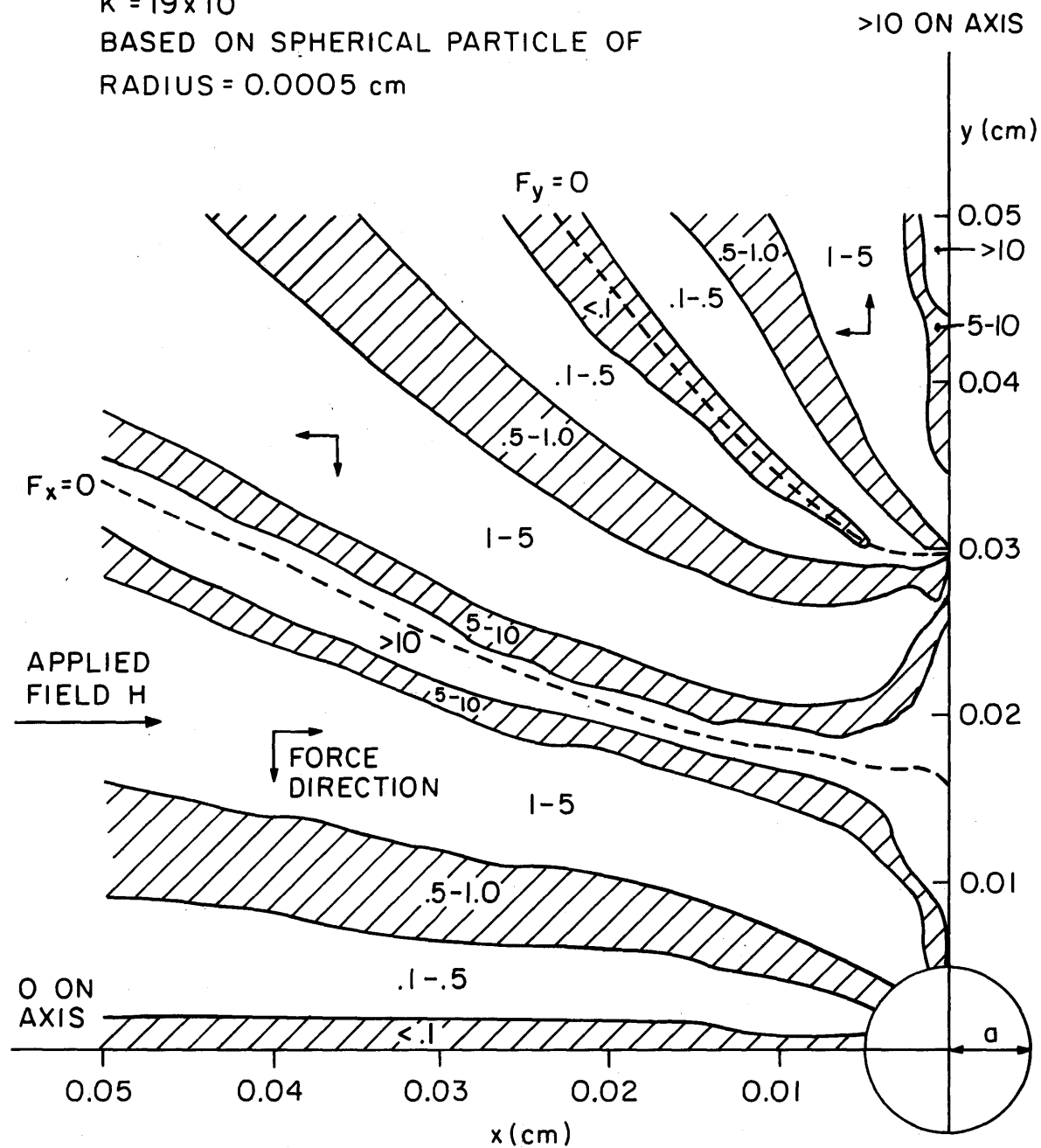
FIGURE 11

should first examine the alternatives to the complete Navier-Stokes equation for incompressible fluids of constant viscosity, η.

$$\rho \left(\frac{\partial \bar{V}}{\partial t} + \bar{V} \cdot \nabla \bar{V} \right) = -\nabla p + \eta \nabla^2 \bar{V} + \rho \bar{g} \qquad (33a)$$

where p is pressure, t is time, $\bar{g}$ is acceleration due to gravity, the only body force considered, ρ is density, and $\bar{V}$ is the velocity vector. For steady state

$$\rho \bar{V} \cdot \nabla \bar{V} = -\nabla p + \eta \nabla^2 \bar{V} + \rho \bar{g} \qquad (33b)$$

The $\rho \bar{g}$ term may be incorporated into the pressure gradient.

$$\rho \bar{V} \cdot \nabla \bar{V} = -\nabla p + \eta \nabla^2 \bar{V} \qquad (33c)$$

There are three standard simplifications, dropping of viscous terms $\eta \nabla^2 \bar{V}$, dropping of inertial terms $\rho \bar{V} \cdot \nabla \bar{V}$, and the boundary layer approximation.

The boundary layer approximation is an order of magnitude analysis in which a boundary layer thickness δ' is assumed to be much less than the characteristic linear dimension L of the submerged

$$\delta' << L \quad \text{or} \quad \delta = \delta'/L << 1 \qquad (34)$$

body (Schlichting, 1968). In length δ, the velocity parallel to the body goes from zero at the body to the free stream velocity. A direct assumption is that the Reynolds number, Re, is very large or

$$\frac{1}{Re} = 0[\delta^2] = \frac{\eta}{2\rho LV} \qquad (35)$$

For the physical phenomena to be described, a typical Reynolds number is 10 (V = 5 cm/sec, a = L = .005 cm, ρ = 1 gm/cm^3, and η = .01 gm/cm sec). Then

$$\frac{\delta'}{L} = \frac{\delta'}{a} \simeq .316 \tag{36}$$

and the original assumption made for δ, equation (34), is not particularly valid at such low Reynolds numbers. Therefore, the boundary layer approximation will not be used.

Dropping the inertial terms may be justified for Re<<1, resulting in the "creeping flow" equation.

$$\nabla p = \eta \nabla^2 \bar{V} \tag{37}$$

However, there is no analytic solution for the equation for flow past a circular cylinder because of boundary condition problems (Happel and Brenner, 1965). Partially taking into account the inertial terms by perturbation techniques (Van Dyke, 1964), several improvements have been made, notably the original by Oseen in 1910 and more recently by Proudman and Pearson (1957) that are valid for circular cylinders. However, the complexity of the analytic forms are an obstacle to economic numerical solutions of particle motion in the velocity field (see section 3.3.4).

Dropping the viscous terms or assuming irrotational flow results in potential or ideal flow, expressed below for two dimensions.

$$\frac{\partial V_x}{\partial y} - \frac{\partial V_y}{\partial x} = 0 \tag{38}$$

Defining a stream function, $\psi(x,y)$, where

$$V_x = \frac{-\partial \psi}{\partial y} \tag{39a}$$

$$V_y = \frac{\partial \psi}{\partial x} \tag{39b}$$

equation (38) becomes the Laplace equation.

$$\nabla^2 \psi = 0 \tag{40}$$

A solution then can be found in terms of a complex potential which satisfies the given geometry (Bird, Stewart, and Lightfoot, 1960). For constant upstream velocity perpendicular to the long axis of a circular cylinder of radius a (figure 12)

$$Vx = V_\infty \left(1 - \frac{a^2}{r^2} \cos 2\theta \right) \tag{41a}$$

$$Vy = V_\infty \frac{a^2}{r^2} \sin 2\theta \tag{41b}$$

where θ is measured from the second quadrant, r is radial distance from the center of the cylinder, and positive Vx is from left to right. One should observe that there is a stagnation point at $\theta = 0$, $r = a$.

This form will be used mainly because of its simplicity. However, it is an extremely valid description of the flow on the upstream side of the cylinder except near the vicinity of the surface where viscous terms become the same magnitude as inertial terms. Although the boundary layer approximation is not truely applicable, an estimate of this region (the boundary thickness) can be obtained from boundary layer theory (Kays, 1966).

$$\delta' = \frac{2/3 \ v^{.5}}{aU_\infty^3} \left[\int_0^x U_\infty^5 a^2 dx \right]^{.5} \tag{42}$$

where δ' is the boundary layer thickness over a body of revolution, v is the kinematic viscosity $= \eta/\rho$, and U_∞ is the

Figure 12   Potential Flow Past a Circular Cylinder

APPROACH
VELOCITY
V_∞

$\psi = 3/2$

θ

a

$\psi = 0$

STREAMLINES

U_∞

X

a

θ
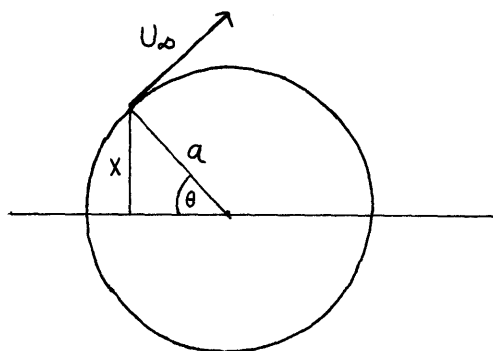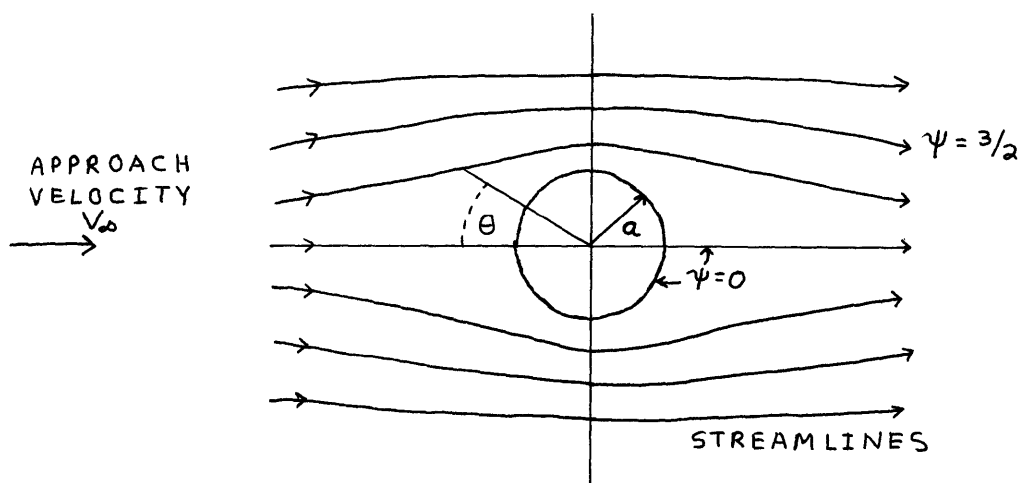
FIGURE 12a

velocity parallel to surface outside the boundary layer.
Referring to figure (12a).

$$U_\infty = 2V_\infty \sin\theta = 2V_\infty x/a \qquad (43)$$

Then for a typical situation (V_∞ = 5 cm/sec, v = .01 cm^2/sec,
a = .005 cm), δ' is about .001 cm or about 20% of the cylinder
radius.

On the downstream side of the cylinder, the streamlines,
in reality, are not symmetric with the upstream side. The phen-
omena of flow separation occurs, but the potential flow des-
cription is reasonably valid except at higher Reynolds num-
bers.

It should be mentioned that the full Navier-Stokes equa-
tions can be solved numerically, case by case, if not analy-
tically. This procedure is more exact when separation occurs.
A more detailed discussion of flow separation and numerical
solutions is given in appendix B.

Given the velocity field described by equations (41a)
and (41b), the fluid drag force acting on a spherical particle
in the stream may be given by (Perry, 1963)

$$\bar{F}_D = \frac{C\pi R^2 \rho \bar{V}_r \cdot \bar{V}_r}{2} \qquad (44)$$

where C is a dimensionless drag coefficient, ρ is the fluid
density, R is the particle radius, and $\bar{V}_r$ is the relative
fluid velocity.

$$\bar{V}_r = \bar{V}_{fluid} - \bar{V}_{particle} \qquad (45)$$

For low Reynolds numbers (Re < .3)

$$C = \frac{24}{Re} = \frac{12\eta}{RV_r\rho} \tag{46}$$

$$\bar{F}_D = 6\pi\eta R\bar{V}_r \tag{47}$$

Equation (47) is Stoke's Law. For $.3 < Re < 1000$

$$C = \frac{18.5}{Re^{.6}} \tag{48}$$

$$\bar{F}_D = \frac{9.25R^2 \bar{V}_r \cdot \bar{V}_r}{Re^{.6}} \tag{49}$$

There is an obvious discontinuity in $\bar{F}_D$ versus Re as constituted. Solving equations (46) and (48) simultaneously, a smooth transition between forms for C can be obtained at a Reynold's number of about 1.92. This value for Reynolds number will be used as the switching criterion.

3.3.3. Consideration of London and Gravitational Forces

Given the description of the magnetic force and fluid drag force, one can calculate the relative size of these forces and compare them with London and gravitational forces. London forces can be described by (Spielman, 1970):

$$F_L = \frac{-2/3 \ Q}{R} \left[\frac{1}{(r/R + 2)^2 (r/R)} \right] \tag{50}$$

where R is the particle radius, r the gap distance between the particle and the collector and Q is a constant equal to 10^{-12} ergs. Assuming the particle center is 3/2 R from the collector's surface, F_L is approximately -4.3×10^{-10} dynes for a particle of radius .0005 cm.

At the same distance and using a spherical particle of the same radius, equation (30) with $\theta = 0°, K=19 \times 10^{-6}$, $a = .005$ cm, $\mu = 6.4$ and $H = 5000$ gauss gives a magnetic force of about -0.09 dynes. The magnetic force, however, will decrease with distance (see figures 9 and 10). A typical fluid drag force, using equation (47) and assuming the same particle radius as before, $\eta = .01$ gm/cm sec, and V_r of 5 cm/sec, is about 4.7×10^{-4} dynes.

The net gravitational force on a spherical particle of the same size and a density of 6 gm/cm^3 is about 2.25×10^{-6} dynes when the particle is in water.

The inertial force on the same particle of density 6 gm/cm^3, assuming a velocity change of .1 cm/sec/10^{-5} sec, is about 3×10^{-5} dynes.

Thus, London forces and gravitational forces seem to be sufficiently smaller than the drag force or magnetic force in the region of interest and neglectable. The inertial force is also smaller than the magnetic force or drag force but larger than either gravitational or London forces. Since the inertial term describes position changes of the particle, it will be included in the model.

3.3.4. Dynamic Equations and Method of Solution

Given equations (32), (41), and (44) which express the magnetic and drag forces as a function of position (x and y) and system variables a, μ, H, K', and V_∞, a force balance around a particle may be written. A major assumption is that the particle is small enough to be considered a point in the

magnetic force field. No such assumption is necessary to describe the drag force, although the particle must be small enough not to disturb the flow around the cylinder. The point at which the magnetic force will be evaluated is at the center of the particle. Then

$$\frac{4}{3}\pi R^3 \overline{F}_M + \overline{F}_D = \frac{4}{3}\pi R^3 \rho * \frac{d\overline{V}}{dt} \qquad (51)$$

where $d\overline{V}/dt$ is the acceleration of the particle and $\rho *$ is the density of the particle.

Equation (51) is actually two simultaneous second order scalar differential equations, since

$$\overline{V} = \hat{x}\frac{dx}{dt} + \hat{y}\frac{dy}{dt} \qquad (52)$$

and θ in equations (32) and (41) is determined by arctan (y/x). Equation (51) may also be written as four first order differential equations via equation (52).

The set of equations (51) were solved simultaneously by the fourth order Runge-Kutta method of numerical integration to find a trapping length, y. A working description of the program will be given here; a more complete description may be found in F.B. Hildebrand, <u>Advanced Calculus for Applications</u> or Jenson and Jeffreys, <u>Mathematical Methods in Chemical Engineering</u>.

Given the differential equation

$$\frac{dy}{dx} = f(x,y) \qquad (53a)$$

$$\int dy = \int f(x,y) dx \tag{53b}$$

the integration over a given region or step, Δx, is approximated by

$$\Delta y = \frac{1}{6}[K_1 + 2K_2 + 2K_3 + K_4] \tag{54a}$$

where

$$K_1 = f(x_0, y_0) \Delta x \tag{54b}$$

$$K_2 = f(x_0 + \frac{\Delta x}{2}, y_0 + \frac{K_1}{2}) \Delta x \tag{54c}$$

$$K_3 = f(x_0 + \frac{\Delta x}{2}, y_0 + \frac{K_2}{2}) \Delta x \tag{54d}$$

$$K_4 = f(x_0 + \Delta x, y_0 + K_3) \Delta x \tag{54e}$$

and x_0 and y_0 are initial values. Then the values of x and y at at the end of step integration are

$$x_1 = x_0 + \Delta x \tag{55a}$$

$$y_1 = y_0 + \Delta y \tag{55b}$$

For a new step x_1 and y_1 become initial values and the process is repeated.

Using the above procedure, equation set (51) with set values for H, V_∞, K' (including ρ^*), a, and R becomes

$$\frac{dV_x}{dt} = \frac{F_{Mx}(x,y)}{\rho^*} + \frac{F_{Dx}(x,y,V_x)}{4/3\pi R^3 \rho^*} = \frac{d^2x}{dt^2} \tag{56a}$$

$$\frac{dx}{dt} = V_x(x,y,t) \tag{56b}$$

$$\frac{dV_y}{dt} = \frac{F_{My}(x,y)}{\rho^*} + \frac{F_{Dy}(x,y,V_y)}{4/3\pi R^3 \rho^*} = \frac{d^2y}{dt^2} \tag{56c}$$

$$\frac{dy}{dt} = V_y(x,y,t) \tag{56d}$$

Then for time step Δt and an initial position and velocity, following the algorithm in figure 13a, one can calculate intermediate velocities (V_x and V_y) which in turn give a new intermediate position for each step of the Runge-Kutta method.

To terminate the integration, an algorithm is needed. Since the problem is symmetric about $y = 0$ (figure 13b), only the first and second quadrants need be considered. Downstream of the cylinder, a value of x such that there is no net force towards the cylinder should be a stopping criteria. A maximum time limit should also be considered as well as limits on y in case the integration "blows up." Finally, a definition of entrapment is needed.

In the actual program, an extremely small step size was necessary to prevent the integration from "blowing up" due to a large derivative value. This step size ($\leq 10^{-5}$ seconds depending on particle size) corresponded to a position change per step of about one tenth of a typical particle radius (.0005 cm), assuming a velocity of 5 cm/sec. No noticeable improvement in accuracy occurred with smaller step sizes. All integrations were started at x = -0.05 and a value of y , the trapping length,to find the maximum initial y at which trapping

Figure 13a   Algorithm for Runge-Kutta Method
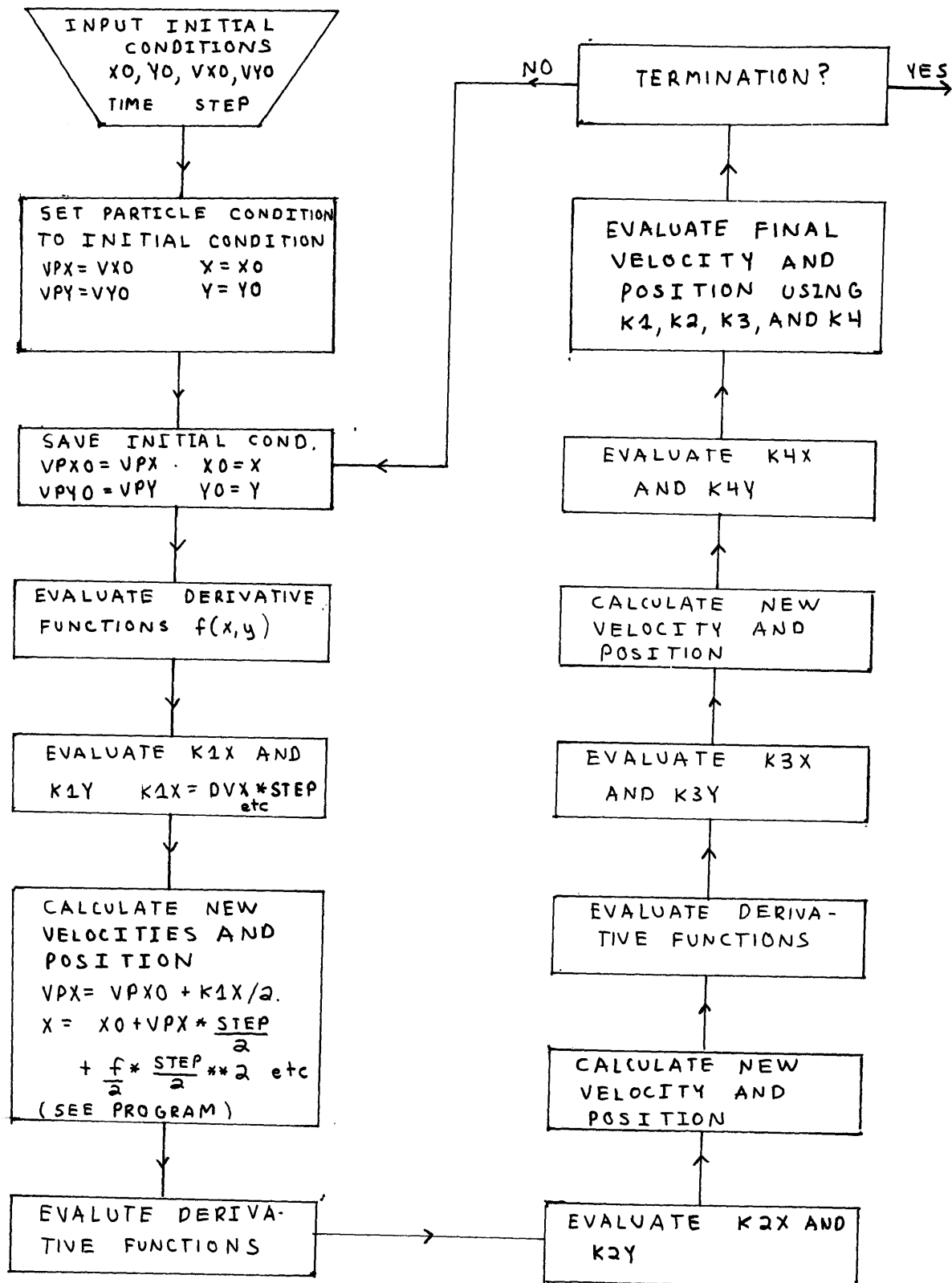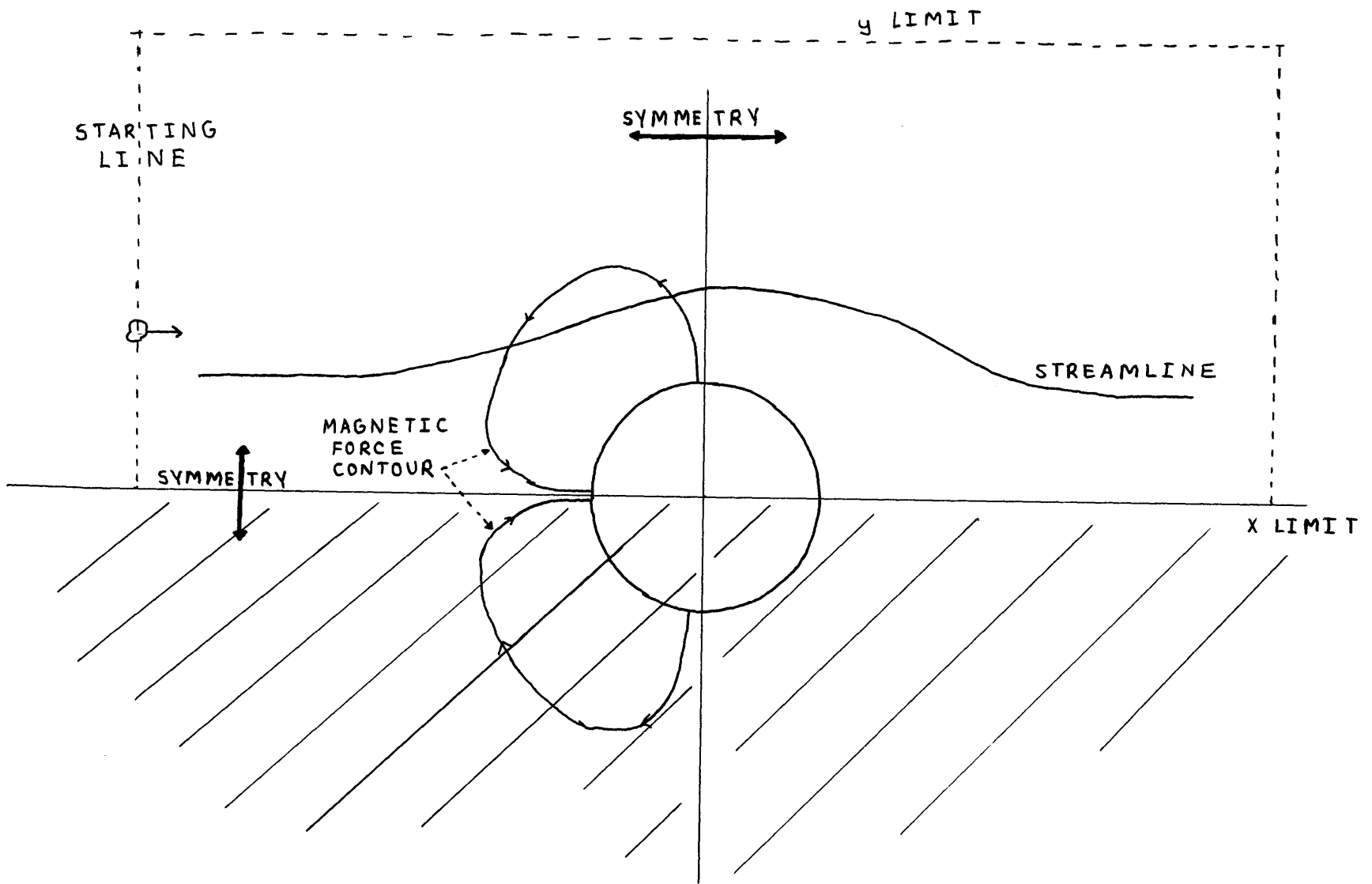
Figure 13b   Region of Interest for Numerical Integration

occurred for given values of H, V_∞, K', a, and R. All trajectories were terminated when x $\geq$ .05 at which point the net force in the x direction was positive. The limit on y was not critical, and y > |.05| was used to terminate the integration. The maximum time limit was .1/V_∞. A collision occurred when

$$r = \sqrt{x^2 + y^2} \leq R + a \qquad (57)$$

All collisions were considered inelastic (no bounce), but terminal only if V_y at collision was negative for θ < 90° or V_x was negative for 90° $\leq$ θ $\leq$ 180°. If neither condition was met, the particle was placed at the surface (r = R+a) and a new step was taken. A summary of terminating conditions is presented in figure 13c. A listing of the final program may be found in Appendix C.

Three final assumptions were made for the calculations. Any effects due to the susceptibility of the media (water) were neglected or considered incorporated in the inherent susceptibility of the test particle. The density and viscosity of water were taken as 1 gm/cm^3 and .01 gm/cm sec, respectively, and assumed constant.

3.3.5. The Two Cylinder Model

In an applied field, ignoring any interactions between the cylinders, two cylinders are identical magnetically except that they occupy different positions. The net magnetic force is simply the superpositioning of the individual forces, taking into account the different radial distances and angles involved (figure 13d).

Figure 13c   Terminating Algorithm for Numerical Integration
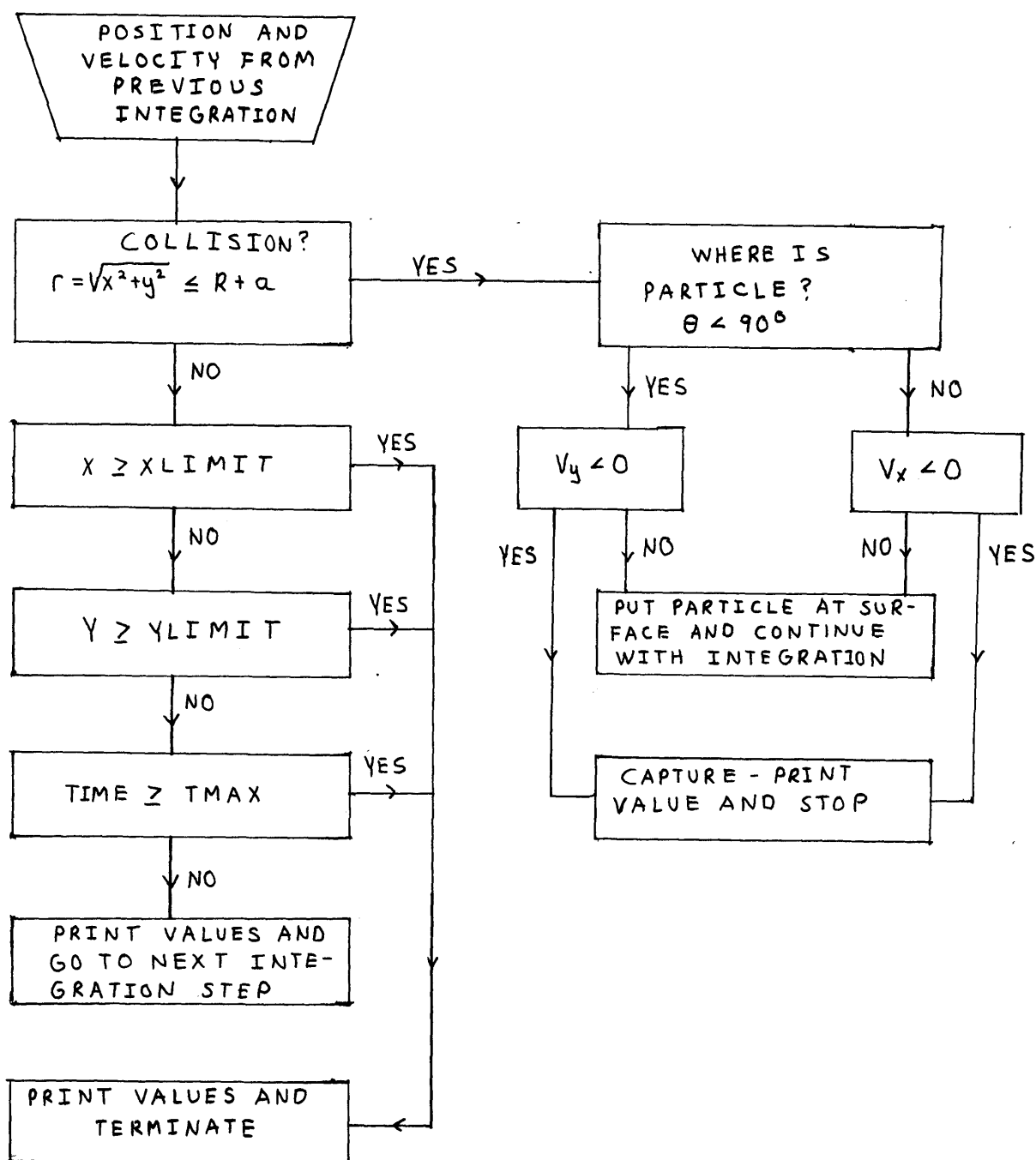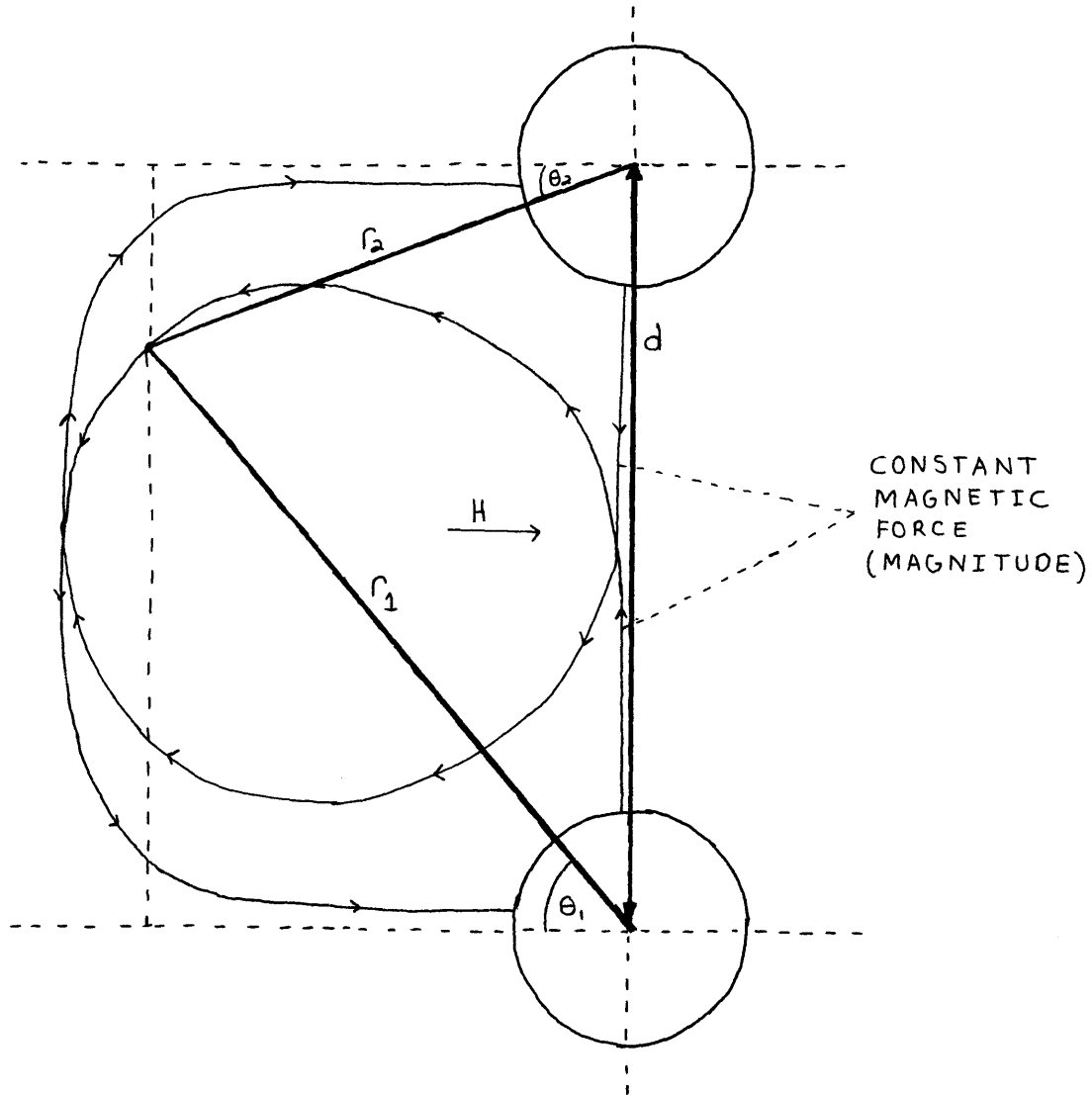
Figure 13d Two Cylinder Magnetic Description

However, the potentials for flow past two cylinders cannot be superimposed to get a proper result. If, for a single cylinder the flow potential is (Robertson, 1965)

$$\phi = V_\infty x + V_\infty \frac{a^2 x}{x^2 + y^2} \tag{58}$$

where a is the cylinder radius and V_∞ is the free stream velocity, two cylinders may be represented by

$$\phi_{1+2} = \phi_1 + \phi_2 \tag{59}$$

Then

$$\phi_{1+2} = V_\infty x + V_\infty \frac{a^2 x}{x^2 + y_1^2} + V_\infty \frac{a^2 x}{x^2 + y_2^2} \tag{60a}$$

$$\phi_{1+2} = V_\infty x + V_\infty a^2 \left[\frac{x}{x^2 + (y - \frac{d}{2})^2} + \frac{x}{x^2 + (y + \frac{d}{2})^2} \right] \tag{60b}$$

using the coordinate system in figure 13e with the cylinders equidistant from the origin. Note that d = f(y). By the definition of potential

$$V_x = \frac{\partial \phi}{\partial x} = \frac{\partial \psi}{\partial y} \tag{61a}$$

$$V_y = \frac{\partial \phi}{\partial y} = \frac{-\partial \psi}{\partial x} \tag{61b}$$

where ψ is the streamline function. Then

$$\psi = V_\infty y \left[1 - \frac{a^2}{x^2 + (y - \frac{d}{2})^2} - \frac{a^2}{x^2 + (y + \frac{d}{2})^2} \right] \tag{62a}$$

x=0
y=d/2

STREAMLINE

d

$V_\infty \rightarrow$

x=0
$\psi = 0$

(0,0)

x=0
$\psi = 0$

$V_\infty \rightarrow$

STREAMLINE

x=0
y=-d/2
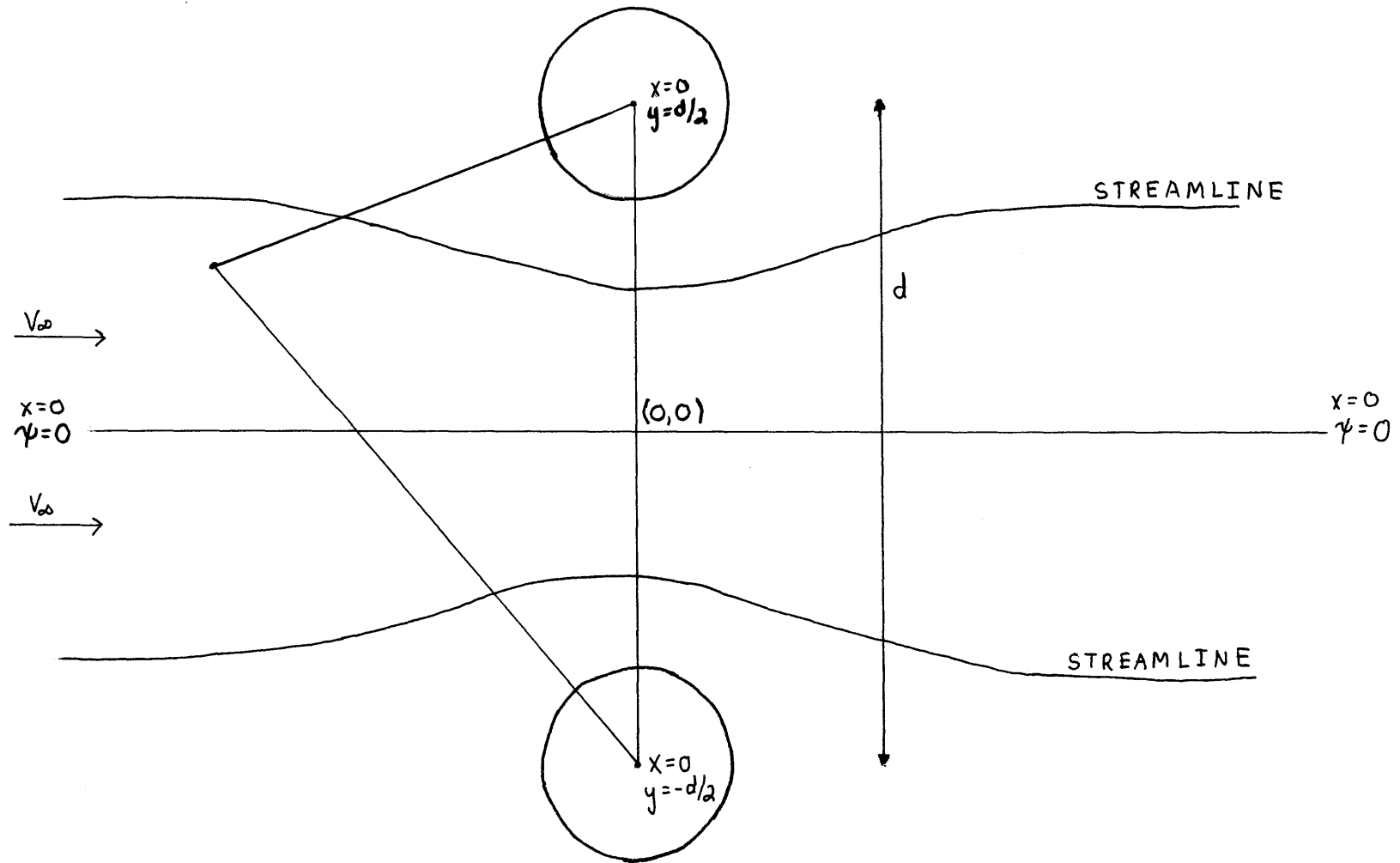
Figure 13e   Potential Flow Between Two Cylinders

$$V_x = V_\infty + V_\infty \, a^2 \left[\frac{1}{x^2 + (y - \frac{d}{2})^2} - \frac{2x^2}{[x^2 + (y - \frac{d}{2})^2]^2} \right]$$

$$+ V_\infty a^2 \left[\frac{1}{x^2 + (y + \frac{d}{2})^2} - \frac{2x^2}{[x^2 + (y + \frac{d}{2})^2]^2} \right] \qquad (62b)$$

$$V_y (y>0) = -2V_\infty a^2 xy \, \frac{1}{[x^2 + (y - \frac{d}{2})^2]^2} + \frac{1}{[x^2 + (y + \frac{d}{2})^2]^2} \qquad (62c)$$

However, the surface of a cylinder is no longer defined by $\psi = 0$. $\psi = 0$ is now the x axis. Going further, let $y = d/2$. Then

$$V_x = V_\infty - V_\infty a^2 \left[\frac{1}{x^2} + \frac{2x^2}{(x^2 + d^2)^2} - \frac{1}{x^2 + d^2} \right] \qquad (63a)$$

$$V_y (y>0) = -dV_\infty a^2 \left[\frac{1}{x^4} + \frac{1}{(x^2 + d^2)^2} \right] \qquad (63b)$$

As separation distance d approaches infinity

$$V_x = V_\infty - V_\infty \, a^2/x^2 \qquad (64a)$$

$$V_y = -dV_\infty \, a^2/x^4 \qquad (64b)$$

The expression for V_x is correct. However, V_y approaches infinity with infinite separation along what corresponds to the streamline $\psi = 0$ for a single cylinder. The proper result at large values of d should be $V_y = 0$ at $y = d/2$. Thus superpositioning of fluid potential is not valid.

The fluid flow past the cylinder will be represented by the potential flow past a single cylinder, although this

approximation is not valid at small separation distances.
Then for a given separation distance, d, the model will be
solved using the fourth order Runge-Kutta method. The problem
is exactly as the single cylinder model except for an additional
magnetic force term. A listing of the computer program may be
found in Appendix C.

CHAPTER 4

RESULTS AND DISCUSSION

4.1. Predictions of Mathematical Models

   4.1.1. Changes Required in Magnetic Description

   The first result is a change in the description of the
magnetic field about the cylinder. With the magnetic field
description of section 3.3.1, the trajectories produced by the
computer program predicted entrapment near the top of the
cylinder (θ = 90°) in most cases (figure 14a). Experimental
observations (see section 4.2) detected almost no trapping in
this region; trapping occurs mainly on the upstream side of
the cylinder near θ = 0° with a small amount of trapping
occuring on the downstream or backside. Even with a flow
rate of zero, trapping, although enhanced, does not occur near
the top (figure 14b). The trajectories predicted by the model
are explainable, since there is an attractive region near the
vicinity of the top of the cylinder of greater magnitude than
any drag force, depending on position and the variables of the
system. The repulsive region appears only at a large distance
from the cylinder.

   The size of the magnetic force and the zones of attraction
and repulsion are directly related to the basic assumptions for
the model, that the cylinder can be treated as a line of point
dipoles. A result is the term $\beta = 2\Pi a^2 (\mu-1)$ in two key places
in equation (28). Since the magnetic force will go to zero or
be repulsive at θ = 90° only when:

$$\frac{\beta}{r^2} \ = \ \frac{2\pi a^2 (\mu - 1)}{r^2} \ \leq \ 1 \tag{65}$$

the change in the direction of the force occurs only when r, the radial distance, is very large when expressed in terms of a, since $\mu > 1$. The other effect is on the magnitude of the magnetic force, since β also appears as a multiplier. Since $\beta \gg 1$, the magnetic force is correspondingly amplified.

Since visual observations do not support the model, the irregularities in the model need to be identified. The basic fault is that no provision was made for what is known as self-demagnetization. This can be determined somewhat empirically by the use of magnetic lines of flux and flux loss (General Electric,1963) or more properly by suitable boundary conditions on the magnetic potential (Stratton, 1941). Intuitively, one can imagine the field lines due only to a ferromagnetic cylinder (Figure 15a) which travel opposite to the applied field at the "top" and "bottom" of the cylinder cross section, cancelling the applied field lines which cause the magnetization and thus "demagnetizing" the cylinder. The final result, regardless of the purity of the approach, is that an infinitely long ferromagnetic cylinder whose long axis is perpendicular to the applied field has a total external field at the surface of only twice the applied field at any field strength below saturation.

$$B \ = \ 2H \ = \ M + H \tag{66a}$$

$$B' \ = \ M \ = \ H \tag{66b}$$

where M is the magnetization of the cylinder.
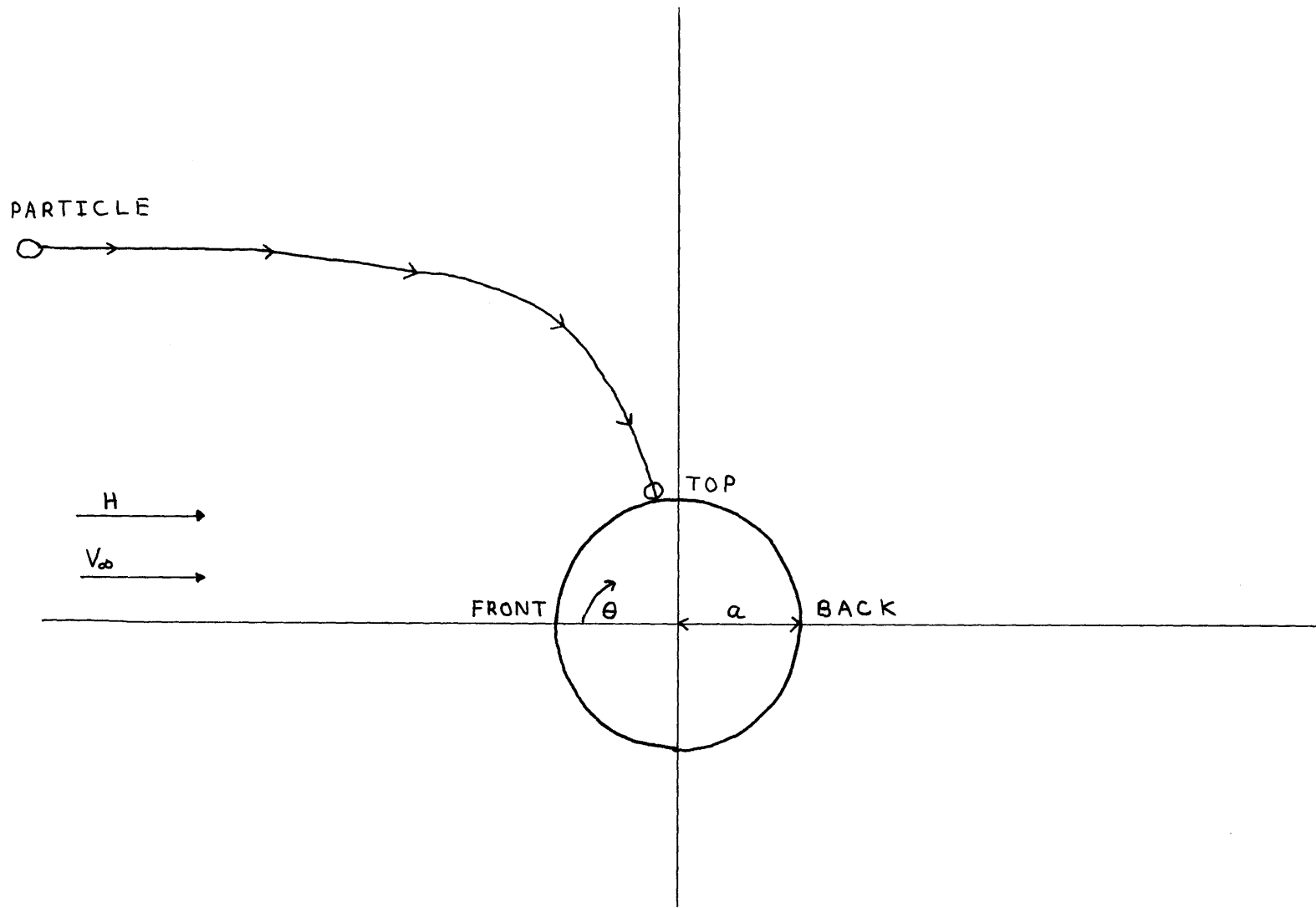
Figure 14a   Trajectory Produced By Original Model

Figure 14b   Actual Trapping on Cylinder at Zero Flow Rate
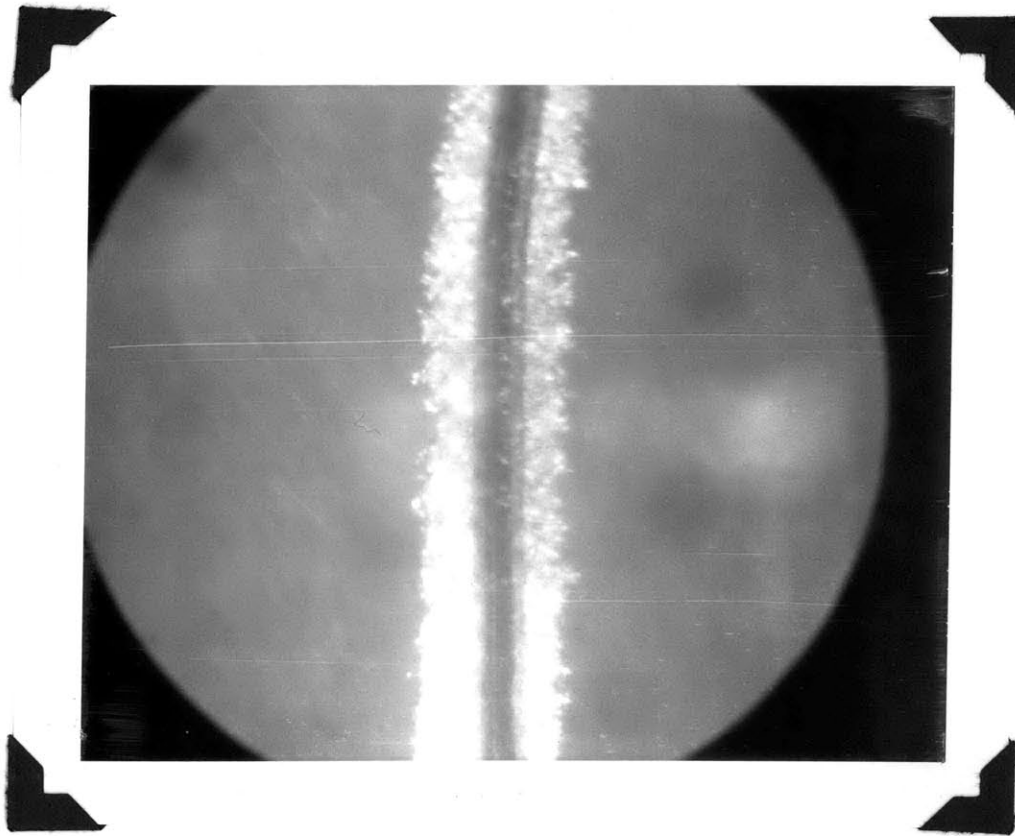
Figure 15a Concept of Demagnetizing Field Lines
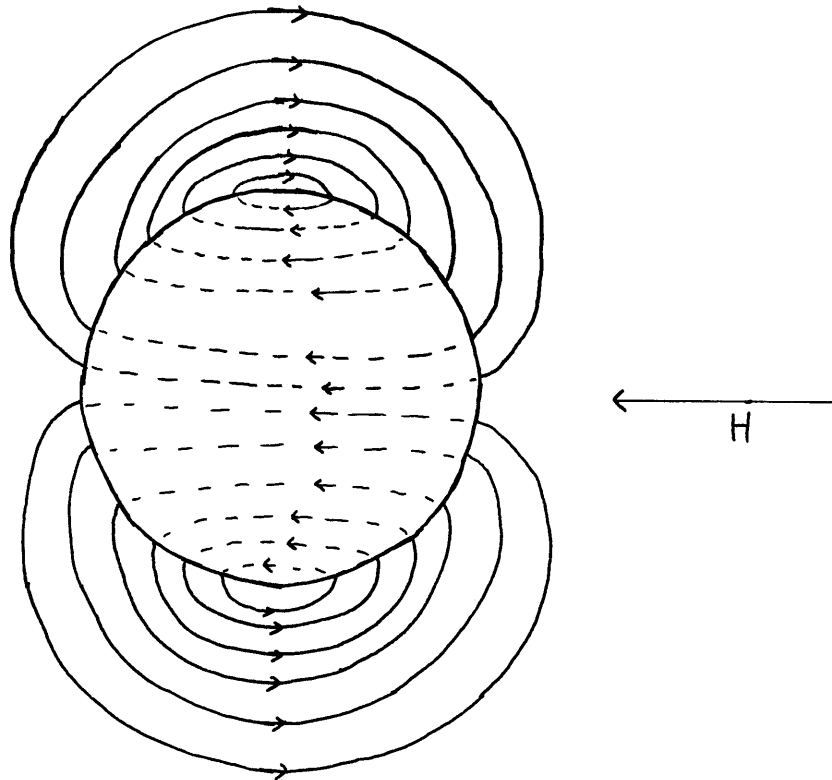
This is also the result of the Stratton solution, equation (8) for a large permeability. However, the permeability (difference between the cylinder and the media) used in the Stratton solution is the inherent permeability. For a ferromagnetic material, the permeability is not constant, although the apparent permeability may be constant. In the Stratton solution, constant permeability was assumed to simplify and linearize the problem. The proper differential equations and boundary conditions should be solvable for a permeability that is a function of applied field. However, the procedure, if not the results would be more complicated.

One can properly use the Stratton solution only if one assumes a constant inherent permeability. This will be done by the following expansion. Let

$$\bar{B} = \int_0^H \frac{dB}{d\bar{H}} \, d\bar{H} \tag{67a}$$

$$\bar{B} = \bar{B}_1 + \bar{B}_2 = \int_0^{H_s} \frac{dB}{d\bar{H}} \, d\bar{H} + \int_{H_s}^H \frac{dB}{d\bar{H}} \, d\bar{H} \tag{67b}$$

where H_s is the apparent applied field necessary to saturate the material. Then the total field may split into two components. For $H \leq H_s$ a constant permeability μ_s equal to the inherent value of permeability at saturation will be used (figure 15b). For $H \leq H_s$, then, one can utilize the Stratton solution directly. For $\mu_2 = 1$, and measuring ϕ from the first quadrant

Figure 15b   Approximation of Constant Permeability
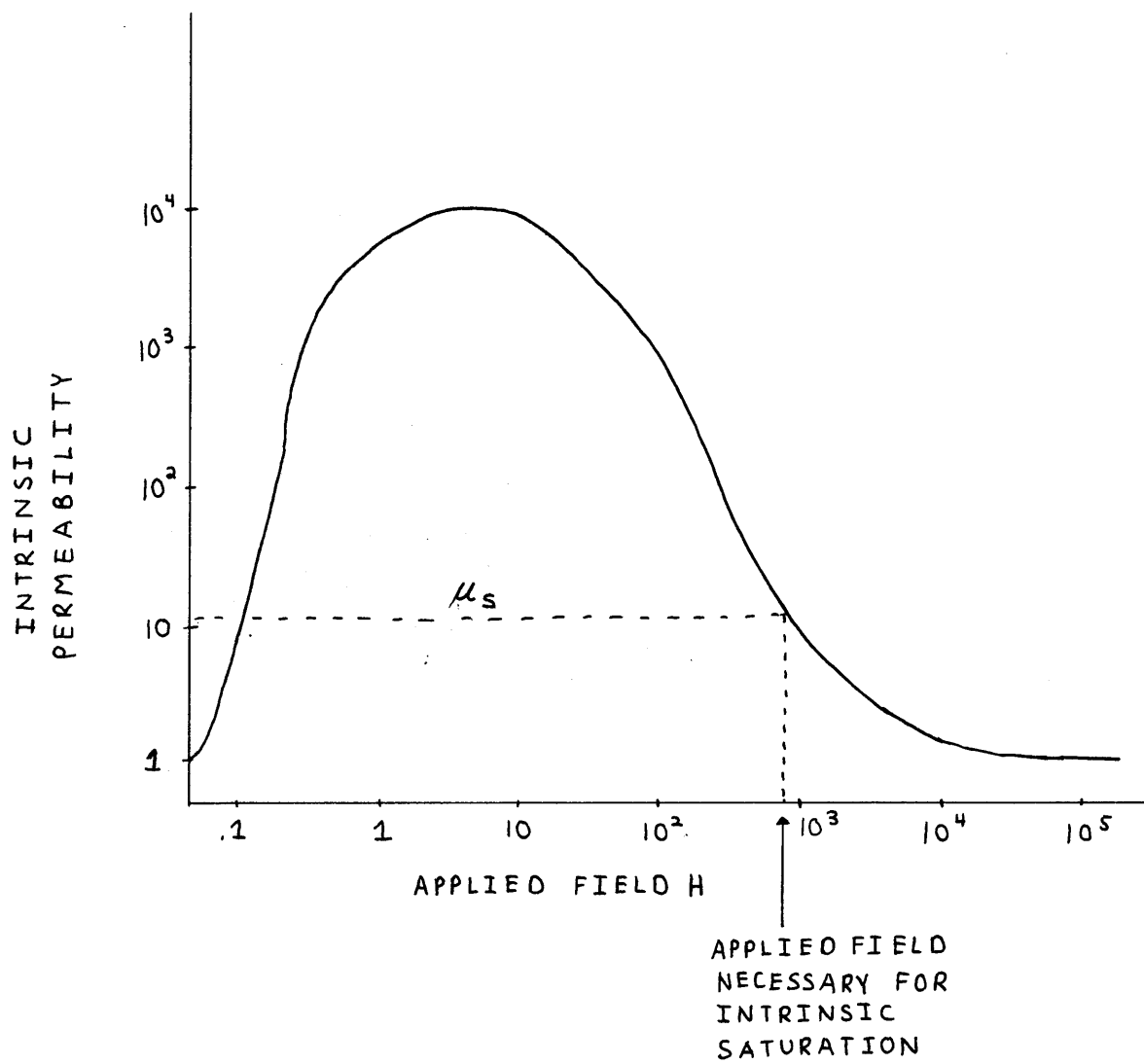
$$\bar{B}_1 = \int_0^{H' \leq H_s} \frac{dB}{dH} d\bar{H} = H'\cos\phi \left[1 + \left(\frac{\mu_s - 1}{\mu_s + 1}\right)\frac{a^2}{r^2}\right]\hat{r}$$

$$+ H'\sin\phi\left[-1 + \left(\frac{\mu_s - 1}{\mu_s + 1}\right)\frac{a^2}{r^2}\right]\hat{\theta} \quad (68)$$

For $H > H_s$, the inherent permeability is one and $\frac{dB}{dH} = 1$. Then

$$\bar{B}_2 = \int_{H_s}^{H} d\bar{H} = (H - H_s)\cos\phi \, \hat{r} - (H - H_s)\sin\phi \, \hat{\theta} \quad (69)$$

again employing the Stratton solution. For $H \leq H_s$, there is no second term in the expansion. Since both terms are linear, they may be superimposed.

$$\bar{B} = \left[\frac{\beta H_s}{r^2} + H\right]\cos\phi \, \hat{r} + \left[\frac{\beta H_s}{r^2} - H\right]\sin\phi \, \hat{\theta} \quad (70)$$

where $\beta = \left(\frac{\mu_s - 1}{\mu_s + 1}\right)a^2$.

Following equations (27) and (29) in section 3.3.1, the magnetic force becomes

$$\bar{F}_M = \frac{-2\beta H_s K'}{r^3}\left[\left[\frac{H_s \beta}{r^2} + \cos2\phi H\right]\hat{r} - H\sin2\phi\hat{\theta}\right] \quad (71a)$$

rearranging, letting $\beta' = \beta H_s/H$

$$\bar{F}_M = \frac{-2\beta HH_s K'}{r^3}\left[\left[\frac{\beta'}{r^2} + \cos2\theta\right]\hat{r} - \sin2\phi\hat{\theta}\right] \quad (71b)$$

$$F_{mx} = \frac{2\beta HH_s K'}{r^3}\left[\left[\frac{\beta'}{r^2} + \cos2\theta\right]\cos\theta - \sin2\theta\sin\theta\right] \quad (71c)$$

$$F_{My} = \frac{-2\beta HH_s K'}{r^3} \left[\left[\frac{\beta'}{r^2} + \cos2\theta \right] \sin\theta + \sin2\theta\cos\theta \right] \quad (71d)$$

This formulation for magnetic force will be used henceforth. For $\mu_s = 10$, the resulting force contours are illustrated in Figures 16 and 17. Again the fields are symmetric. Note that a repelling region does occur at the top ($\theta = 90°$). Also, the magnitude of the magnetic force is much smaller than with the dipole model. The repelling regions for F_{Mx} construct a funneling mechanism which aids in directing particles towards the cylinder.

4.1.2. Implications of the Required Change

The major implication of the new model is that the effective available trapping area per cylinder decreases above the saturation magnetization. The force per unit volume increases, however, the regions of attractive magnetic force decrease in size. The "lines of force" may be represented by

$$\frac{F_r}{dr} = \frac{1}{r} \frac{F_\theta}{d\theta} \quad (72a)$$

$$-\frac{1}{r} \frac{dr}{d\theta} = \frac{\frac{\beta}{r^2} + \cos2\theta}{\sin2\theta} \quad H \leq H_s \quad (72b)$$

$$-\frac{1}{r} \frac{dr}{d\theta} = \frac{\frac{\beta'}{r^2} + \cos2\theta}{\sin2\theta} \quad H > H_s \quad (72c)$$

When the magnetic force is zero, $dr/d\theta = 0$, and

$$\frac{\beta}{r^2} + \cos2\theta = 0 \quad H \leq H_s \quad (73a)$$
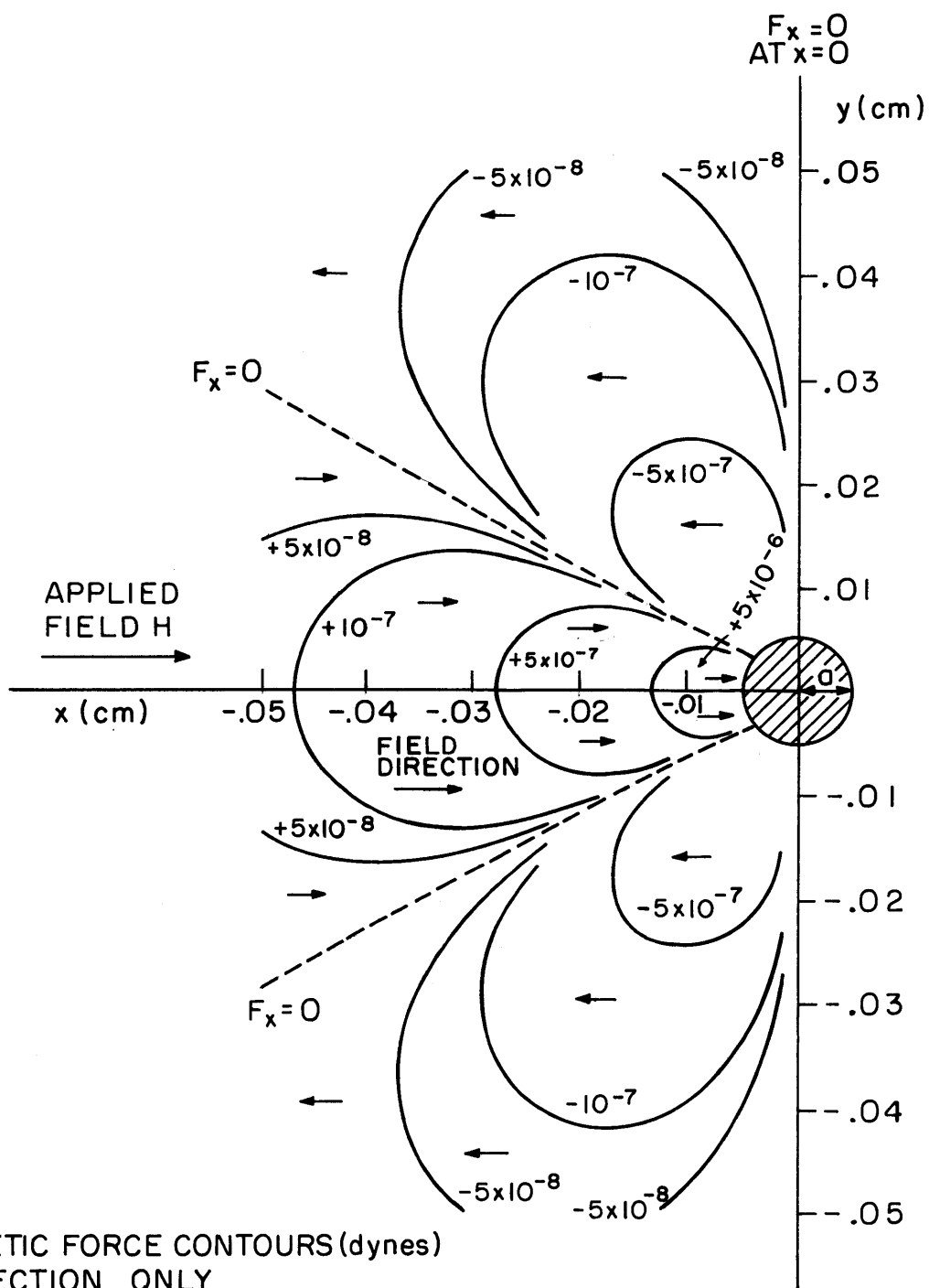
MAGNETIC FORCE CONTOURS (dynes)
x DIRECTION ONLY
BASED ON A SPHERICAL PARTICLE OF
RADIUS .0005 cm
H = 5000 GAUSS
a = .005 cm
μ = 10
K' = 19×10^{-6}

FIGURE 16

MAGNETIC FORCE CONTOURS (dynes)
y DIRECTION ONLY
BASED ON A SPHERICAL PARTICLE OF
RADIUS .0005 cm
H = 5000 GAUSS
a = .005 cm
μ = 10
$K' = 19 \times 10^{-6}$

$F_y = 0$

-5×10^{-8}

$+10^{-7}$

APPLIED
FIELD H

-5×10^{-8}

$+5 \times 10^{-7}$

$+5 \times 10^{-6}$

-5×10^{-7}

-5×10^{-6}

x (cm)

$F_y = 0$ AT y = 0

-.05 -.04

-.03

-.02 -.01

$+5 \times 10^{-8}$

$+5 \times 10^{-6}$

-5×10^{-6}

FORCE
DIRECTION

$+5 \times 10^{-7}$

$+5 \times 10^{-8}$

-5×10^{-7}

-10^{-7}

$F_y = 0$

y (cm)

.05
.04
.03
.02
.01
-.01
-.02
-.03
-.04
-.05

a
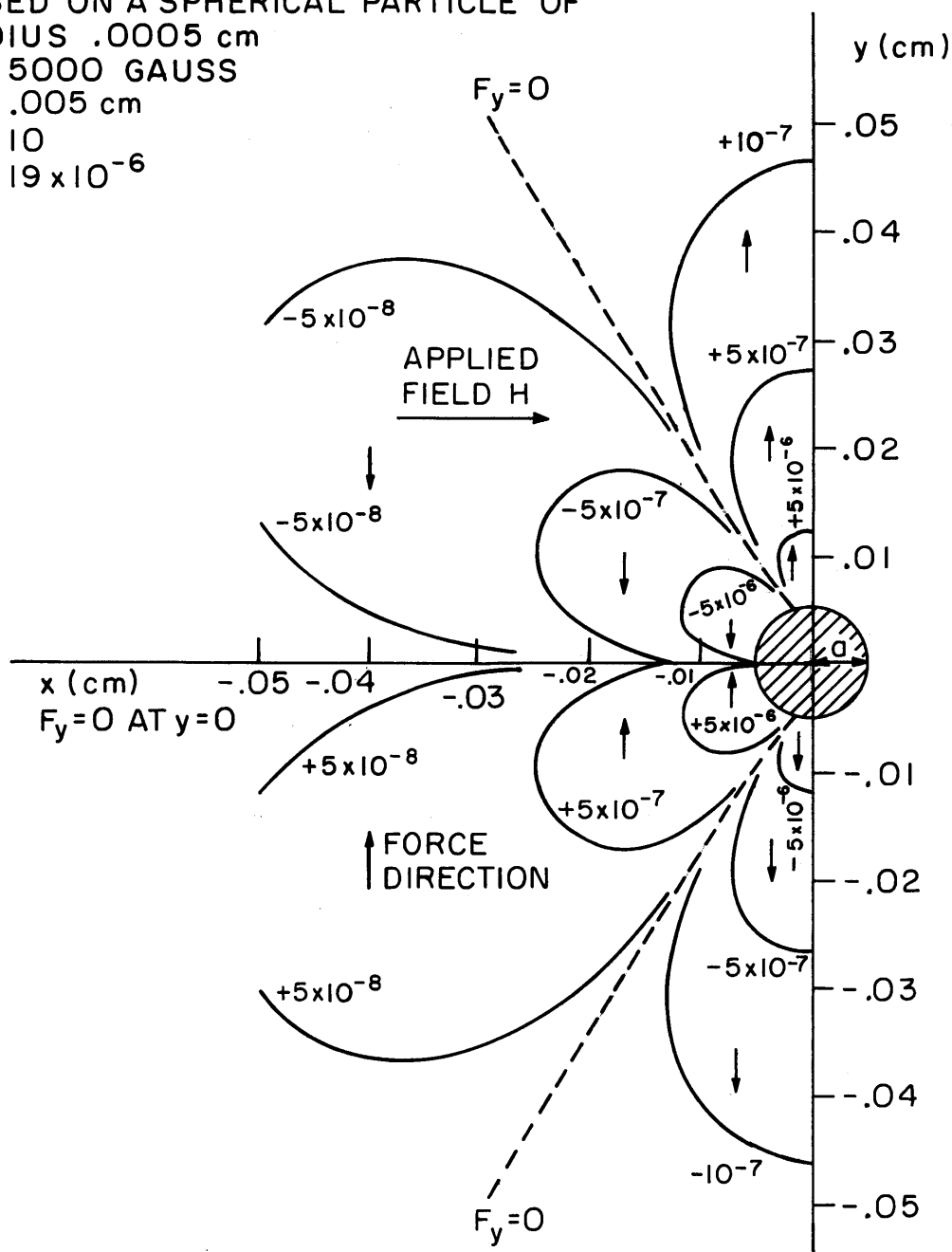
FIGURE 17

$$\frac{\beta'}{r^2} + \cos 2\theta = 0 \quad H > H_s \tag{73b}$$

Since $\cos 2\theta = (x^2 - y^2)/r^2$

$$y = \pm\sqrt{x^2 + \beta} \qquad H \leq H_s \tag{74a}$$

$$y = \pm\sqrt{x^2 + \beta'} \qquad H > H_s \tag{74b}$$

Similar expressions can be derived for F_x and F_y, separately. For a given value of x, as β' decreases with increasing H, the corresponding value of y also decreases. In the limit as H approaches infinity and β' approaches zero, $y = \pm x$. The effect is to make the cylinder appear more like an applied magnetic field and less like a permanent magnet (Figure 18).

Another aspect of the model change concerns the validity of using dipole analogs to describe magnetic fields about ferromagnetic trapping objects. Unless boundary conditions are taken into account, an improper result will occur as seen. A dipole model may be used if the boundary effects are later added as a model correction, but true magnetic field descriptions are highly dependent on the geometry of the object in the applied field. Moreover, the more complex a geometry is, the more difficult it becomes to accurately describe the field. For example, the field about an ellipsoid is analytically describable only in terms of an elliptical integral for each point in the field.

Finally, a reassessment of force magnitudes needs to be made. For the same conditions as in section 3.3.4, except using a permeability of 10 and a radial distance of four cylinder

Figure 18 Position Changes of Zero Force Lines
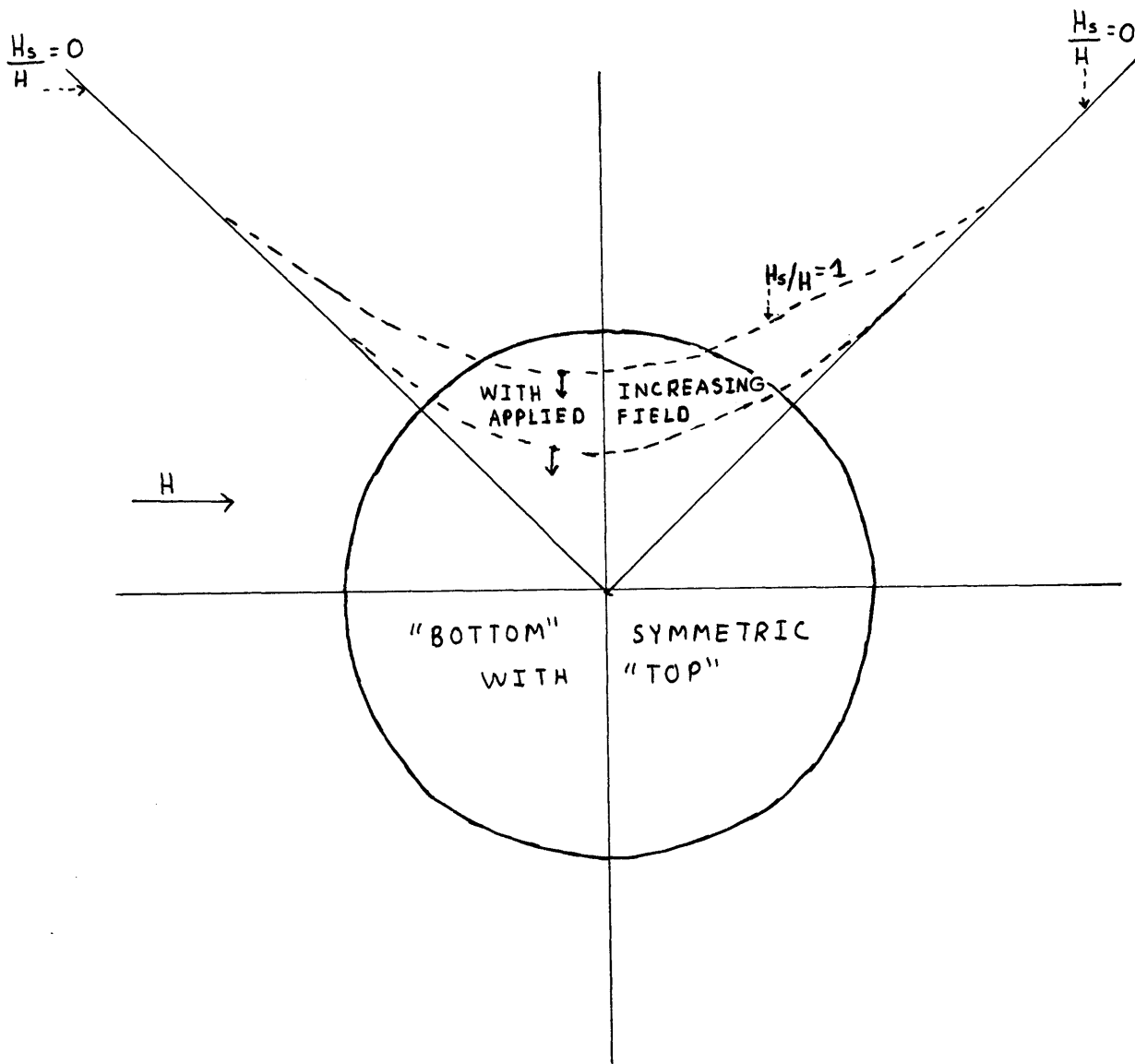
radii, a, the magnetic force is only about 1.6×10^6 dynes in size at this field strength and position. At this position, the inertial terms may be approximately the same size as the magnetic forces at low fields, and the drag force, much greater. The gravitational force now is of the same magnitude as the magnetic force and is added to equation (51) and (56c) as a force in the y direction.

$$\frac{4}{3}\pi\rho*R^3 \frac{dV_y}{dt} = F_{My} \frac{4}{3}\pi R^3 + F_{Dy} - 980\left[\frac{4}{3}\pi R^3 (\rho* - 1)\right] \quad (75)$$

4.1.3. Results of the New Single Cylinder Model and Variable Correlations

With the model change described in section 4.4.1, the trajectories are in much better agreement with the experimental results. Typical trajectories are shown in Figures 19a, b, and c. Almost all trapping occurs on the front or upstream side. All case descriptions and resulting trapping lengths generated by the computer program may be found in Appendix D.

Given Equations (71c) and (71d), one needs to determine the effect different values of H_s have on the trapping length y. For constant a, K (equivalent to K'), V_∞, $\rho*$, μ_s, and R; y versus H was determined for $H_s = 10,000$ and $20,000$ gauss (Figure 20). The loss in magnetic attractive force due to H_s/H has a more pronounced effect when the material saturates at a higher applied field, causing the decrease to occur at a larger absolute magnetic force. The result is a temporary decrease in trapping length. The decrease is only temporary, since H_s/H soon approaches zero while $H_s H$ increases linearly

Figure 19   Typical Particle Trajectories

(19a)

.01cm

-.025   -.02   -.01   .01cm

FRONTSIDE   CAPTURE

(19b)

.01cm

-.025   -.02   -.01   .01cm

BACKSIDE   CAPTURE

(19c)

.01cm

-.025cm   -.02   -.01   .01cm

NO   CAPTURE
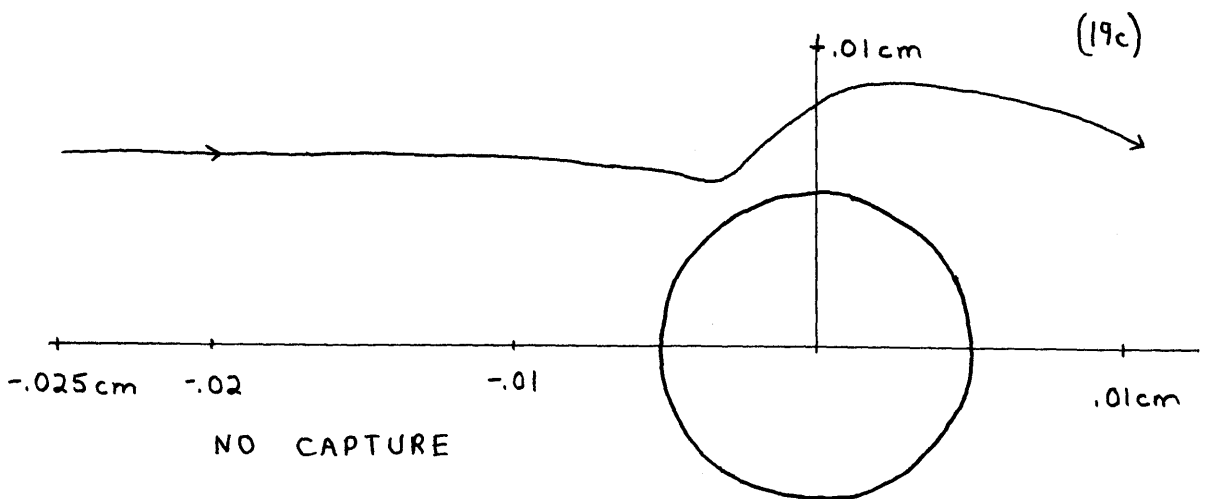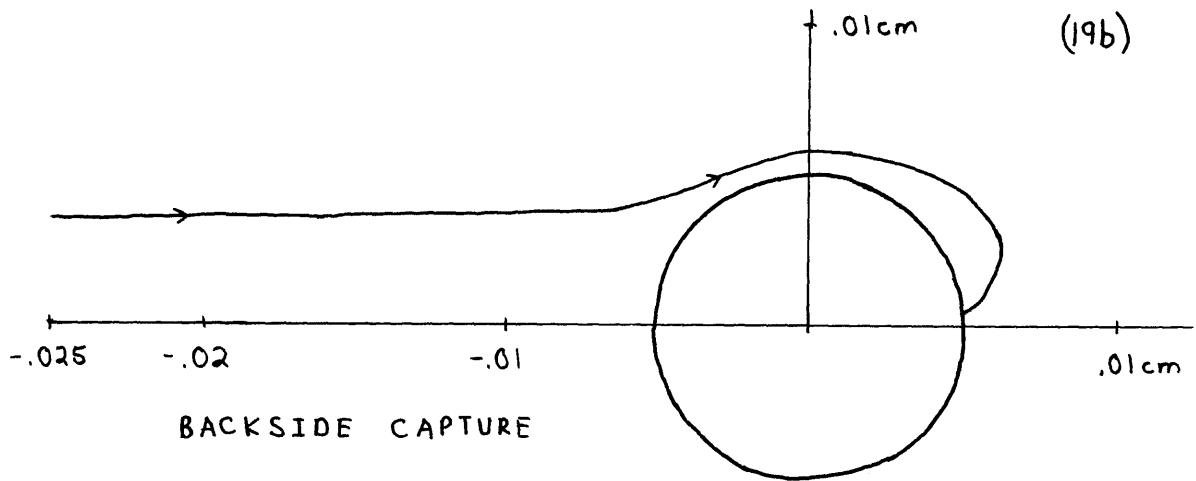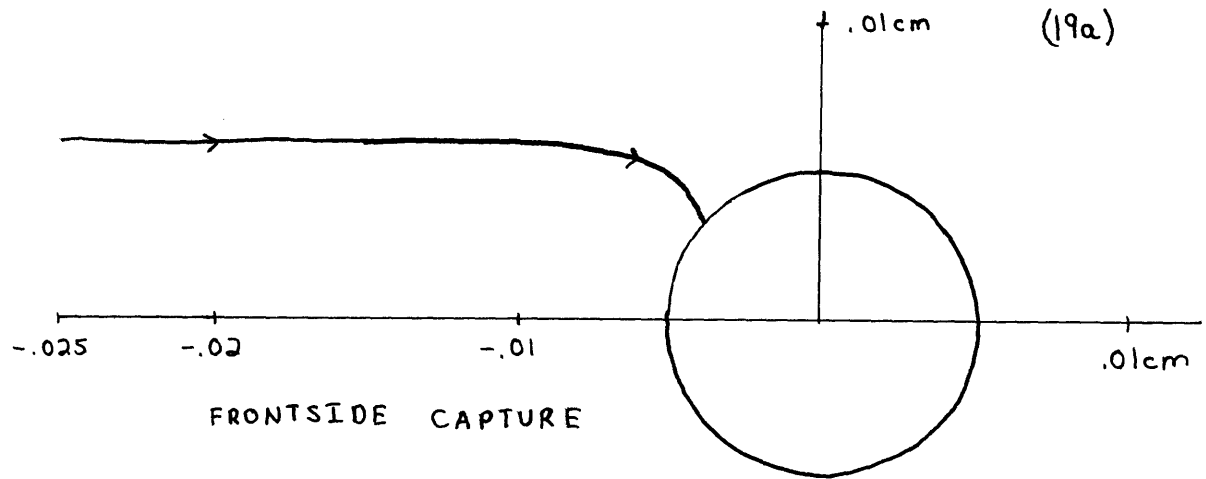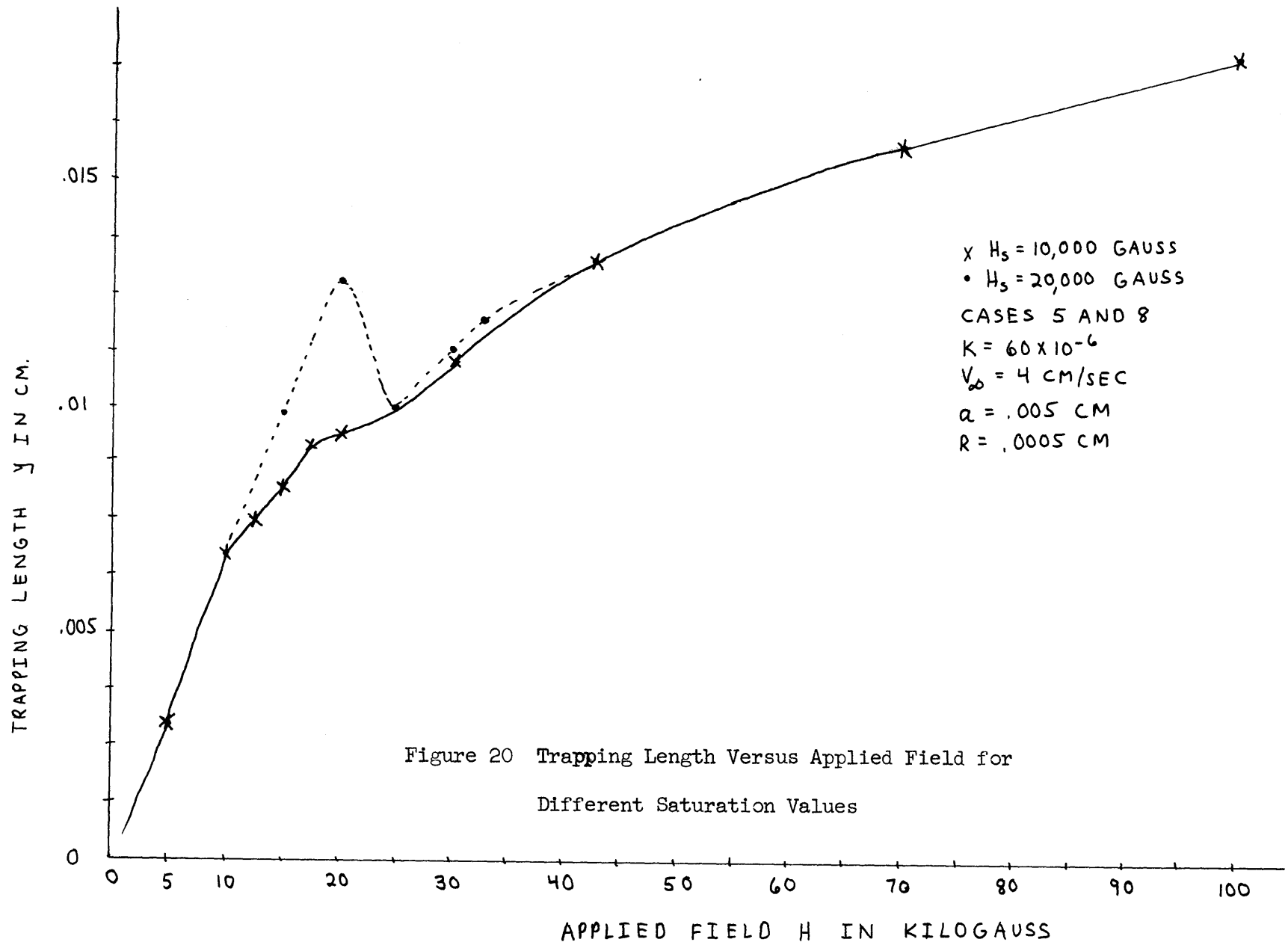
Figure 20   Trapping Length Versus Applied Field for

Different Saturation Values

The figure shows a graph with axes labeled:
- Y-axis: TRAPPING LENGTH y IN CM. (with markings at 0, .005, .01, .015)
- X-axis: APPLIED FIELD H IN KILOGAUSS (with markings at 0, 5, 10, 20, 30, 40, 50, 60, 70, 80, 90, 100)

Legend:
$\times$ $H_s = 10,000$ GAUSS
• $H_s = 20,000$ GAUSS
CASES 5 AND 8
$K = 60 \times 10^{-6}$
$V_\infty = 4$ CM/SEC
$a = .005$ CM
$R = .0005$ CM

with increasing H. The temporary decrease in y should macro-
scopically correspond to a drop in retained feed in actual
separators if the material saturates at about 20,000 gauss.
However, the phenomena has not been noticed. It may have been
overlooked, since it occurs in only a short range of field
strengths above H_s. Since the phenomena, whether real or not,
will only obfuscate matters, an H_s value of 10,000 gauss will
be used. This might actually be closer to the true saturation
magnetization of steel wool. Corresponding to this will be a
constant inherent saturation permeability μ_s of 10, i.e. in a
torroidal arrangement M_s = 10,000 gauss at H = 1000 gauss.

Although not the first variable inspected, the first
variable discarded is ρ^*, the density of the particle.
Keeping K constant by varying χ_M, the molar susceptibility,
with ρ^* (at constant V_∞, a, R, and H), ρ^* was varied. The
results are illustrated in Figure 21. The effect of particle
density is almost negligible except for its effect on K, the
volume susceptibility. Gravitational forces are thus
unimportant. This may be better understood by calculating the
terminal settling velocity for a spherical particle in water.
Letting R = .0005 cm, ρ^* = 12 gm/cm^3, the terminal velocity is
only .15 cm/sec, or only 5% of a freestream velocity. The
density effect is only about this size.

Holding all other variables constant, the functionality
of y with H is shown in Figure 20. A logarithmic plot is
shown in Figure 22. A change in slope occurs at H = H_s = 10,000
gauss, when the magnetic force function changes. A third region

η IN CM

.009

.007

.005

.003

.001

CASE 9
H = 10,000 GAUSS
α = .005 CM
R = .0005 CM
V_∞ = 4 CM/SEC
K = 60 X 10^{-6}

0   1   3   6   9   12

ℓ^* DENSITY GM/CM^3
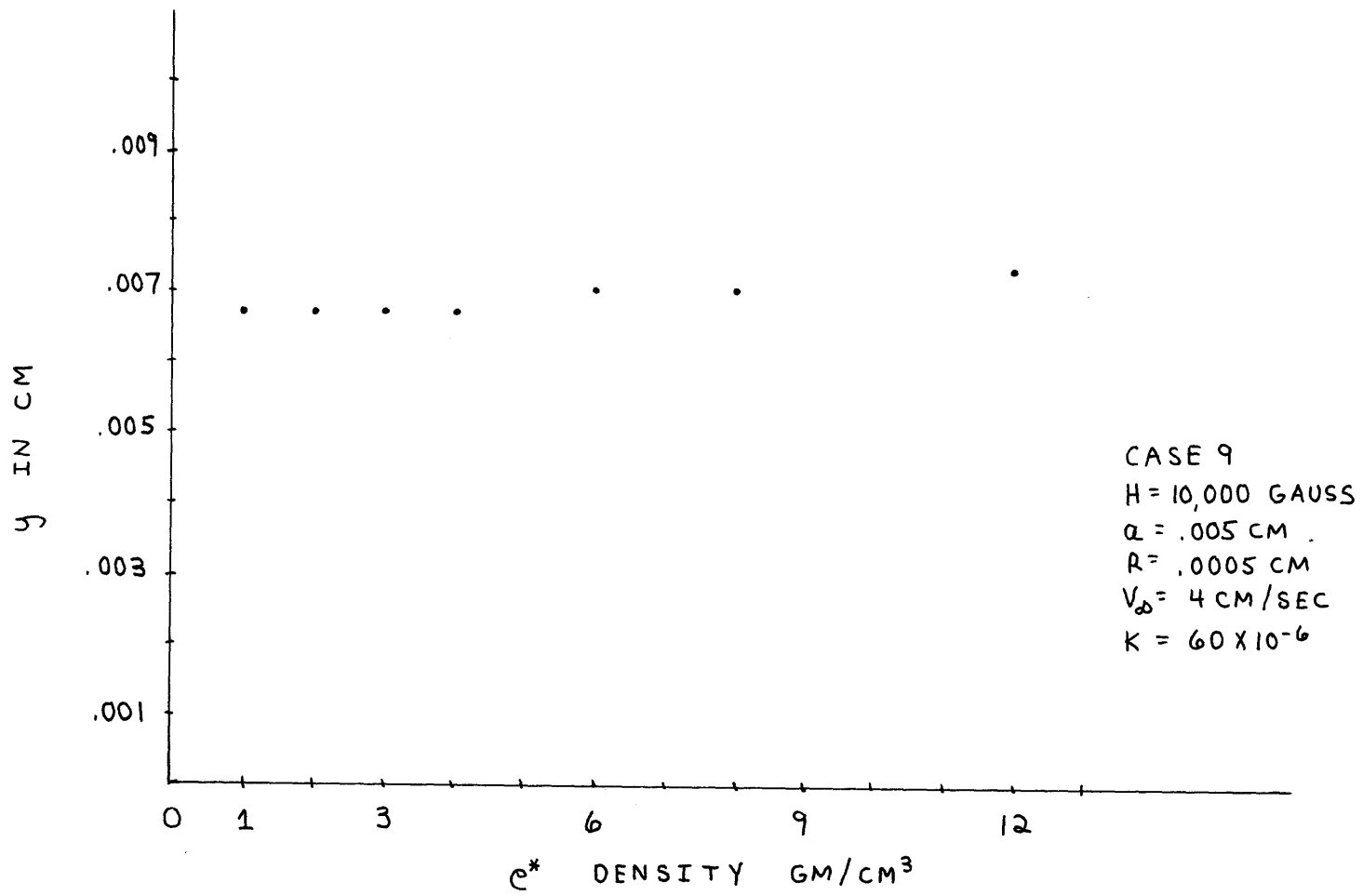
Figure 21   Trapping Length versus Particle Density

Figure 22   Logarithmic Plot of Trapping Length versus

Applied Field
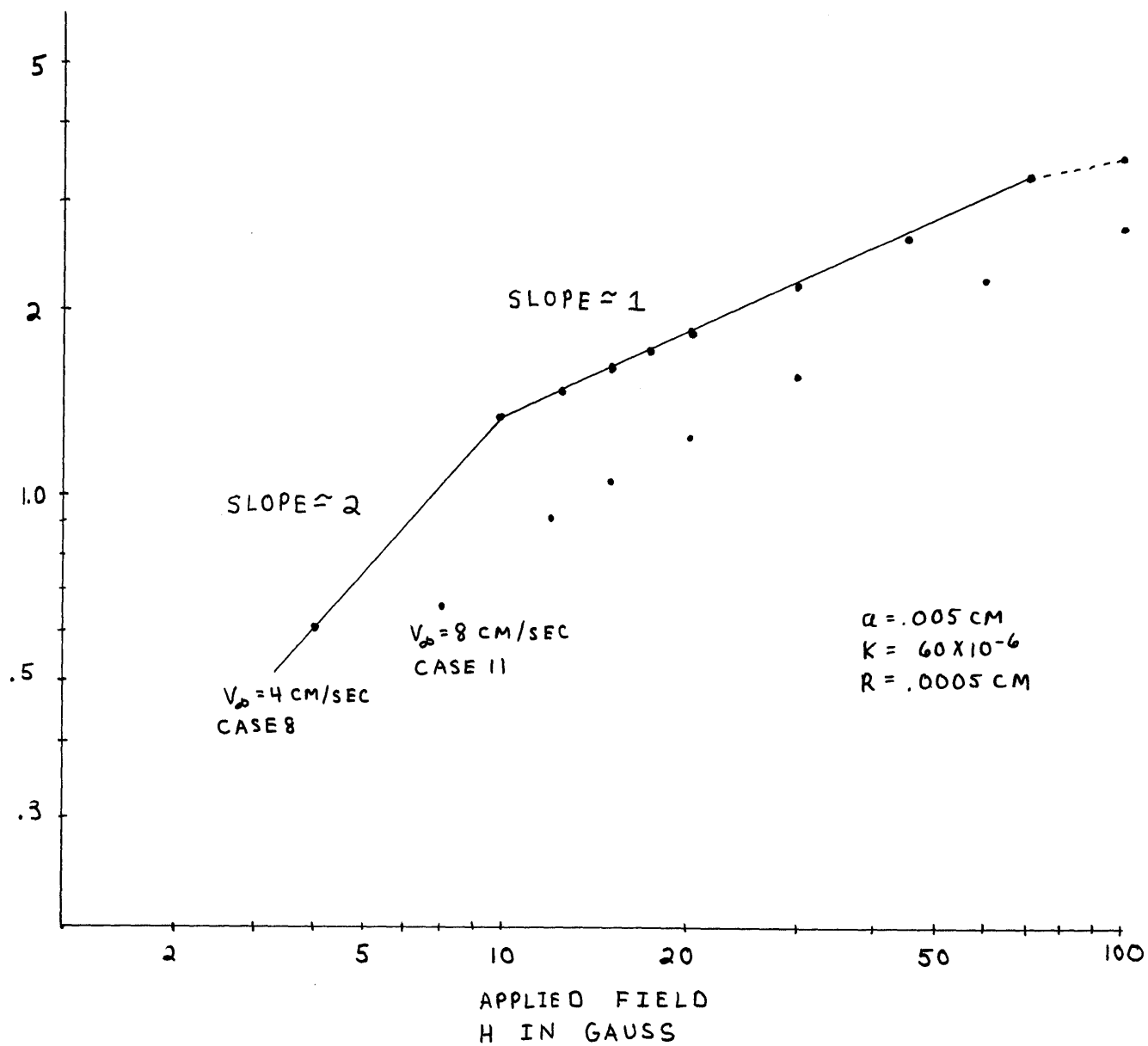
might exist at $H > 70,000$ gauss.

For different field strengths, holding a, r, and K constant y versus V_∞ is shown in Figures 23a and 23b. The trapping length is proportional to $V^{-.57}$. A more complex dependence will be presented with the dimensionless analysis. At low field strengths, depending on the velocity used, the model breaks down and predicts a trapping length of zero. Particles will hit the cylinder (Figure 24), but with a positive V_y and do not stick. In the model the velocity at the surface of the cylinder is zero only at $y = 0$, $x = \pm a$. In reality, the fluid velocity at the surface is zero. The drag force near the surface is overestimated by the model.

The functionality of y with K, the particle susceptibility, is shown in Figure 25 for different field strengths, holding all other variables constant. Trapping length versus a, the cylinder radius is shown in figures 26a and 26b for constant H, V_∞, R, and K. Discussion of these two variables will be postponed until the dimensionless analysis.

Trapping length versus R, the particle radius, is shown in Figure 27 The functionality is complex, since there is an inflection in the curve. At fields above 10,000 gauss for low R, the model predicts a lower or zero value for trapping length at intermediate field strengths and certain a/R ratios (see cases 18 and 20 in Appendix D). This is due to the lack of a no slip condition ($V = 0$) at the surface of the cylinder. Also, upon reaching the surface of the cylinder, a particle may roll along the

Figure 23   Trapping Length versus Velocity

(23a)

$a = .005$ CM
$K = 60 \times 10^{-6}$
$R = .0005$ CM

TRAPPING LENGTH y IN CM

.01

.005

.003

H = 45,000

H = 30,000

H = 20,000

VELOCITY V_∞ CM/SEC

(23b)

$a = .005$ CM
$K = 60 \times 10^{-6}$
$R = .0005$ CM

TRAPPING LENGTH $y \times 200$ (CM)

H = 45,000
H = 30,000
H = 20,000

VELOCITY V_∞ CM/SEC

V_∞

H

PARTICLE
BEING
RETURNED
TO SURFACE

F_M

F_M
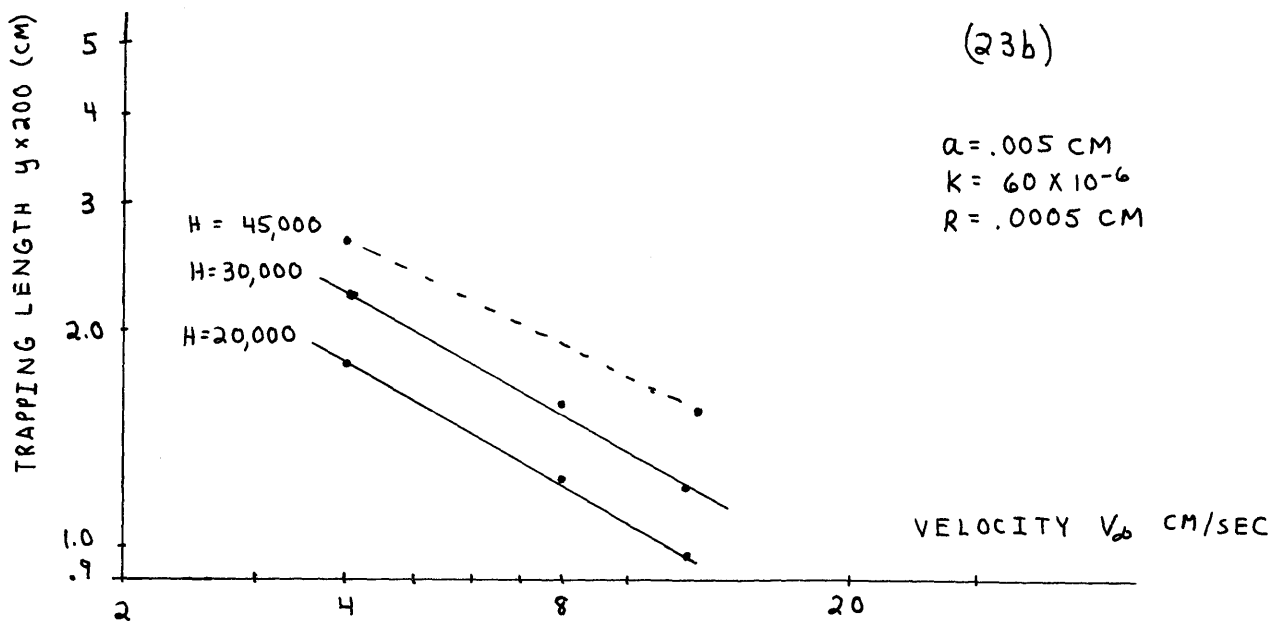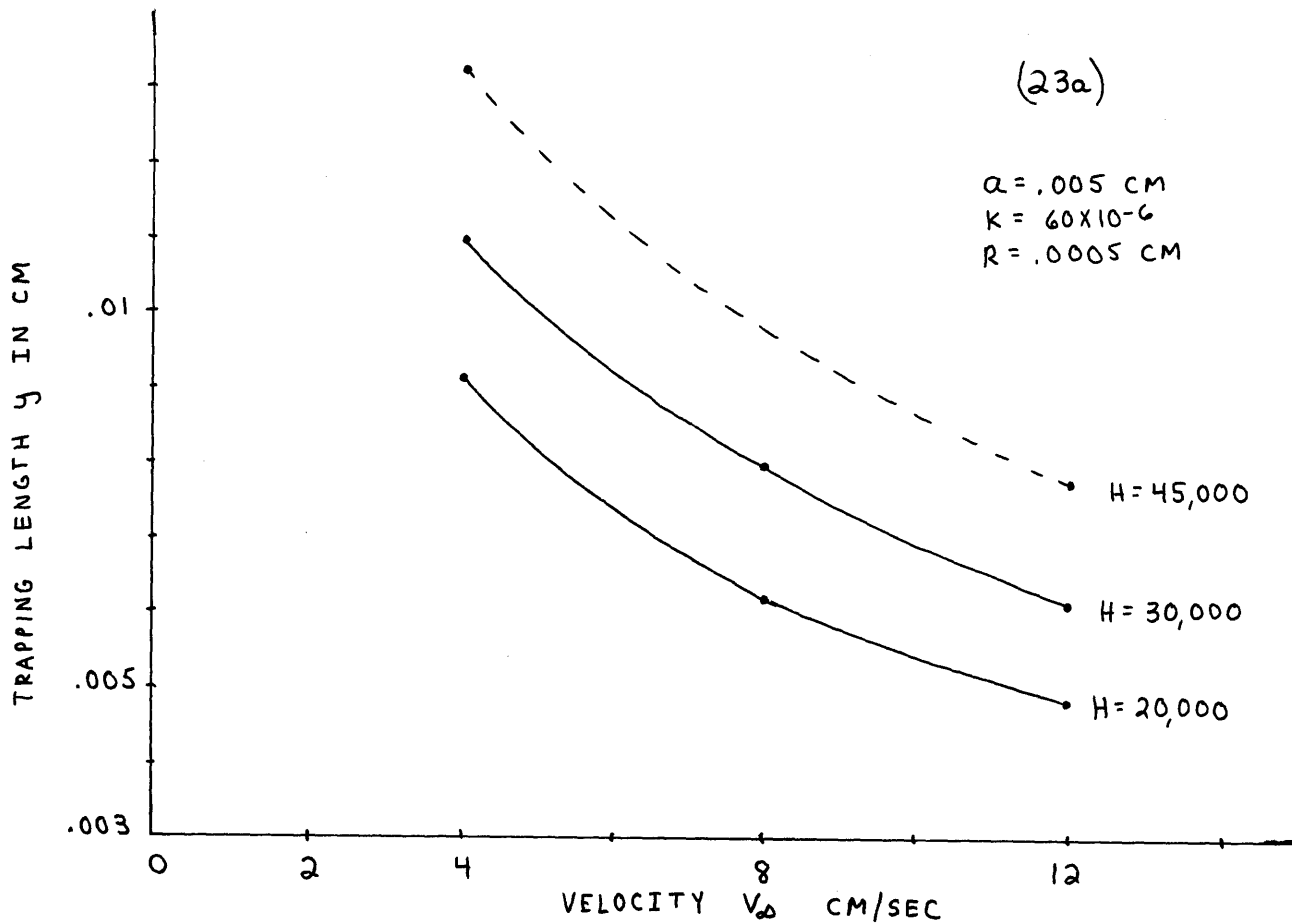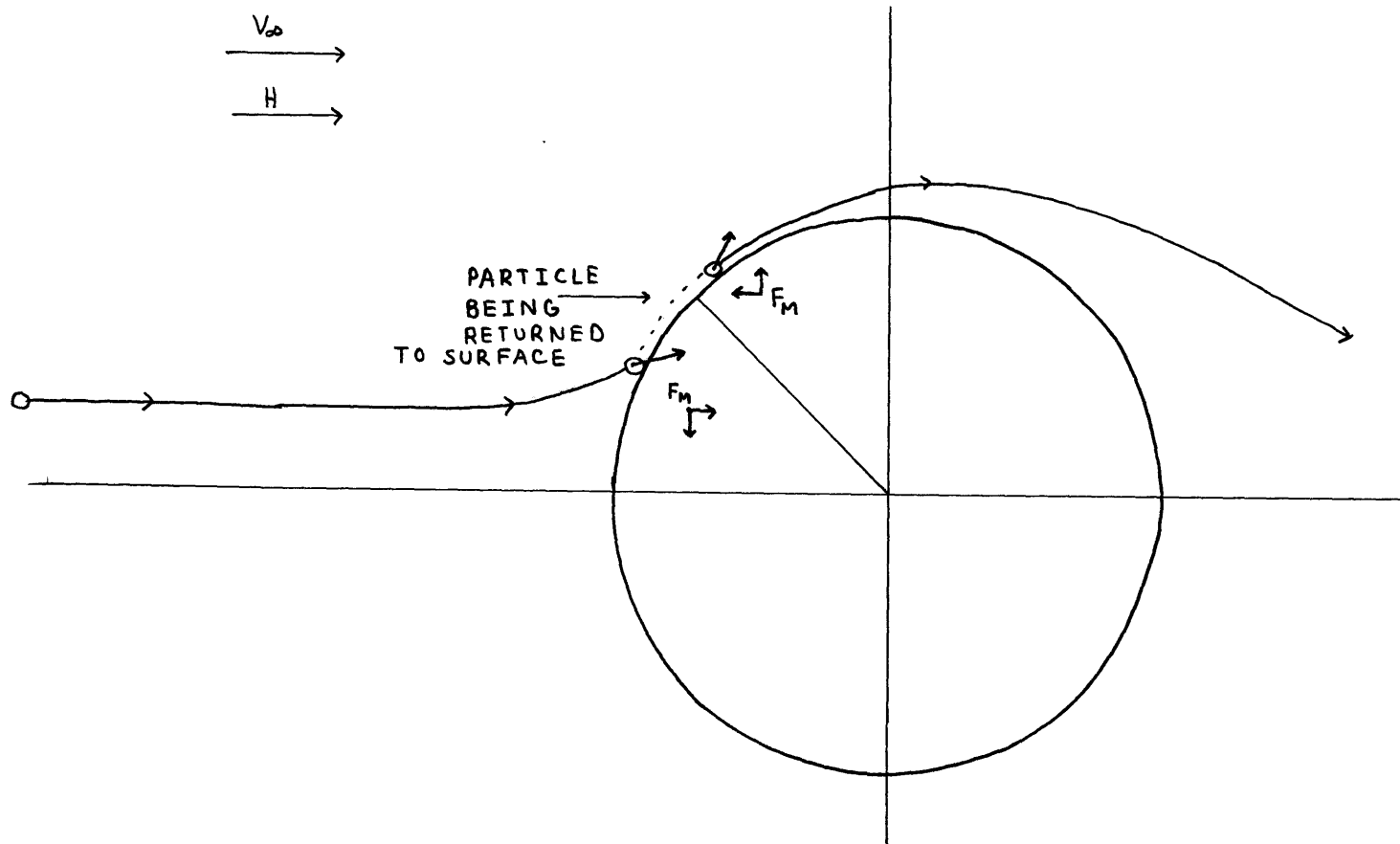
Figure 24 Collision without Entrapment

Figure 25 Trapping Length versus Particle Susceptibility

In the figure:

H = 30,000

H = 20,000

H = 10,000 GAUSS

$a = .005$ CM
$V_\phi = 4$ CM/SEC
$R = .0005$ CM

Y-axis: TRAPPING LENGTH y CM — values .001, .005, .01

X-axis: VOLUME SUSCEPTIBILITY K $\times 10^6$ — values 0, 20, 40, 60
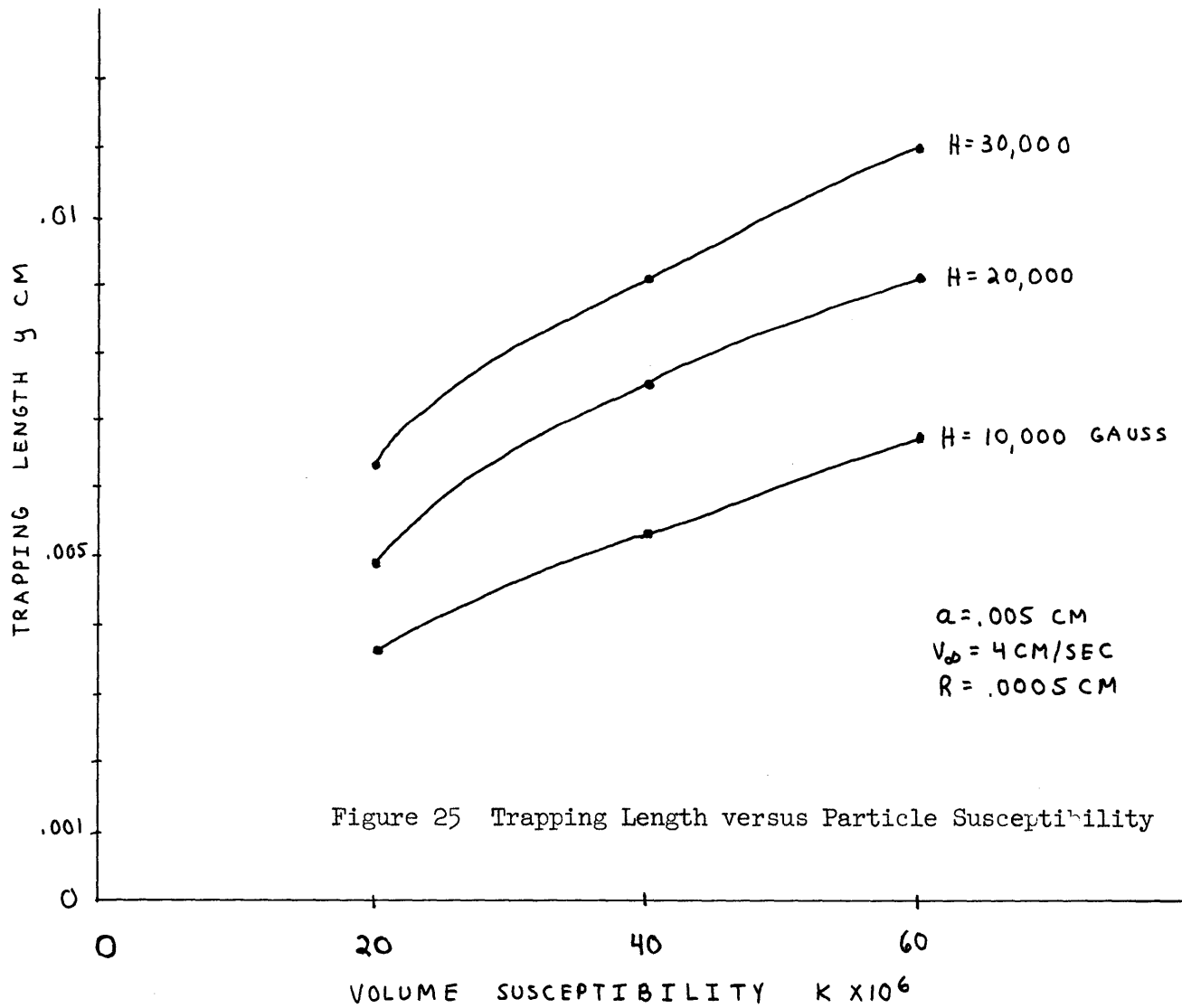
Figure 26   Trapping Length versus
Cylinder Radius
                                        103

(26a)

TRAPPING LENGTH y CM

H = 30,000 GAUSS

H = 20,000

$K = 60 \times 10^{-6}$
$R = .0005\,CM$
$V_\infty = 4\,CM/SEC$

CYLINDER RADIUS a CM

(26b)

TRAPPING LENGTH y x 200 CM.

H = 30,000

H = 20,000

$K = 60 \times 10^{-6}$
$R = .0005\,CM$
$V_\infty = 4\,CM/SEC$

CYLINDER RADIUS a CM
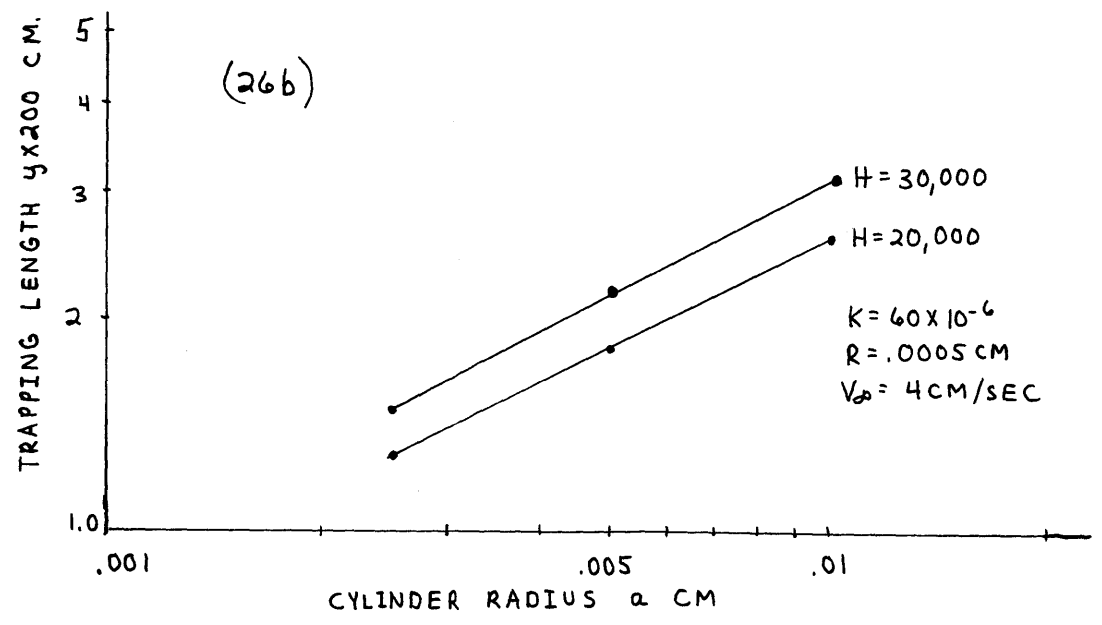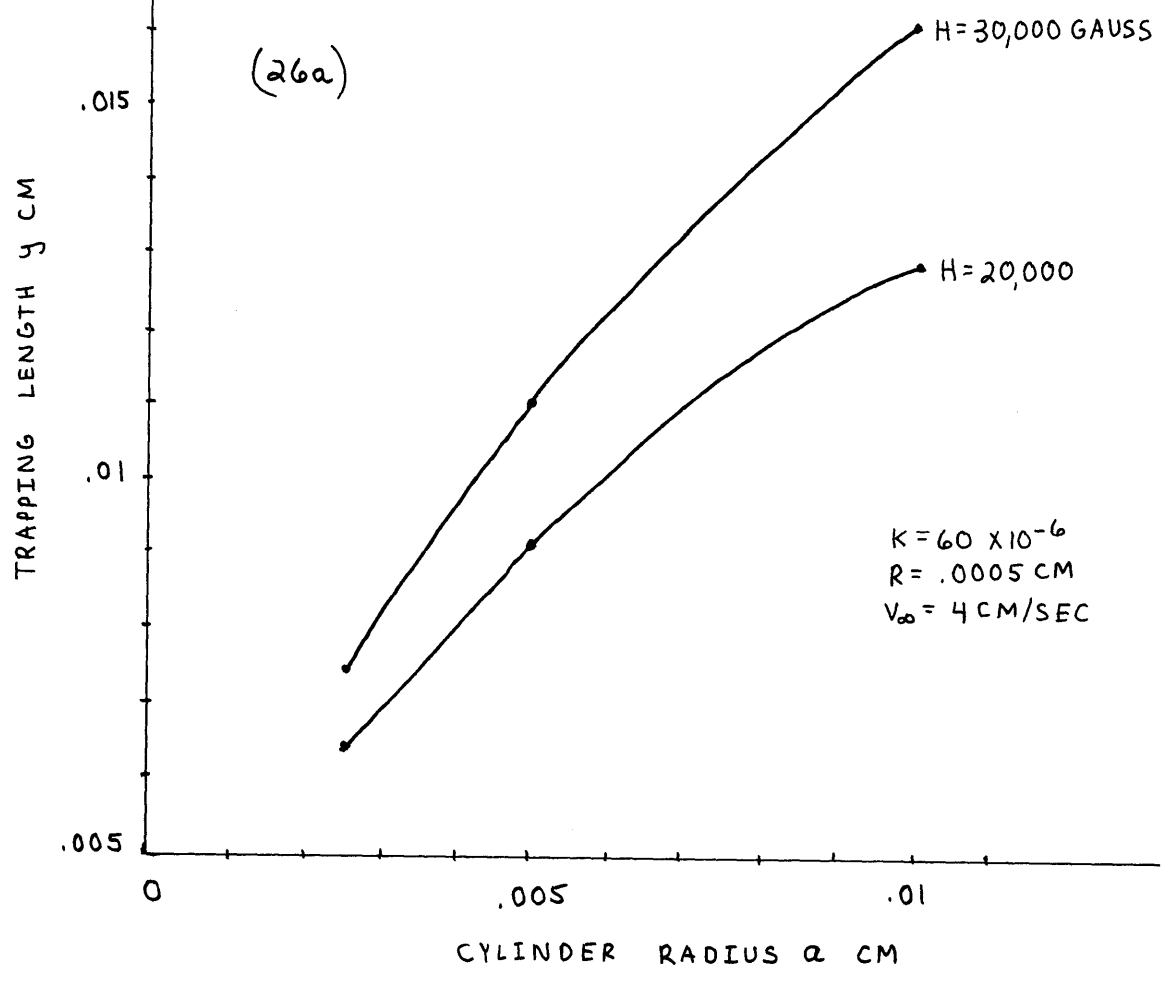
Figure 27   Trapping Length versus Particle Radius
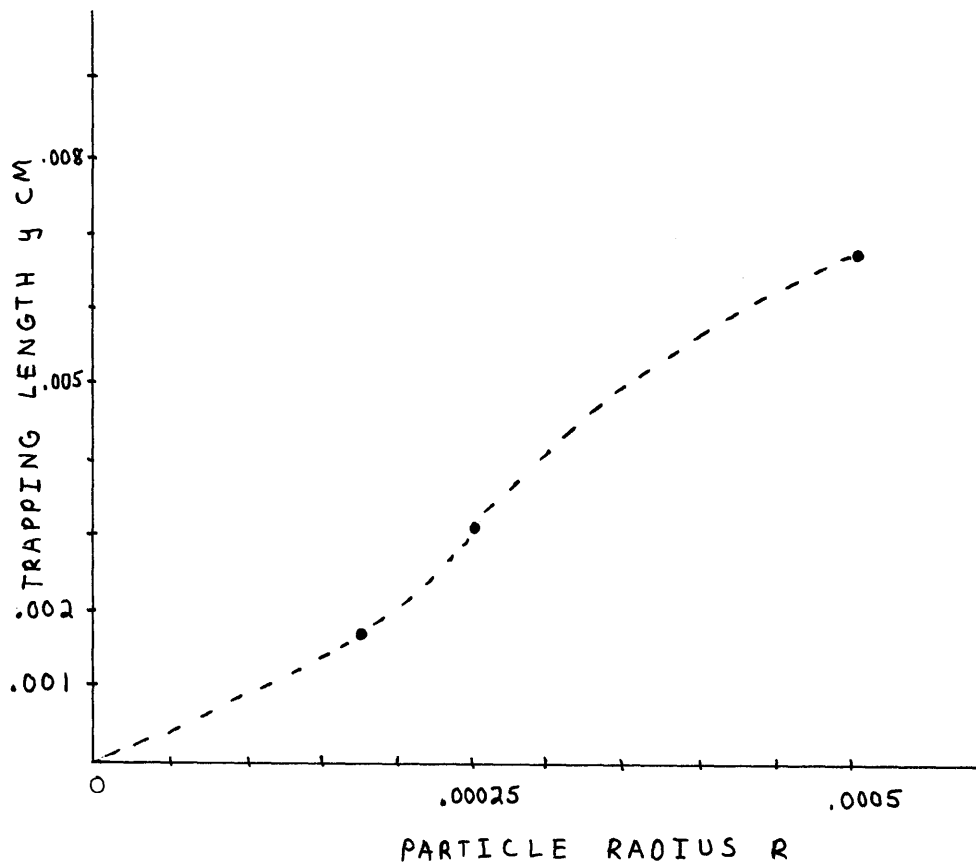
H = 10,000 GAUSS
a = .005 CM
K = 60 × 10⁻⁶
V_∞ = 4 CM/SEC

surface carried by the oversized drag forces until a repulsive region is reached. At this point (Figure 28) the particle leaves the surface and accelerates down the backside of the cylinder, not to be trapped. At the intermediate field strengths above H_s, the repulsive regions increase in area and magnitude, pushing the particle well away from the cylinder. At low fields the particle may not be repulsed enough to avoid backside capture. At high fields the particle will trap at the front and not roll along the surface.

To describe the interactions between any two parameters, a set of dimensionless correlations are needed. By using Buckingham's Pi theorem, one can deduce that four dimensionless groups are needed (Appendix E). By inspection, it was found that $KH^2/\rho_f V_\infty^2$, y/R, $2aV_\infty\rho_f/\eta$, and R/R_o were correlatable groups.

Figure 29 is a plot of y/R versus $KH^2/V_\infty^2\rho_f = S$ ($KHH_s/V_\infty^2\rho_f$ for $H > H_s$) for values of $2aV_\infty\rho_f/\eta$ or Reynolds number based on the cylinder, Re(a), all at constant R. Note that while y/R increases with increasing Re(a), there is also an increase in H necessary to keep S constant if V_∞ is being changed. The ability to change either V_∞ or a in the Reynolds number is demonstrated in Figure 30. The discrepancy at Re(a) = 2 is probably due to the effect a has on the β or β' term in the magnetic force which may become increasingly important at low Reynolds numbers when compared with the a^2 dependence in the fluid velocity description. As a approaches zero, the fluid behaves like the freestream and the repulsive force regions
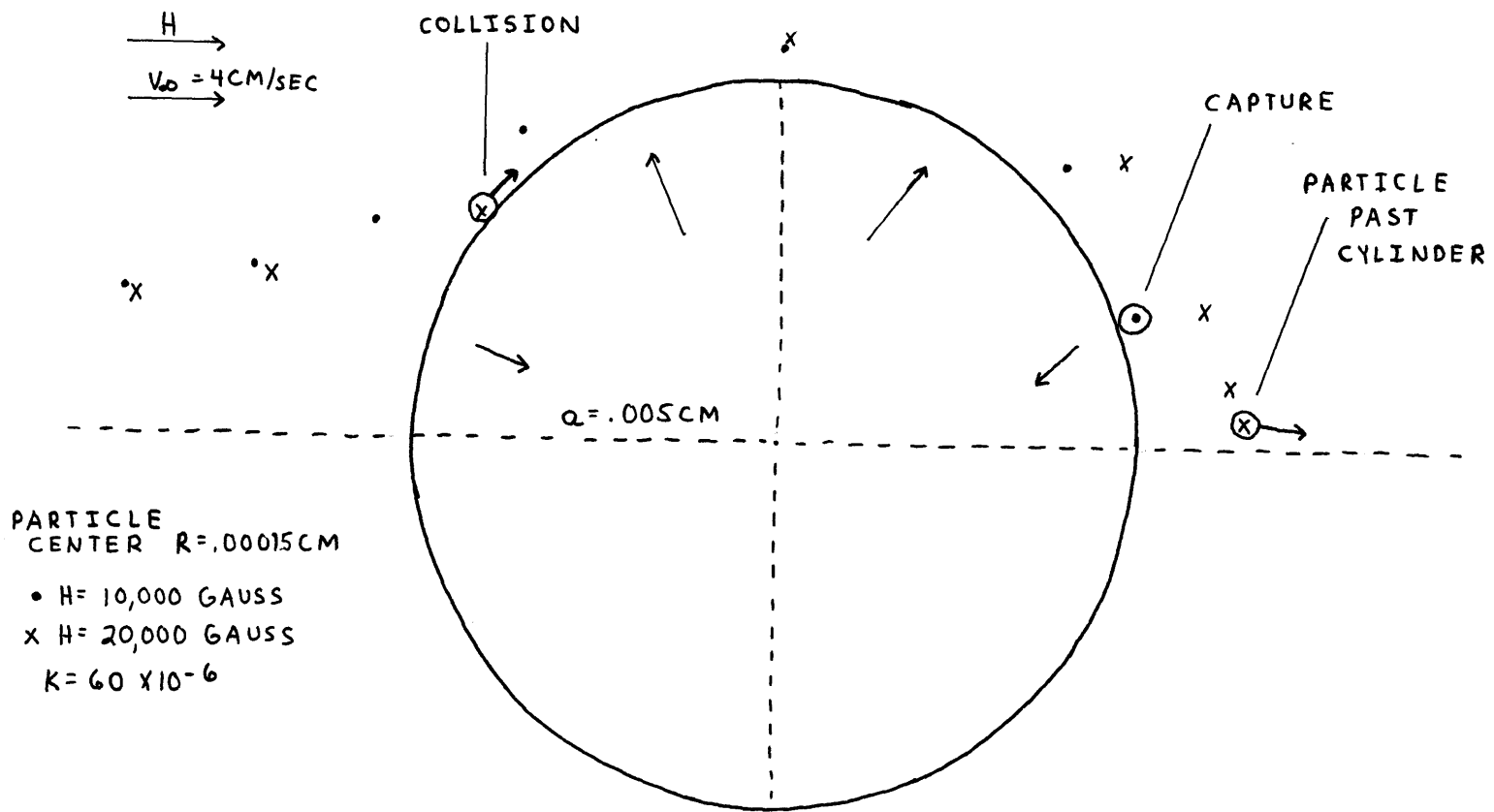
Figure 28   Collision without Entrapment
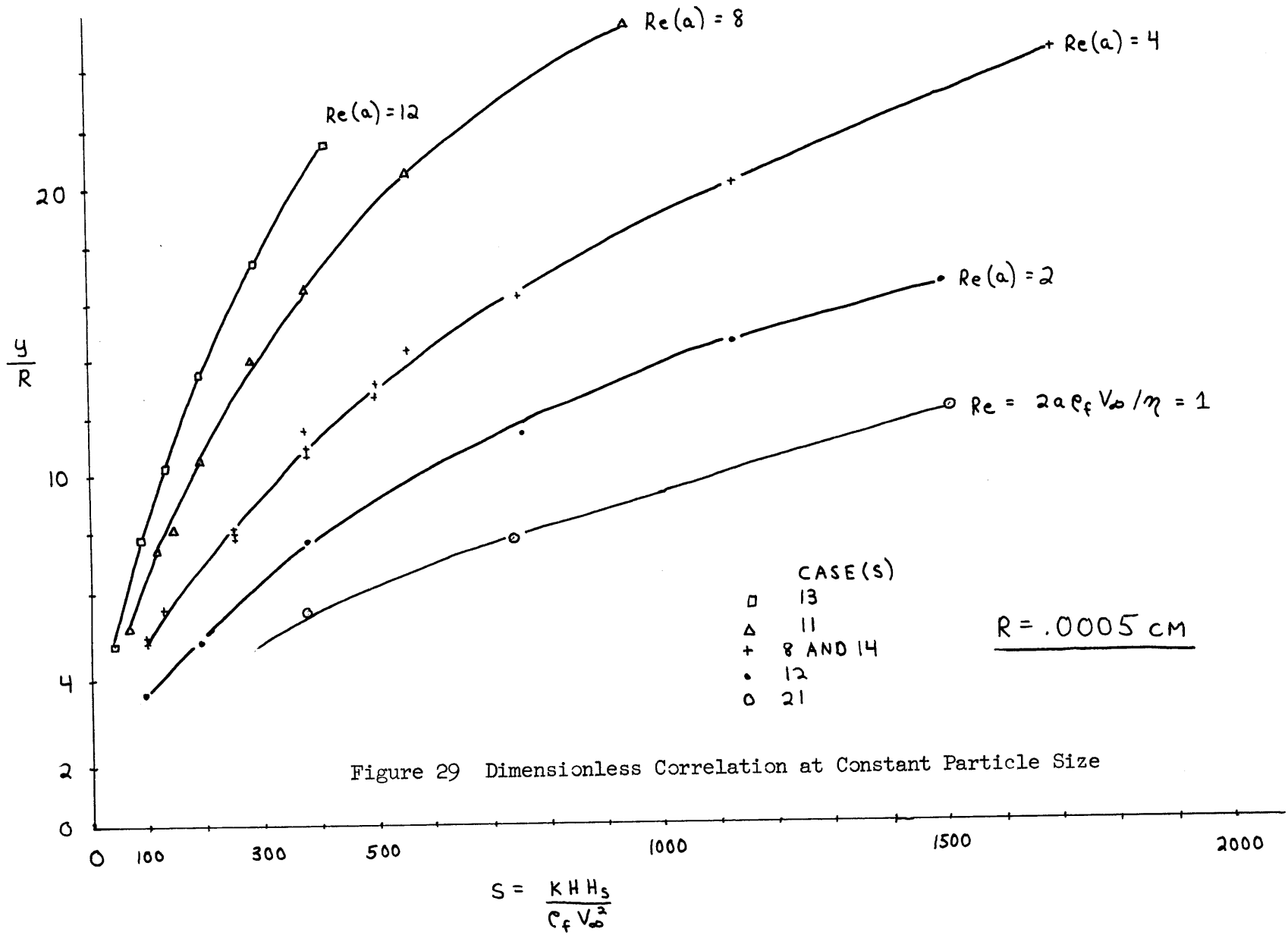
Figure 29   Dimensionless Correlation at Constant Particle Size

$$S = \frac{K H H_s}{C_f V_\infty^2}$$

Figure 30   Variation of Parameters within Reynolds Number Based on Cylinder

On the figure:

$\square$ $Re(a) = 8$

$+ \leftarrow Re(a) = 2$

$R = .0005$ CM

$\bullet$ CASE 12 $V_\infty = 2$ CM/SEC , $a = .005$ CM
$+$ CASE 16 $V_\infty = 4$ CM/SEC , $a = .0025$ CM
$\square$ CASE 11 $V_\infty = 8$ CM/SEC , $a = .005$ CM
$\triangle$ CASE 17 $V_\infty = 4$ CM/SEC, $a = .01$ CM

Y-axis: $\dfrac{y}{R}$ (20, 10, 4, 2)

X-axis: $S = KHH_s / \rho_f V_\infty^2$ (100, 300, 500, 1000, 1500, 2000)
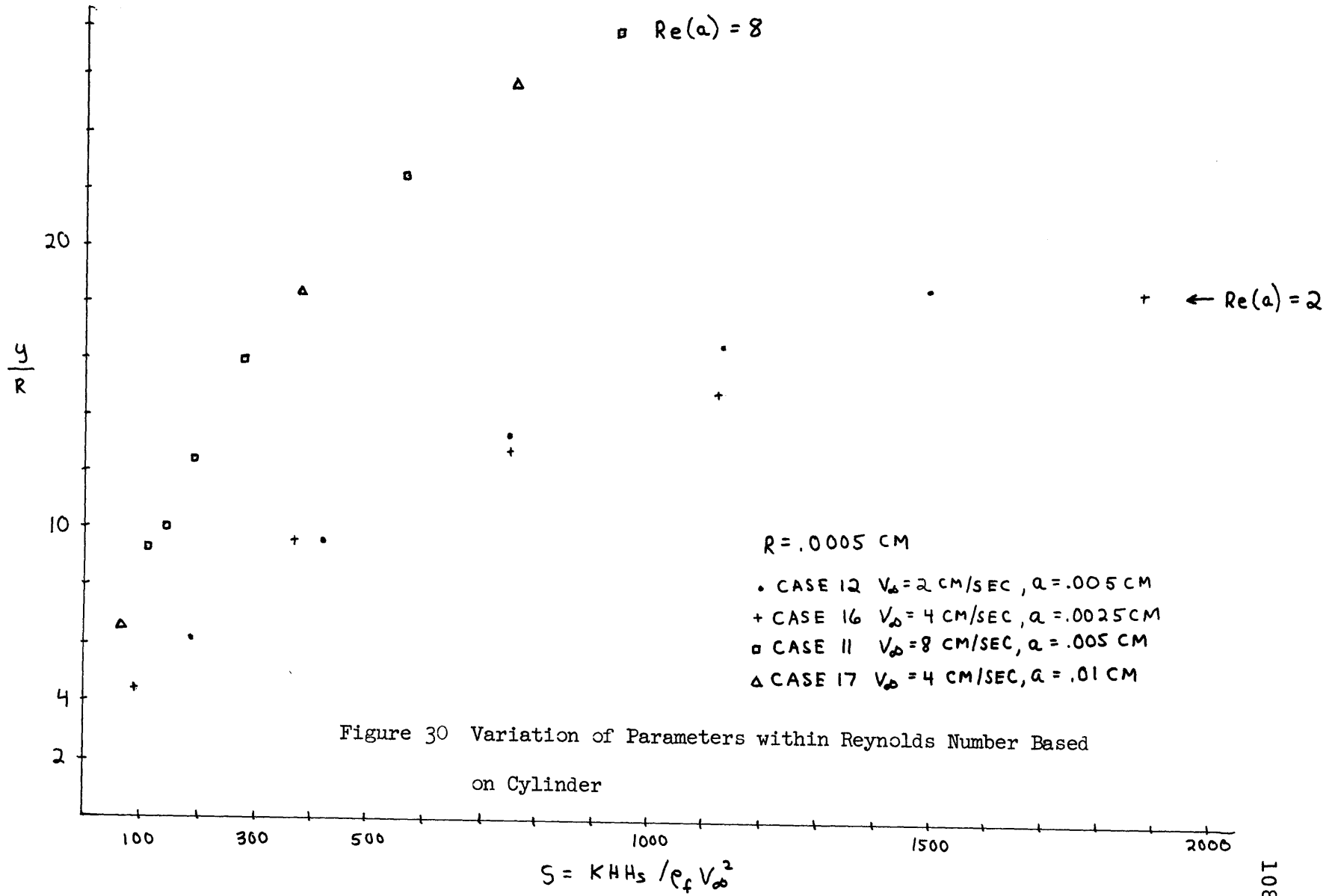
behave as if $H_s/H \to 0$ regardless of the field strength. At

higher $Re(a)$ there is no discrepancy caused by varying a.

Figure 31 demonstrates the differences in Y/R due to changing

K or H. The differences are probably due to the function change

for magnetic force which is dependent only on H.

V_∞ and R cannot be paired to produce a Reynolds number at

constant a (Figure 32). The dependence of magnetic force is

with R^3 while the drag force dependence is only R^2 and V_∞^2.

Decreasing R will have a greater effect on the y parameter

than an equivalent change in V_∞. V_∞ and a seem to correlate

precisely because of the a^2 dependence in fluid velocity and

the V^2 term in drag force; changing a changes the fluid velocity

and then the drag force by the same power as the change in a.

Since $Re(a)$ is used, a direct measure of trapping y/a

cannot be used, since a is not constant. Since R is held

constant in Figure 29, y/R becomes the third group by default.

Figure 33 is a logarithmic plot of Figure 29. The slope is

approximately 1/2, indicating a y/R dependence on $\sqrt{HH_s}/V_\infty$ at

constant R.

The fourth dimension of the correlation still must be

found. An obvious choice is $Re(R) = 2\rho_f RV_\infty/\eta$, but that would

cause the surfaces of constant $Re(a)$ to intersect at various

values of y/R and $Re(R)$ as in Figure 34. Since there is a

maximum value arbitrarily placed on R (.0005 cm) to avoid the

particle affecting the flow about the cylinder ($10R \leq a$), a

better, although more contrived group would be R/R_0 where

R_0 = .0005 cm. y/R versus R/R_0 at constant S for various $Re(a)$

is shown in Figures 35a, 35b,   and 35c. As stated earlier,

Figure 31   Variation of Parameters within S Grouping

$Re(R) = .2$

$Re(R) = .2$

$a = .005\,cm$

• CASE 12 $V_0 = 2\,cm/sec$ $R = .0005\,cm$

+ CASE 15 $V_\infty = 4\,cm/sec$ $R = .00025\,cm$

$\dfrac{y}{a}$

$S = KHH_s / \rho_f V_\phi^2$
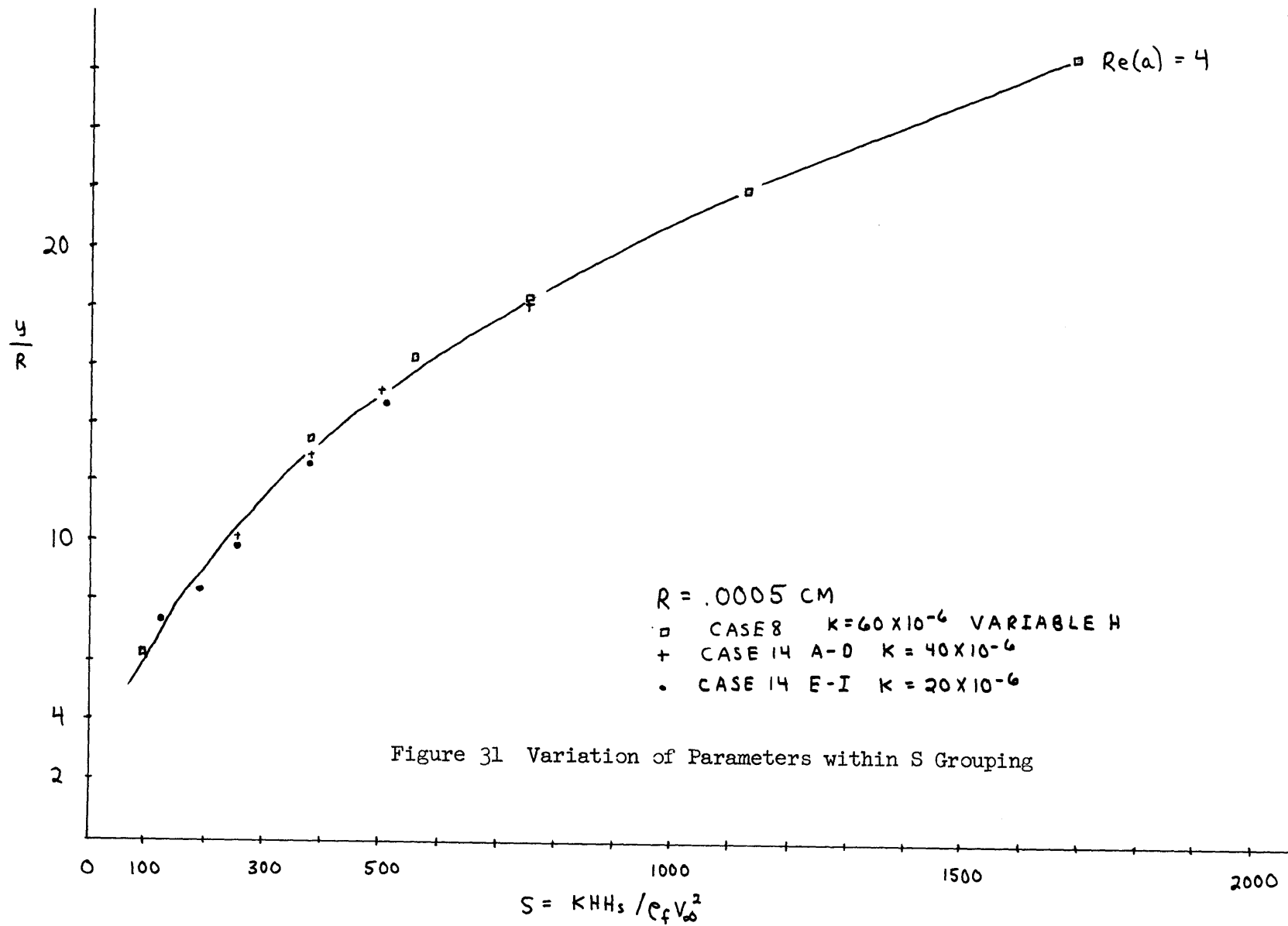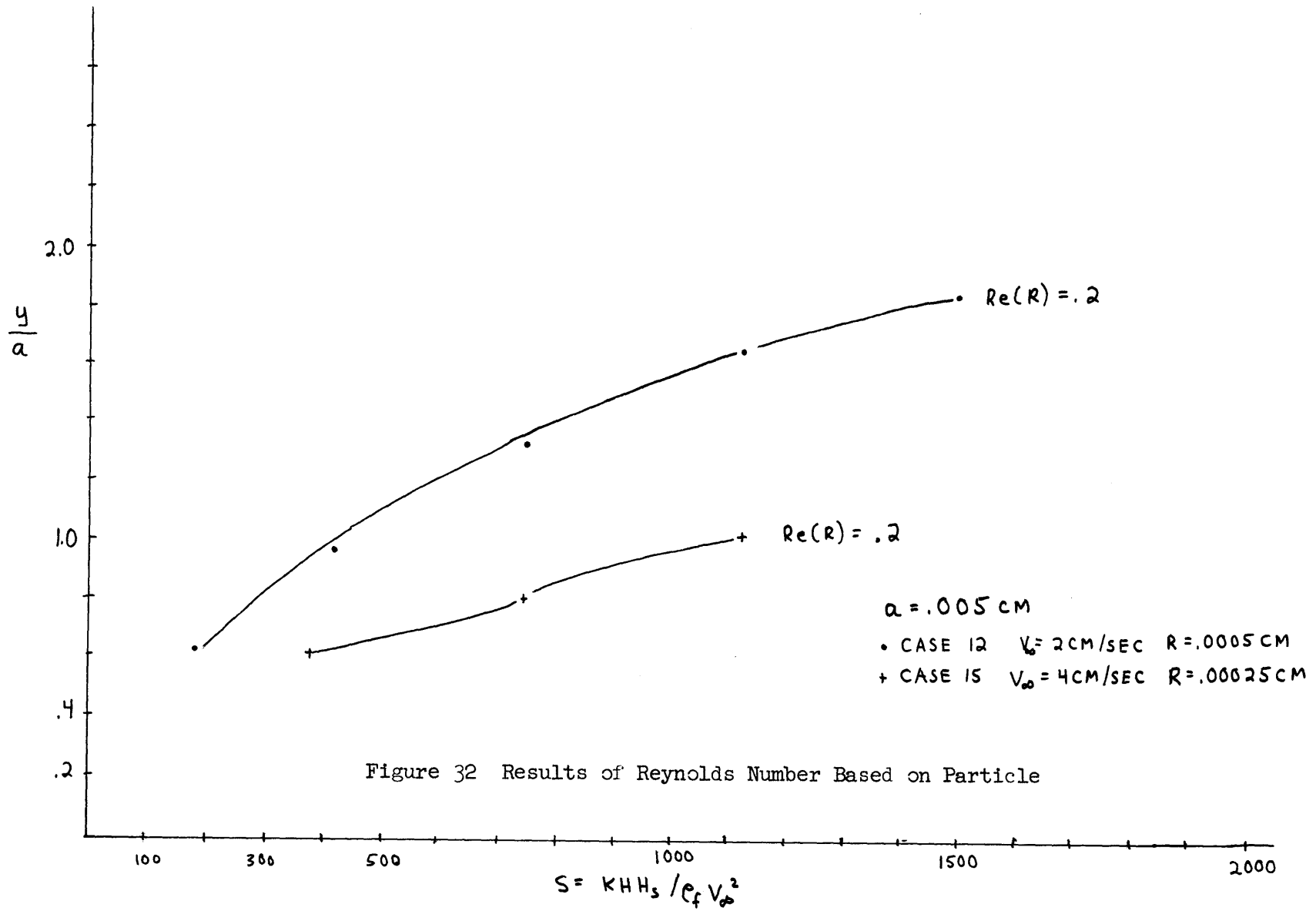
Figure 32   Results of Reynolds Number Based on Particle

Figure 33   Logarithmic Plot of Figure 29

$$S = KHH_s / \rho_f V_\infty^2$$
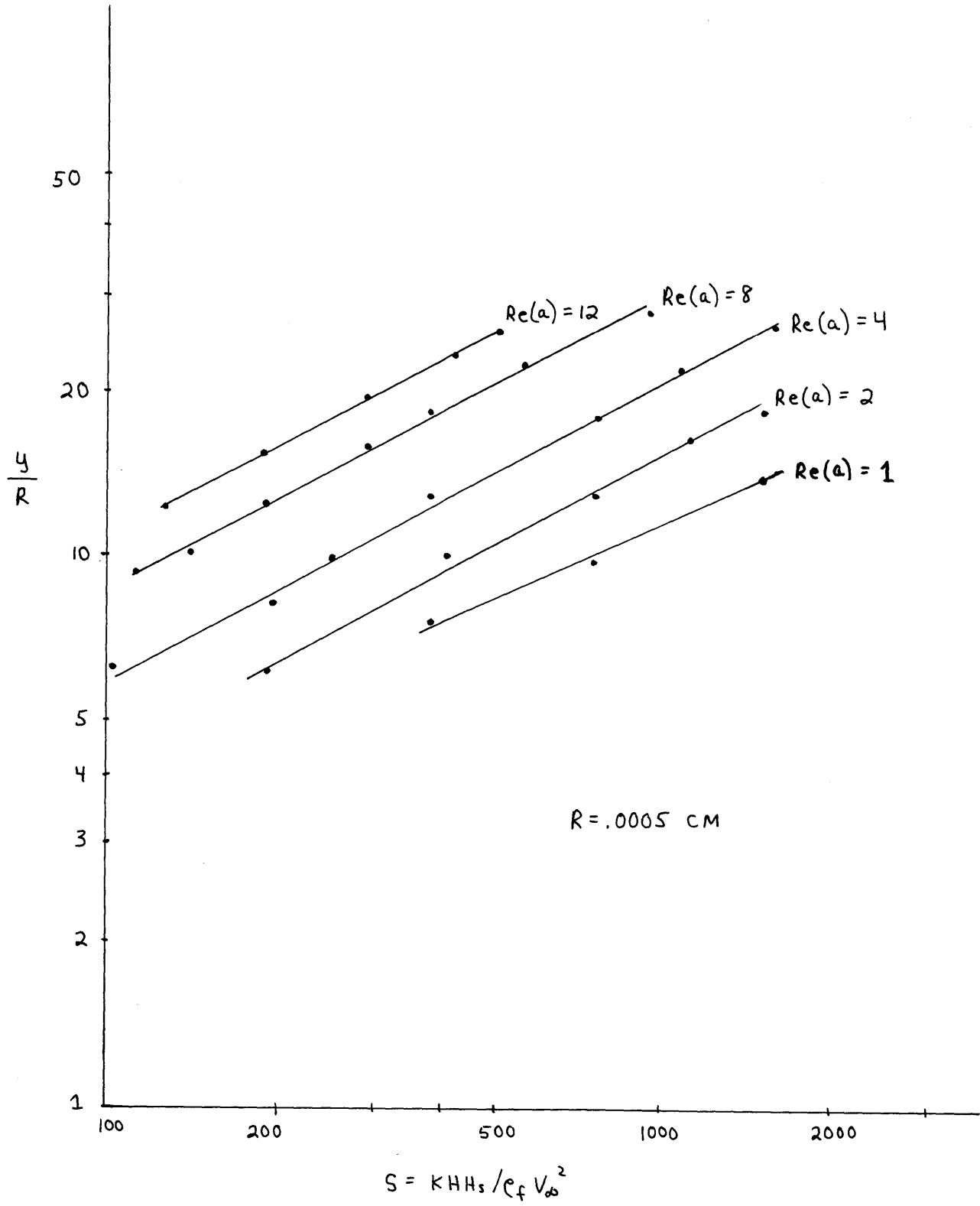
Figure 34   Surfaces Produced by Reynolds Number Based
on Particle
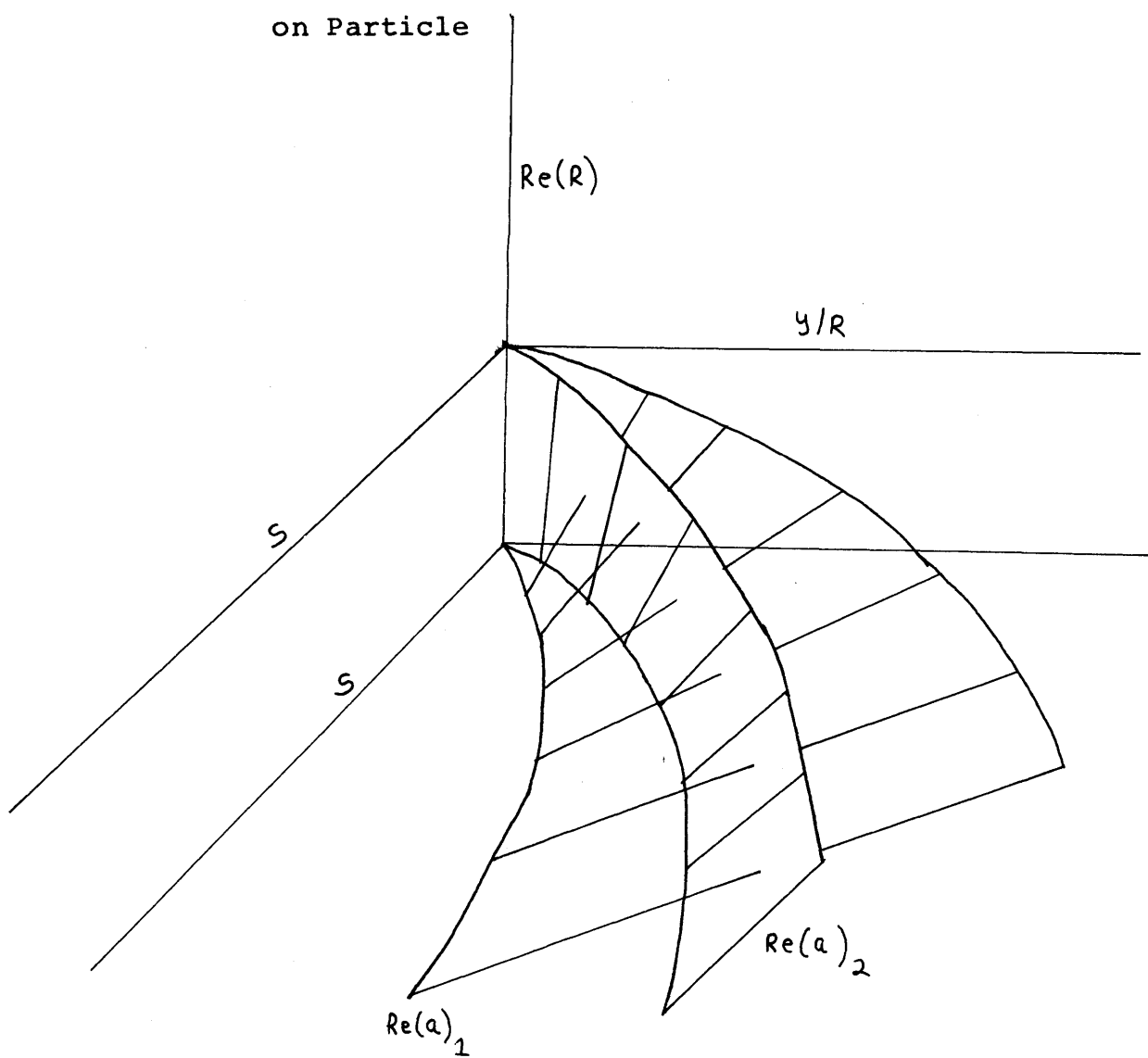
Figure 35   Trapping Length versus Dimensionless Particle
           Radius

(35a)

$\frac{y}{R}$

• a = .01 CM

• a = .005 CM

• a = .0025 CM

S = 375

R/R_0

(35b)

$\frac{y}{R}$

• a = .01 CM

• a = .005 CM

• a = .0025 CM

S = 750

R/R_0

(35c)

$\frac{y}{R}$ vs R/R_0

a = .01 CM

a = .005 CM

a = .0025 CM

S = 1125
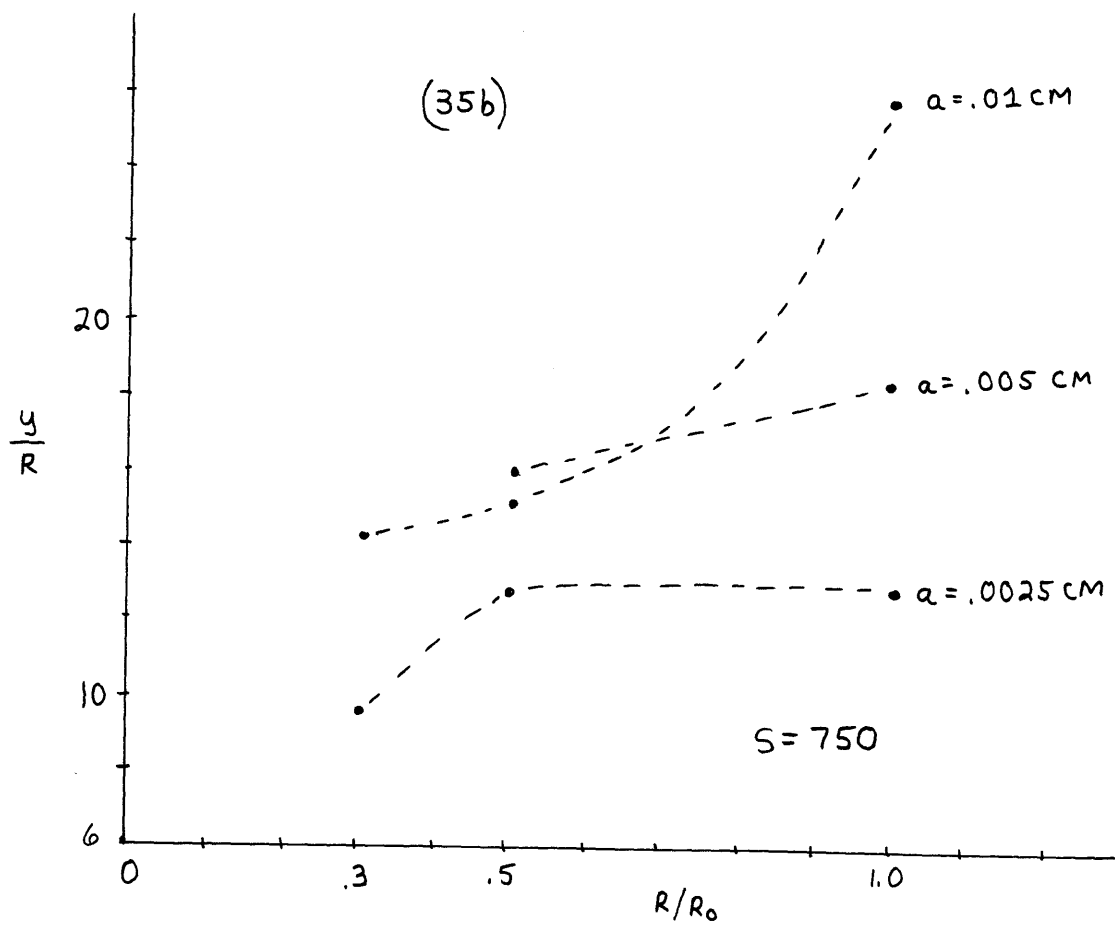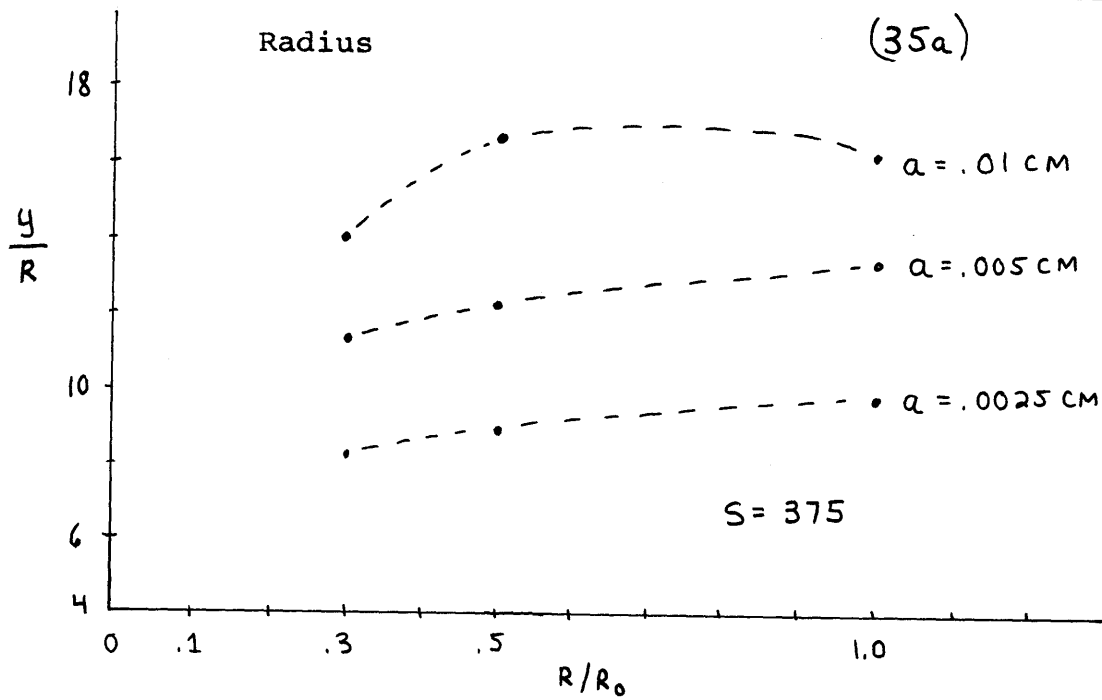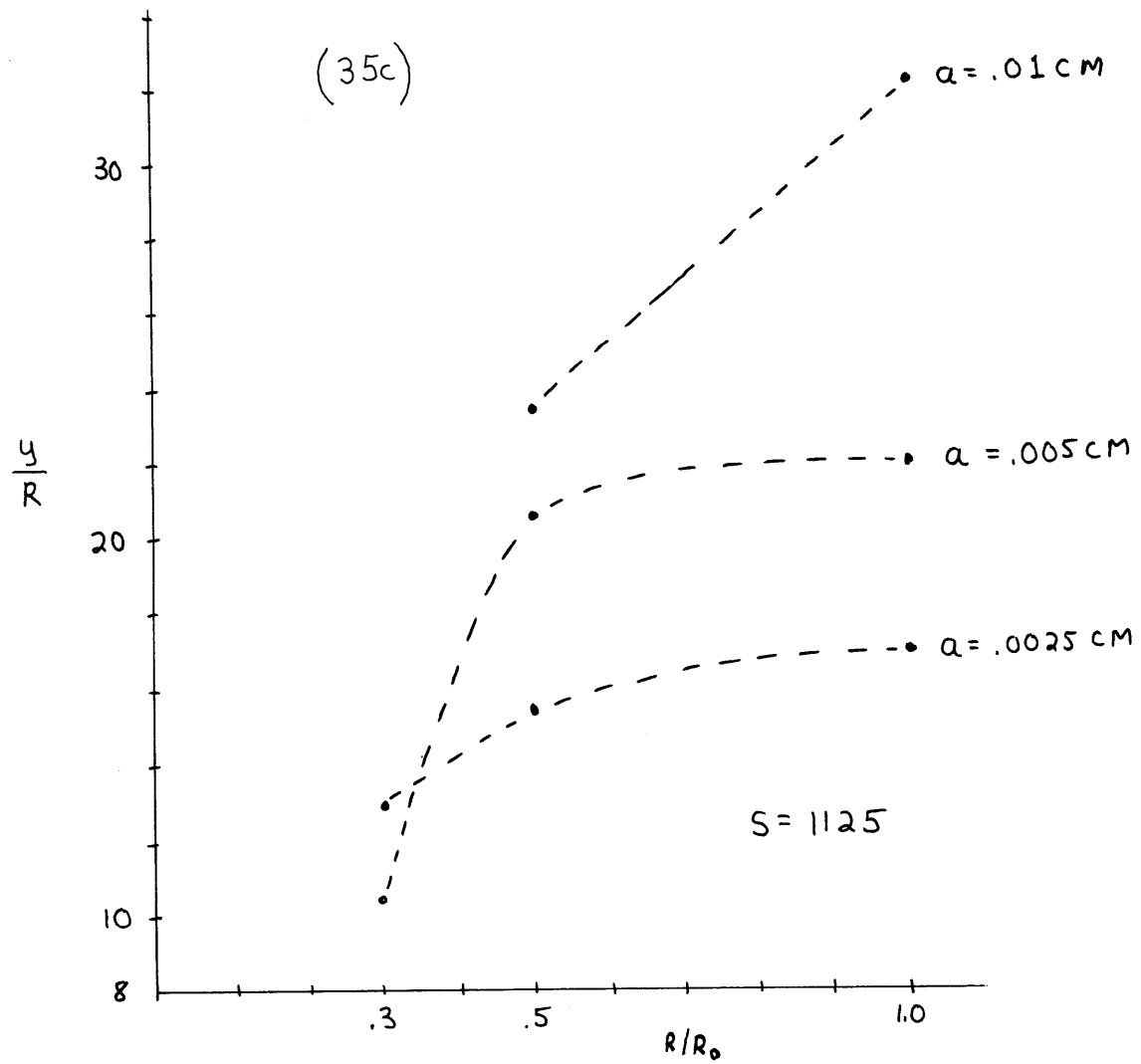
y/R as a function of R has an unusual dependence with H or S.

4.1.4. Results of the Two Cylinder Model

The effect on the trapping length y predicted by the single cylinder model of an identical magnetic force source at a point (O,d) above the origin is shown in Figure 36. Except when y > d/2, the effect is small and decreases with increasing d or decreasing applied field strength H. One would also expect only a small variation in y for any staggered orientation if y < d/2. When the separation distance d is less than 2y, the particle is attracted to the other source. In the model the region of attraction towards the other source includes some values of y less than d/2, but no fluid dynamic description was assumed for the "other cylinder." This result is misleading, since for fluid flow perpendicular to the plane of the cylinders, the midline between the two cylinders is a streamline in the absence of rotational flow. One should assume that with respect to the magnetic force, other cylinders do not affect the trapping length unless y > d/2, or, if there are magnetic interactions between the cylinders.
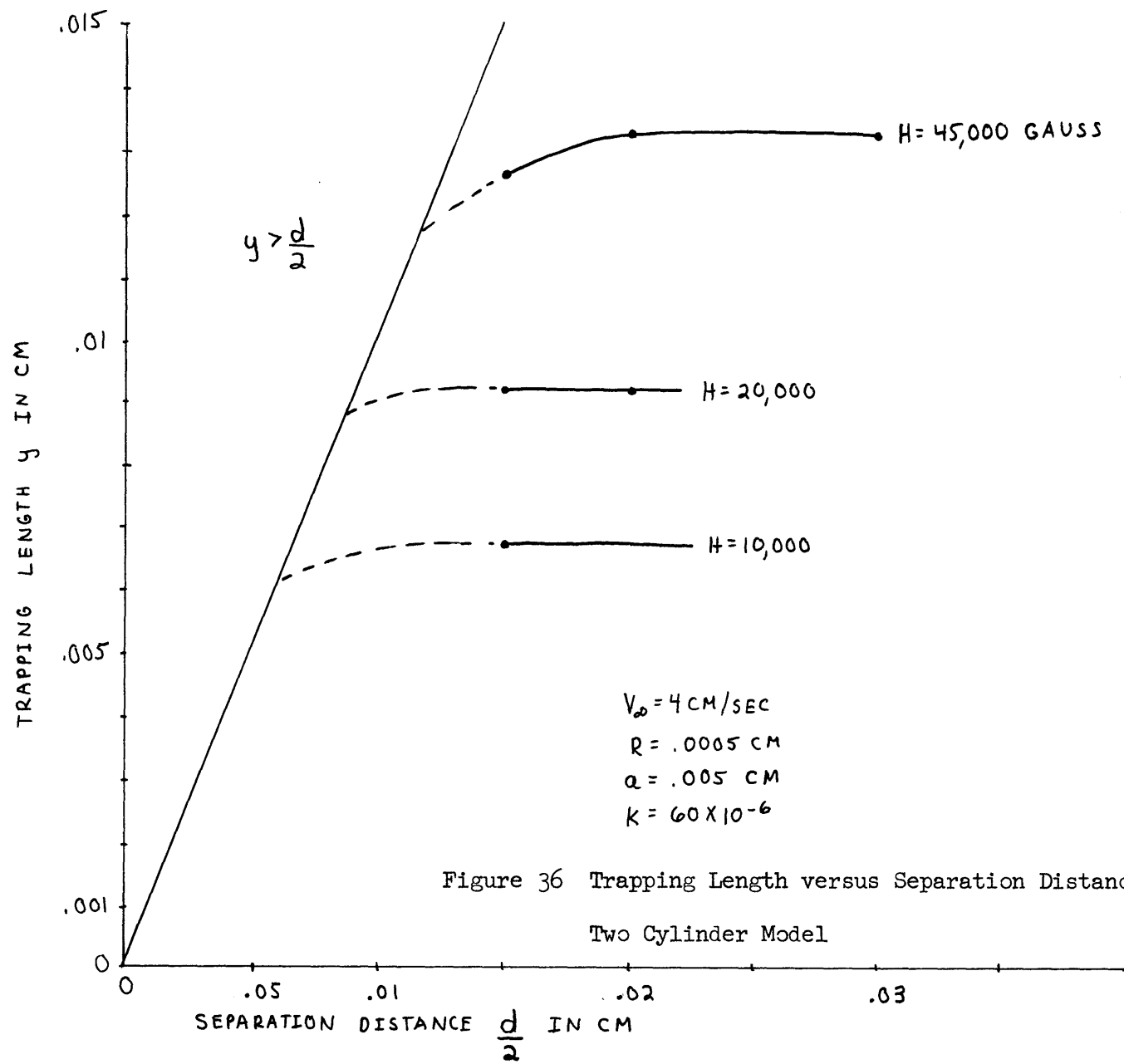
Figure 36 Trapping Length versus Separation Distance for Two Cylinder Model

$V_\infty = 4$ CM/SEC

$R = .0005$ CM

$a = .005$ CM

$k = 60 \times 10^{-6}$

4.2. Experimental Results and Correlation with Mathematical
      Model

Experimental results for most materials were poor.
Tabulated values of molar susceptibility were found to be
quite different from measured values for some of the materials
used; trace impurities, decomposition, or hydration may all
affect material susceptibility. Particle size variations
between materials were large because of different densities
or agglomeration. Only $CO_3(PO_4)_2 \cdot 2H_2O$ gave satisfactory
results. Even for this material, the results seemed very
dependent on the sample injected. This is attributed to small
variations in particle size due to the difficulty in preparing
identical samples by a simple stirring and settling technique.
However, since the particles are about .001 cm in diameter,
the amount of effort necessary to get very uniform particles
would be tremendous.

The data for $CO_3(PO_4)_2 \cdot 2H_2O$ is presented in Figure 37
where y' is the thickness of the build-up or wedge on the
upstream side of the wire and amperes A are used instead of
applied field H (for the magnet used 10 amperes is approximately
5000 gauss and the relationship is linear). Almost all data
fall in the region (of S) where the mathematical model tended
to break down. The average values of y' were used in the
figure. Averaged data may be found in Appendix F. Example
photographs are shown in Figure 38. One should note the for-
mation of a build-up or wedge of particles on the upstream
side. The perception of depth is lost in the photograph, but
an example of the wedge shape is shown in Figure 39.
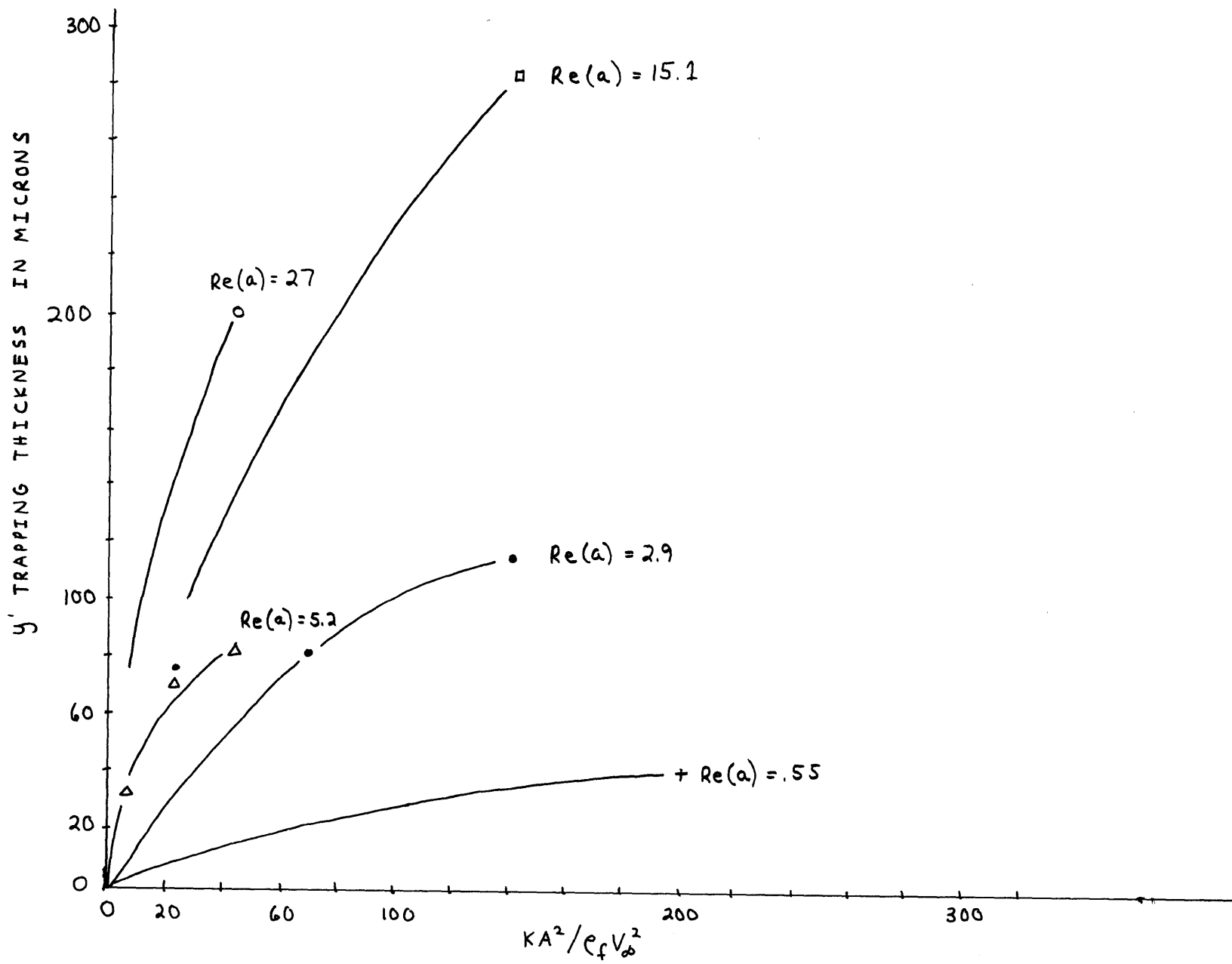
Figure 37 Dimensionless Correlation of Experimental Data
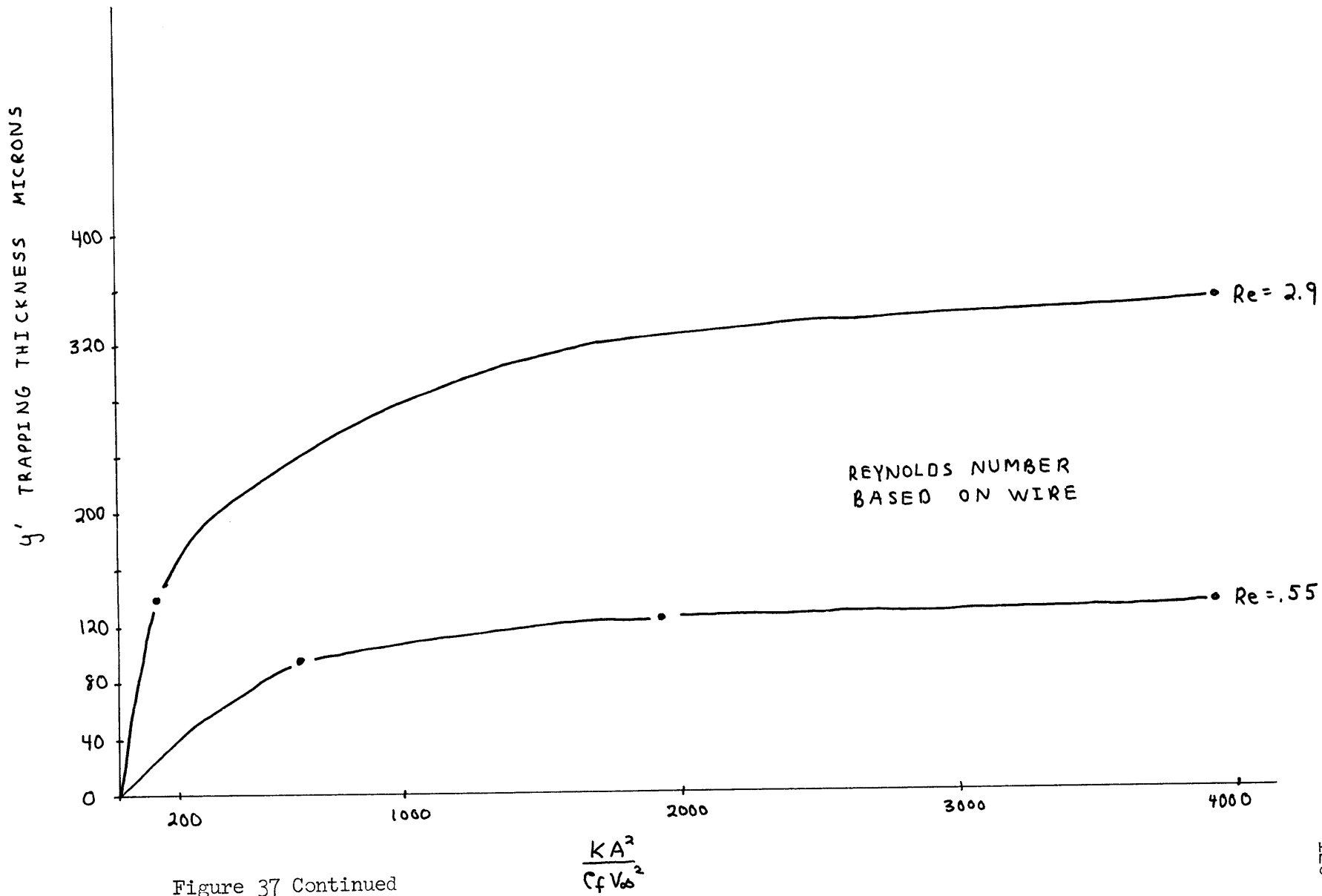
Figure 37 Continued

Figure 38 Pictorial Experimental Results

Flow direction is from left to right

10 amps
$V_\infty = .55$ cm/sec

Bare
Wire
$a = .005$ cm

122

7 amps
$V_d = .55\,cm/sec$

4 amps

$V_d = .55\,cm/sec$

123
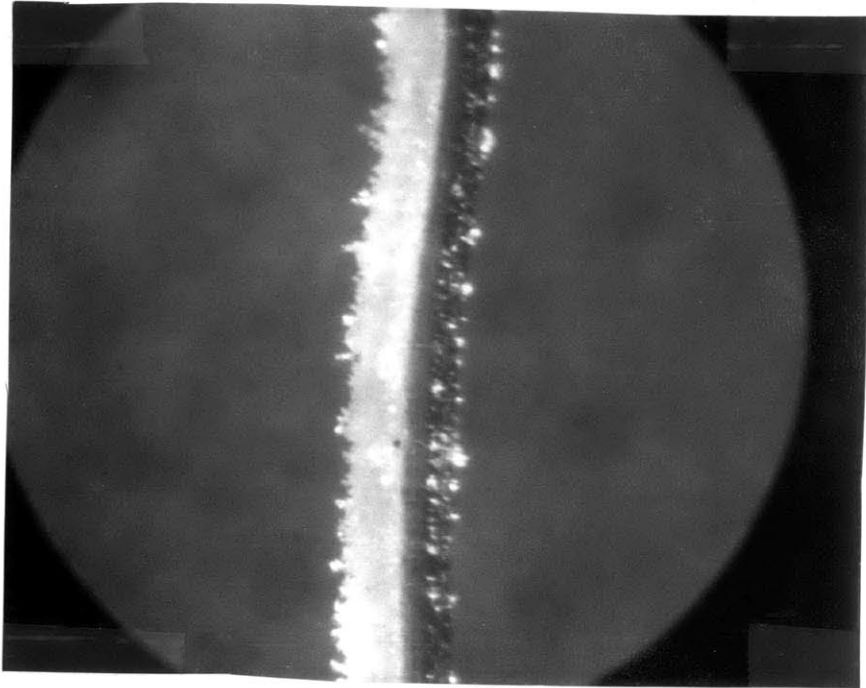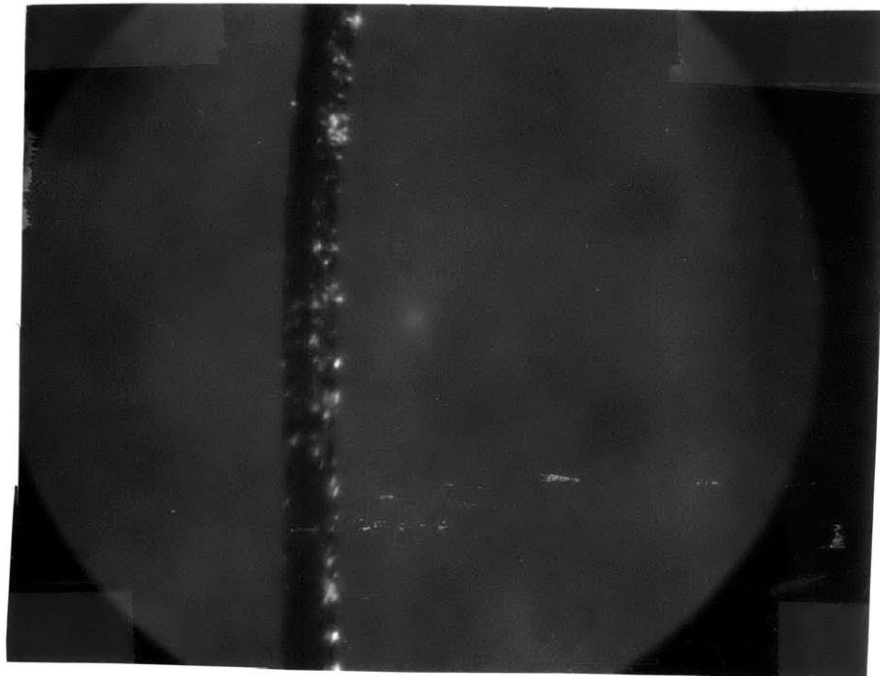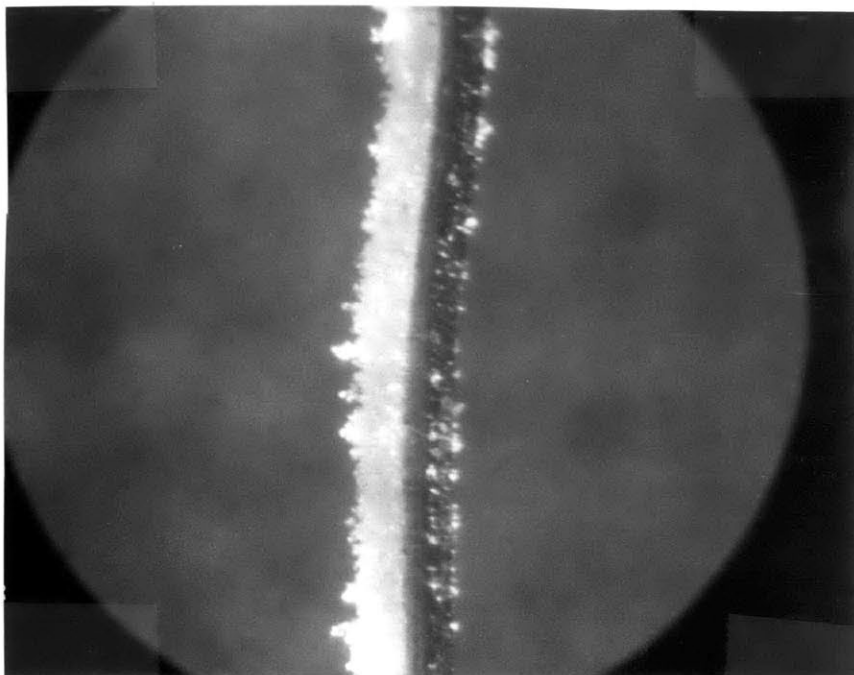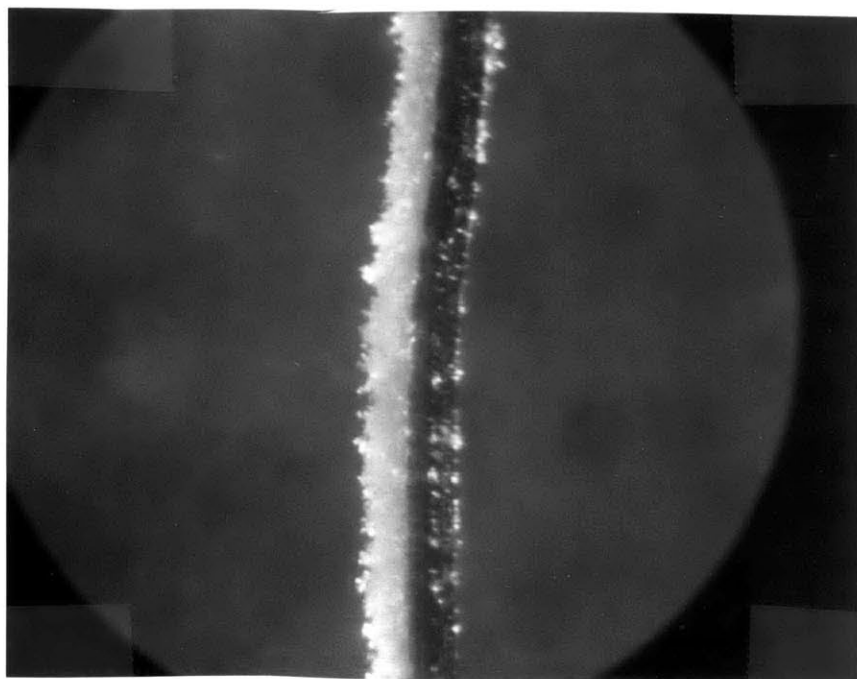
10 amps

$V_b = 2.9\,cm/sec$

$a = .005\,cm$
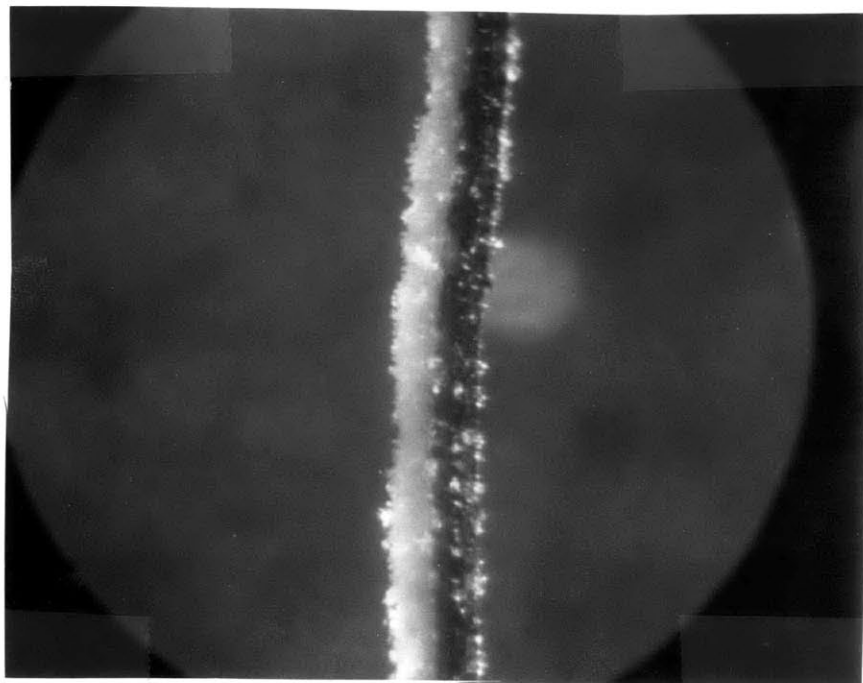
10 amps

$V_b = .55\,cm/sec$

$a = .026\,cm$
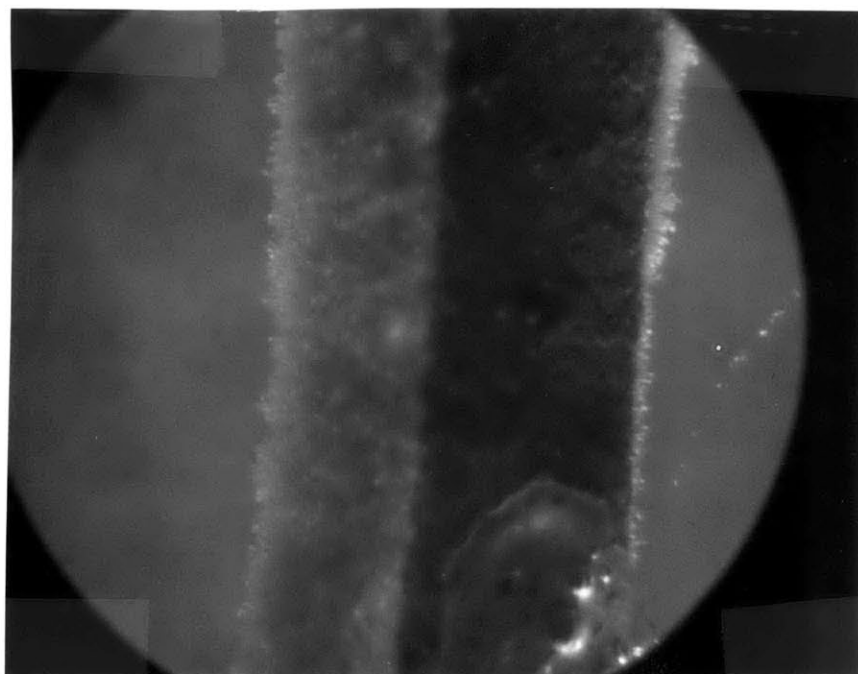
Bare Wire
   a = .026 cm
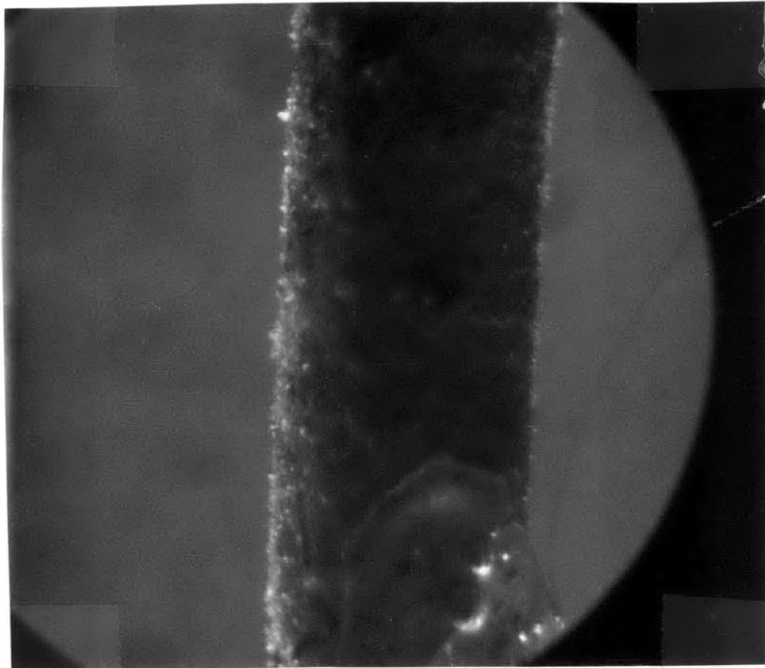
Figure 39   Shape of Particle Build-up on a Wire
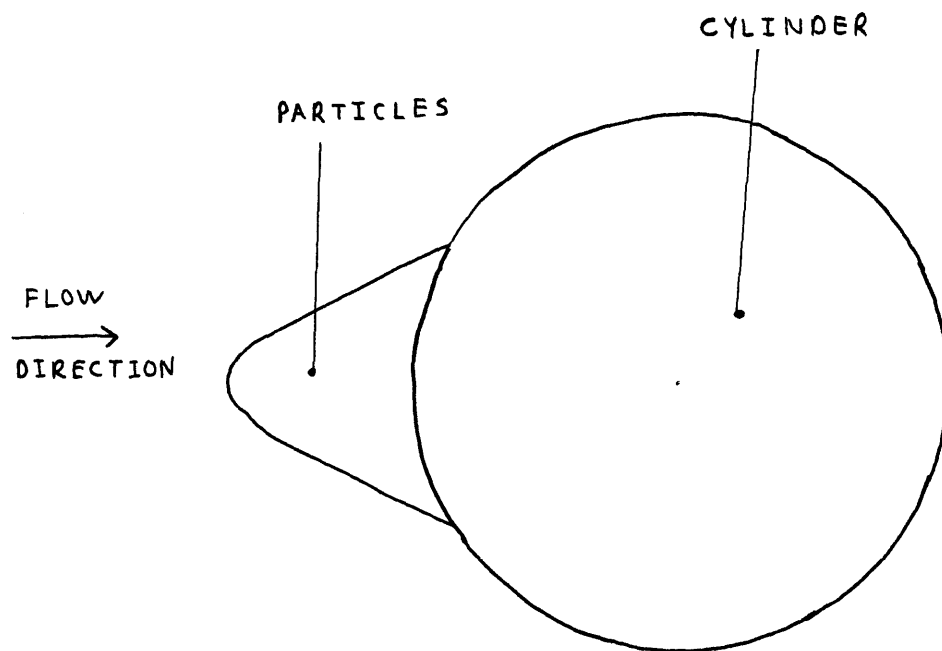
The experimental data confirm the validity of the derived dimensionless correlation for constant particle size. The lines of Reynolds numbers have the same forms with increasing Re(a). The trapping layer or wedge thickness decreases with increasing velocity, decreasing field strength, or decreasing wire radius, although logarithmic plots do not yield the dependence. This is partially due to the change in geometry as a wedge builds up in front of the cylinder.

Note that y' increases with increasing wire size at constant V_∞ and H, as does y with a in the dimensionless correlation, Figure 29. This result suggests that the size of the trapping material used can be optimized with respect to volumetric trapping per cylinder and number of cylinders per unit volume of separator for given operating conditions.

4.3. Other Visual Phenomena

At zero flow velocity and loading the chamber with a large amount of $CO_3(PO_4)_2 \cdot 2H_2O$, an applied field will cause the particles to stick only near the vicinity of the poles (Figures 14b and 40). A useful generalization one can make is that particles tend to be attracted toward the induced poles (ignoring drag forces). A particle will not always procede to a pole because of other particles blocking the way. The shape of the resulting wedge at zero flow indicates where $-F_M \hat{r} > F_M \hat{\theta}$.

At a Reynolds number of 10 - 15 with the large iron wire (a = .026 cm), twin vortices were observable on the downstream side of the cylinder as expected (see Appendix B). Normally,

Figure 40   Shape of Build-up at Zero Flow
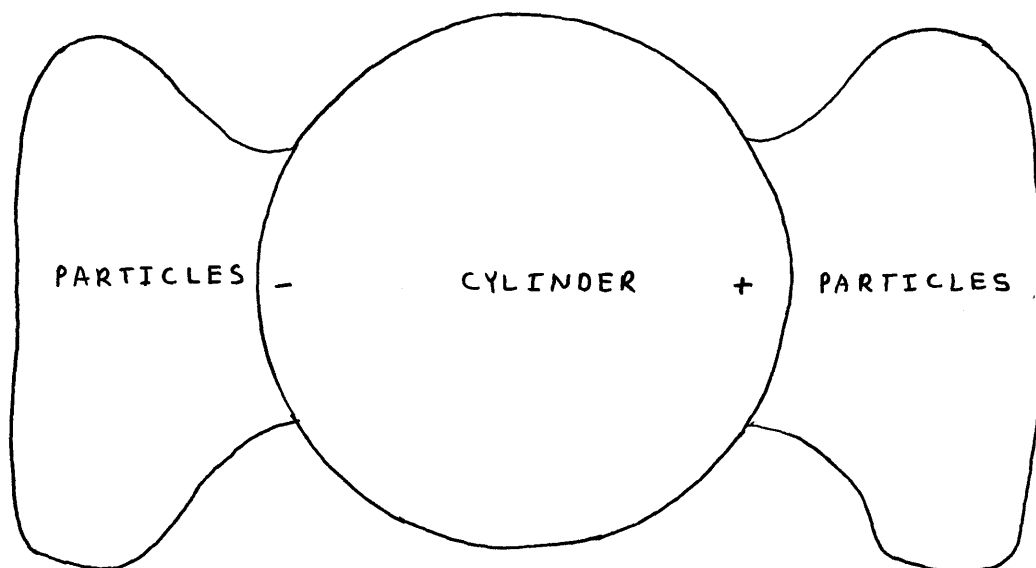
several particles became entrained in the vortices due to the streamlines in the vortex and the magnetic force (particles were released by lowering the applied field). For magnetic separations involving a low concentration of material to be removed, instead of using high fields, one might try to utilize the trapping ability of the vortex.

With applied field on, particles can be "blown" from the front to the back or downstream side of the wire by increasing the flow rate to cause turbulent flow in the chamber. Up to 50% could be transferred. While a poor method in that much is lost or not captured at all, the total capacity of a bed of wires might be increased by running at low flow rate, a turbulent flow rate, then again a low flow rate and use recycle to catch what was lost or didn't trap during the turbulent phase. Also with iron wire, unless the wire is demagnetized well, it is hard to remove all trapped material, since some will just transfer from the upstream to the downstream side with backwashing because of the large permanent magnetization.

Finally, trapping does not occur when flow is parallel to the major axis of the trapping object except at an end. A particle will not stick to a "flat plate" surface because the perpendicular magnetic force (Figure 3b) is not large enough to overcome the drag force except near the extremities. If the long axis is parallel to the magnetic field, these ends become induced poles, and the magnetic gradient and force is quite large. This is illustrated in Figure 41 where both field and flow are parallel to the long axis of the wire.

Figure 41 Trapping for Wedge Form

Flow is from left to right
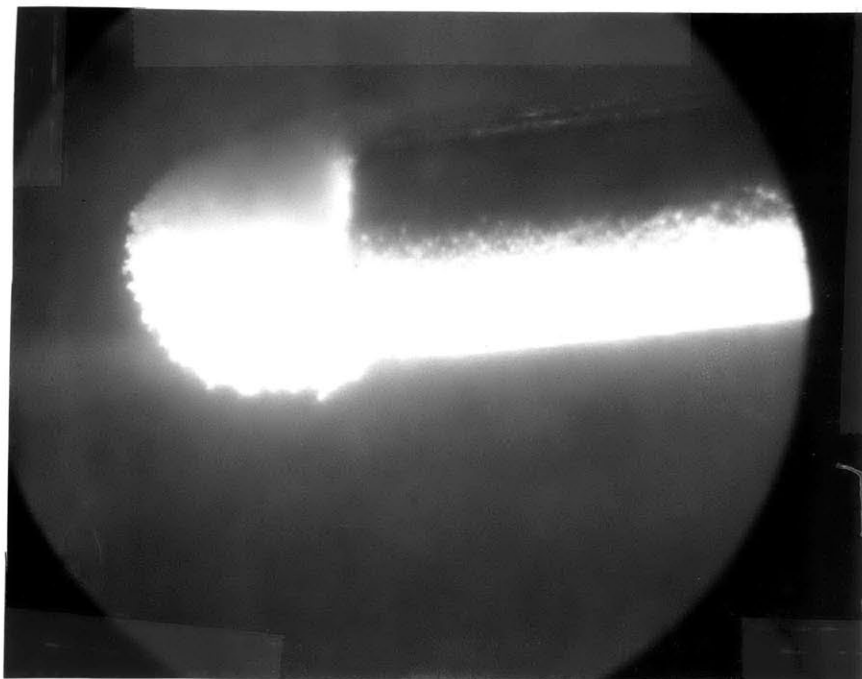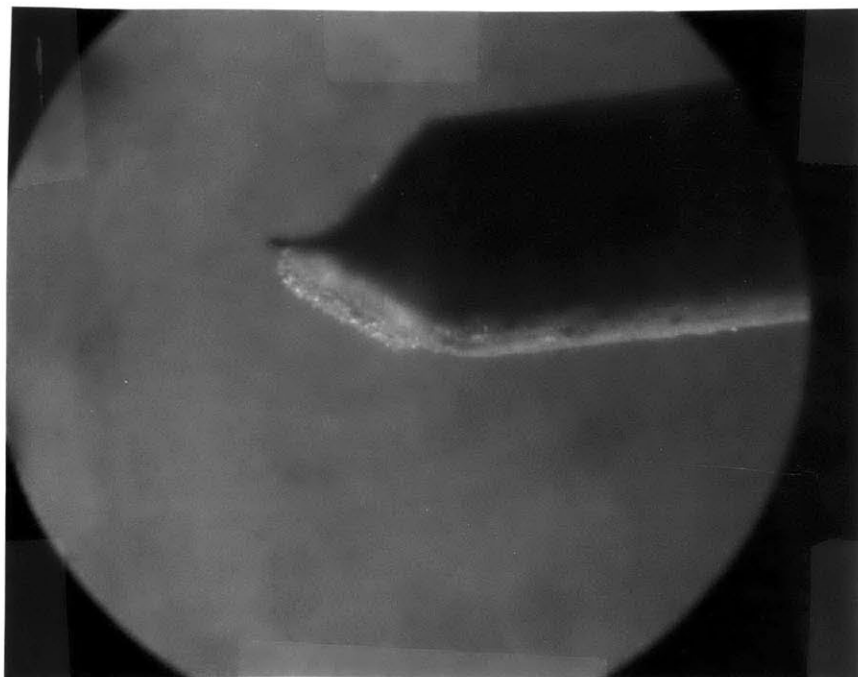
This figure also suggests that a wire containing sharp points, i.e. a barbed or nicked wire, directed in the flow and field direction may be advantageous.

4.4. Macroscopic Predictions of the Cylinder Model and Implications

Assuming that each particle can be described as a point, particles can be assumed to trap when they are within 2y, the trapping length, of a cylinder of diameter 2a, if the particles are initially moving perpendicular to the cylinder and parallel to the applied field. For n cylinders per unit volume arranged as in Figure 42a, the fraction of N particles trapped per length $d\ell$ is:

$$\frac{dN}{N} = -\gamma n\alpha d\ell \tag{76}$$

where α is the effective cross section of the cylinder 2yg (g in the length of the cylinder) and γ is the joint probability of the cylinder being aligned both perpendicular to the field and perpendicular to the initial direction of the particle (Figure 42b). If the probability of capture per length $d\ell$ is small, N does not change much and the expression may be integrated over length L directly.

$$\int_{N_o}^{N(L)} \frac{dN}{N} = -\int_0^L \gamma n 2yg d\ell \tag{77}$$

Letting $n = \frac{1}{efg}$ where e and f are separation distances between cylinders,

$$N(L) = N_o \exp [-2yL\gamma/ef] \tag{78}$$

Figure 42   Diagrams for Macroscopic Model of Cylinders

(42a)

V_∞

H

e

f

g

(42b)

V_∞

H

$\gamma = 1$

$\gamma \neq 1$

$\gamma = 1$

$\gamma \neq 1$
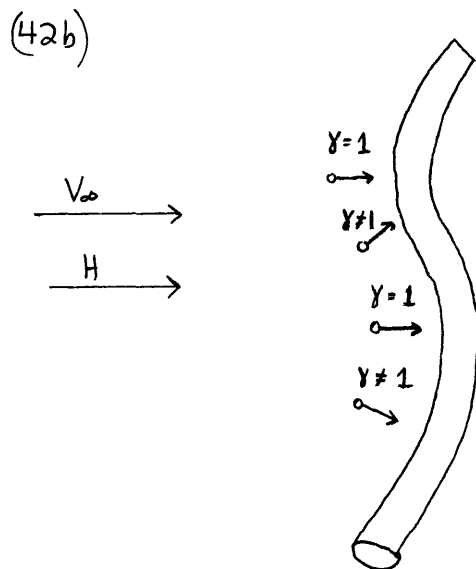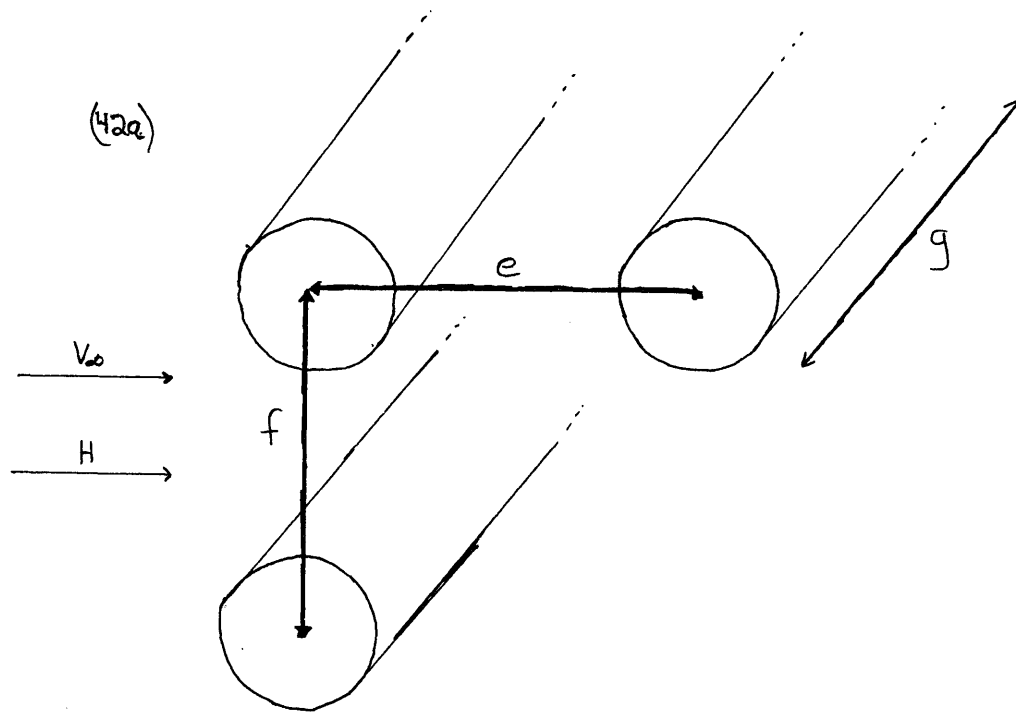
If N_o is the total feed, $N(L)$ is equal to the number of particles passing through the filter. Assuming uniform particle size and density, $N(L)$ and N_o could be expressed in weight or mass.

Going directly to the experimental data of Oberteuffer, et al. (1971) for a case where $V_\infty = 10$ cm/sec, $H = 60,000$ gauss, $K = 20 \times 10^{-6}$, Re(a) $= 10$, and assuming a particle size of .0005 cm, α from Figure 29 is equal to .026 cm^2/cm. Using separation distances $f = e = .04$ cm,

$$N(L) = N_o \exp[-16.25\gamma L] \qquad (79)$$

If $\gamma = 1$ and $L = 15$ cm, for $N_O = 50$ gm, $N(L)$ should be approximately zero while $N(L)$ is actually 10.5 gm. With $\gamma = 1$, L must be less than .1 cm or about 2 cylinders deep. The fraction trapped per length dℓ is not small, invalidating equation (77).

If γ is less than one, L will increase accordingly to produce the actual experimental result, but if the model correctly describes the workings of an actual separator, the separator should be modeled as an adsorber column in which trapping occurs in a series of small zones (Treybal, 1968) until reaching the end of the column. The ease of trapping in each zone is initially high, but falls off as the trapping capacity is filled.

The model of a single particle approaching a cylinder will not give any information about the total number of particles that can be trapped at given operating conditions.

Each particle sees a clean cylinder. To properly describe
bulk trapping at a cylinder, a model which adds trapped par-
ticles into the description would need to be developed, since
the effect of captured particles is to increase the minimum
distance at which the magnetic force can act and to change the
fluid velocity field. A better fluid description than
potential flow is needed, since the no slip condition at the
surface of the wedge becomes important.

One can make an estimate of the maximum amount (by volume)
that can be trapped under given conditions by looking at the
experimental data, although the pictures are only two dimen-
sional. For $H = 5000$ gauss and $V = 2.5$ cm/sec, the maximum
volume available for trapping is approximately 33% of the wire
volume. If 50 grams of steel wool has a density of 7.0 gm/cm^3,
the trapping volume is about 2.3 cm^3. Using a density of 6.0
gm/cm^3 for CuO, one would have a capacity of about 14 grams,
if γ as defined before is equal to one. The actual amount
trapped in the separator (Oberteuffer, et al., 1971) was 52
grams. Some of the additional trapping may be due to mechanical
trapping caused by overlapping wires or wedges. One could
observe trapping on several wires to determine the magnitude
of this effect. However, since photographic evidence obscures
perception of depth, a better approach might be a conventional
breakthrough analysis for different bed lengths.

CHAPTER 5

CONCLUSIONS AND RECOMMENDATIONS

On the basis of the mathematical model, one should model a magnetic separator as an adsorber, since the model predicts much more trapping per unit length of separator than what actually occurs. The length of separator predicted by the model that is required to meet experimental separator results is a short zone. This leads one to expect that in reality, a single cylinder reaches a maximum loading; this is confirmed by experimental evidence. Since the model developed always regards the cylinder as being unloaded, a model which accounts for particles already trapped should be developed to accurately model the maximum loading. The formulation of this model should include a proper boundary layer description of flow and include flow separation, since the current model overestimates drag forces near the surface of the cylinder and neglects backside loading caused by rotational flow. Possible mechanical trapping due to wedge build-up or adjacent wires should be taken into account. Alternatively or jointly, one could study the maximum loading volume phenomena visually or by a breakthrough analysis for different bed lengths.

The model also highlights the effects of variables on trapping ability and suggests how they may be correlated for an actual separator (section 4.1.3). The model predicts that cylinder size can be coupled with fluid velocity to form a Reynolds number, $Re(a)$, indicating that the flow pattern about

the cylinder is the controlling factor in the drag force that must be overcome to hold a particle at the cylinder. The magnetic potential energy (KH^2) and the free stream kinetic energy $(\rho_f V_\infty^2)$ can be paired. The final correlation expresses y/R in terms of $KH^2/\rho_f V_\infty^2$ for values of Re(a) at constant particle radius, R. The stipulation of constant R is necessary, since the magnetic force is dependent on R^3 while the drag force is dependent on R^2. The trapping length y is highly dependent on R.

The model also suggests that a small cylinder is not necessarily better since y/R and the trapping volume per cylinder increase with Re(a) at constant V_∞ and H. However, the volume occupied by the cylinder also increases, decreasing the number of cylinders available. One should be able to optimize the total trapping ability as a function of wire or cylinder size for given operating conditions. One should also be aware that trapping ability is enhanced around a sharp point because of the high field gradient. The sharp point may or may not be advantageous for increasing trapping volume.

Finally, a better description of the magnetic field and magnetic force field about a cylinder has been developed and tested. It predicts a temporary drop in efficiency just above the applied field necessary for saturation for trapping materials saturating at around 20,000 gauss (One should be able to check this result with an actual separator if the saturation properties of the packing are known). Experience gained in the development of this model casts doubt on the use of dipole

analogs to accurately describe magnetic forces. A magnetic force is better described analytically, although the result may be extremely complicated.

LITERATURE CITATIONS

1) Bean, C. P., <u>Bulletin of the American Physics Society</u>, <u>16</u>, 350 (1970).

2) Bird, R. B., Stewart, Warren, and Lightfoot, Edwin, "Transport Phenomena," John Wiley and Sons, New York (1960).

3) Bozorth, Richard M., "Ferromagnetism," Van Nostrand, New York (1951).

4) Chang, Paul K., " Separation of Flow," Pergammon Press, New York (1970).

5) Foex, G., et al, "Constantes Selectionées Diamagnétisme et Paramagnétisme; Relaxation Paramagnétique," Mason et Cie, Paris (1957).

6) Gardini, A., Perona, G., and Sesini, R., <u>Nuclear Engineering and Design</u> (1967),199.

7) Gill, S. J., Malone, C. P., <u>Review of Scientific Instruments</u>, <u>34</u>, 788 (1963).

8) General Electric, "Permanent Magnet Handbook," (1963).

9) Happel and Brenner, "Low Reynolds Number Hydrodynamics," Prentice Hall, Englewood Cliffs, New Jersey (1965).

10) Kaiser, Robert, Colton, Clark, Miskolczy, Gabor, and Mir, Leon, "Water 1971," <u>A.I.Ch.E. Symposium Series</u>.

11) Kays, W. M., "Convective Heat and Mass Transfer," McGraw-Hill, New York (1966).

12) Kelland, D. R., "High Gradient Magnetic Separation Applied to Mineral Benefication," <u>1973 Intermag Conference</u>, Paper #80, Catalog 590,100.

13) Kolm, Maxwell, Oberteuffer, Kelland, deLatour, and Marston, "High Intensity Magnetic Filtration," Magnetism and Magnetic Materials Conference Proceedings, Chicago, 1971.

14) Lorrain, Paul, Corson, Dale, "Introduction to Electromagnetic Fields and Waves," W. H. Freeman, San Francisco (1962).

15) Kinzel and Franks, "Alloys of Iron and Chromium, Vol. II," Alloys of Iron Research Monograph Series, McGraw-Hill, New York (1940).

16) National Magnet Laboratory, 1972 Annual Bulletin, Cambridge, Mass.

17) Oberteuffer, Maxwell, Kolm, Kelland, and deLatour, working paper (1971).

18) Perry, John H., ed., "Chemical Engineer's Handbook," McGraw-Hill, New York (1963).

19) Proudman, Ian and Pearson, J. R. A., Jr. Fluid Mech., 2, 237 (1957).

20) Purcell, E. M., "Electricity and Magnetism," McGraw-Hill, New York (1965).

21) Robertson, James, "Hydrodynamics in Theory and Application," Prentice Hall, Englewood Cliffs, New Jersey (1965).

22) Schlichting, Herman, "Boundary Layer Theory," McGraw-Hill, New York (1968).

23) Schraub, Kline, Henry, Runstadtler, and Littell, ASME Paper No. 64 WA/FE-20.

24) Spielman, Lloyd, Goren, Simon, Env. Science and Tech., 4, 135 (1970).

25) Steckly and Tarr, working paper, MCA, Cambridge, Mass.

26) Stratton, J. A., "Electromagnetic Theory," McGraw-Hill, New York (1941).

27) Treybal, Robert, "Mass Transfer Operations," McGraw-Hill, New York (1968).

28) Trindade, Sergio, "Studies on the Magnetic Demineralization of Coal," Ph.D. thesis, M.I.T., Cambridge, Mass. (1973).

29) Thom, A., Royal Soc. Proc., Ser. A, 141, 651 (1933).

30) Van Dyke, Milton, "Perturbation Methods in Fluid Mechanics," New York Academic Press, New York (1964).

31) Watson, J. H. P., working paper, Corning Co., Corning, New York (1972).

32) Zebel, G., Jr. of Colloid Science, 20, 522 (1965).

NOMENCLATURE

A - amperes

$\overline{A}$ - magnetic potential vector

a - cylinder radius

B - magnitude of magnetic field

$\overline{B}$ - magnetic field vector

B' - induced field = M

b - particle radius

C - friction coefficient

C_{in} - inlet concentration

C_{out} - outlet concentration

d - particle diameter, distance between centers

d_1 - separation distance between cylinders

d_2 - separation distance between cylinders

D_t - tube diameter

e - separation distance between cylinders

F_D - magnitude of drag force

F_G - magnitude of gravitational force

F_L - magnitude of London force

F_M - magnitude of magnetic force

$\overline{F}_D$ - drag force

$\overline{F}_M$ - magnetic force

F_{Mx} - magnetic force in x direction

F_{My} - magnetic force in y direction

g - length of cylinder

$\overline{g}$ - acceleration due to gravity

H   - magnitude of applied field

H_s - applied field necessary for saturation

$\overline{H}$ - applied field

K   - volume susceptibility

K'   - relative volume susceptibility

K_1, K_2, K_3, K_4 - constants for Runge-Kutta integration

L   - total bed length

ℓ - differential bed length

M   - magnitude of magnetization

M_s - saturation magnetization

$\overline{M}$ - magnetization

m   - molecular weight

$\overline{m}$ - magnetic dipole moment

N   - number of particles per unit volume

N_o - initial number of particles per unit volume

n   - number per unit volume

p   - pressure

q   - number of quantities

R   - particle radius

Re   - Reynolds number

r   - radial distance

$\hat{r}$ - unit radial vector

S   - dimensionless group, $KH^2/V_\infty^2 \rho_f$

t   - time

u   - number of fundamental groups

V   - magnitude of velocity

V_∞ - initial or freestream velocity

V_v - volumetric flow rate

v - kinematic viscosity

w - vorticity

X - voids fraction

y - trapping length

y' - trapping thickness

α - effective cross section

β $= [(\mu - 1)/(\mu + 1)] \, a^2$

β' $= \beta H_s/H$

γ - probability of proper alignment

δ - boundary layer thickness, dimensionless

δ' - boundary layer thickness

θ - angle measured from second quadrant

$\hat{\theta}$ - angular polar unit vector

η - viscosity

λ - impact parameter (distance)

μ - magnetic permeability

μ_s - saturation permeability

ρ - density

ρ^* - particle density

ϕ - angle measured from first quadrant

$\hat{\phi}$ - polar angular unit vector

χ_M - molar susceptibility

ψ - streamline function

Appendix A

Definition of Magnetic Dipoles

The definition of a magnetic dipole $\bar{m}$ is $\bar{m}$ = current times area (enclosed by current). In the case of an induced dipole, one must consider an imaginary induced current. For a dipole induced into the cross section of a cylinder, the dipole has the same direction as the inducing field. The imaginary current induced by the field must be perpendicular to the inducing field and the dipole. An imaginary circular current loop perpendicular to the circular cross section of the cylinder but of the same area can be invented (figure A-1). This imaginary current loop must carry current I equal to the induced field $(\mu-1)H$ to give rise to the proper strength dipole. Then

$$\bar{m} = I\pi a^2 \qquad\qquad\qquad (A-1a)$$

$$\bar{m} = (\mu - 1)\bar{H}\pi a^2 \qquad\qquad (A-1b)$$
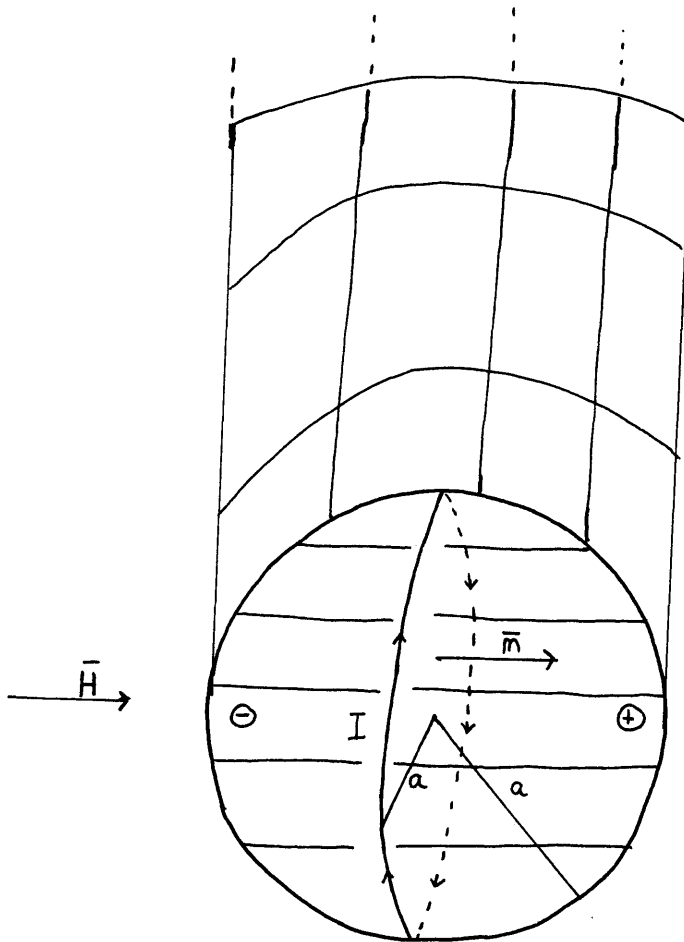
Figure A1   Imaginary Current Loop

Appendix B

Numerical Solutions of the Navier-Stokes Equation

Flow separation is caused by a positive pressure gradient along the flow path of streamline (Chang, 1970). At flows with very small Reynolds numbers (creeping flow), the viscous terms dominate the inertial terms and no separation occurs. At higher Reynolds numbers the boundary layer widens, then separates into two sheets, with reversing flow or vortices occuring between the sheets (figures B-1 and B-2).

For a circular cylinder, at low Reynolds numbers the pressure field satisfies the potential equation and there is no pressure gradient (d' Alembert's paradox). At about at Reynolds number of 10, depending on the proximity of the bounding walls, reverse flow and vortices occur, the point of separation being at $\theta = 80^{\circ}-85^{\circ}$ (figure B-3). At intermediate Reynolds numbers there is a large boundary layer or stagnation region on the downstream side. The twin vortices in figure (B-2) will persist until a Reynolds number of about 100 is reached when von Karmon vortex streets or shedding vortices occur. Other wake forms occur at higher Reynolds numbers, however, since the Reynolds number range of interest is from about 1 to 20, only the case of twin eddy separation need be considered.

Fluid velocity fields at Reynolds numbers above those at which the potential equation holds can be calculated numerically

FLOW SEPARATION
B-1

BOUNDARY
LAYER

FLOW SEPARATION
B-2

BOUNDARY LAYER

ROTATIONAL
FLOW

B-3

SEPARATION
POINT MOVES
FORWARD WITH
INCREASING REYNOLDS
NUMBER

θ
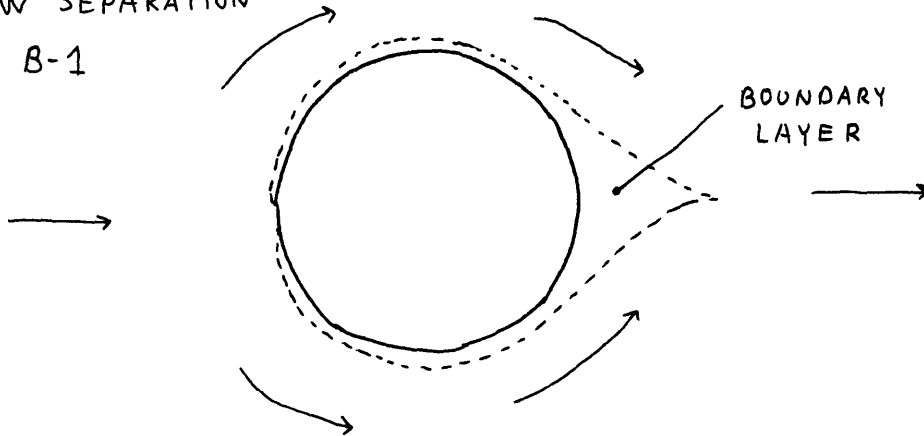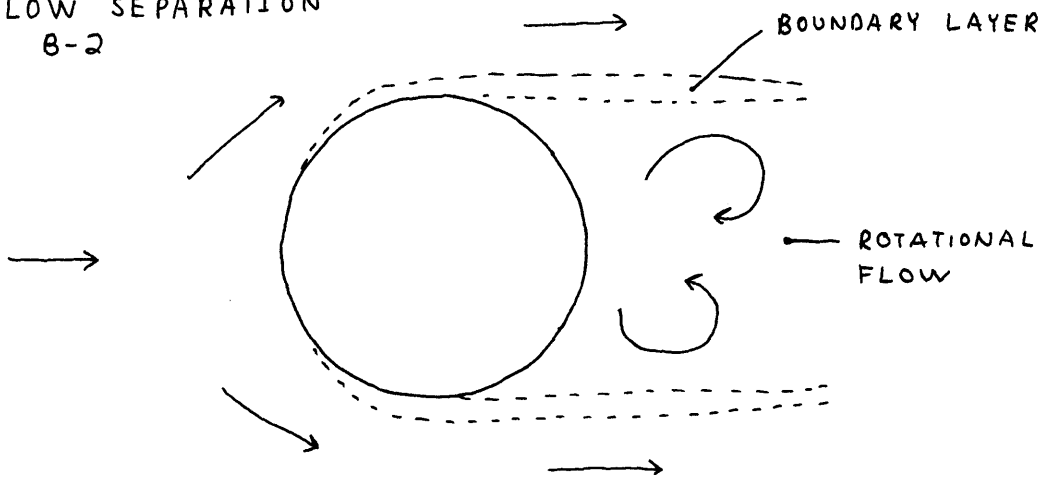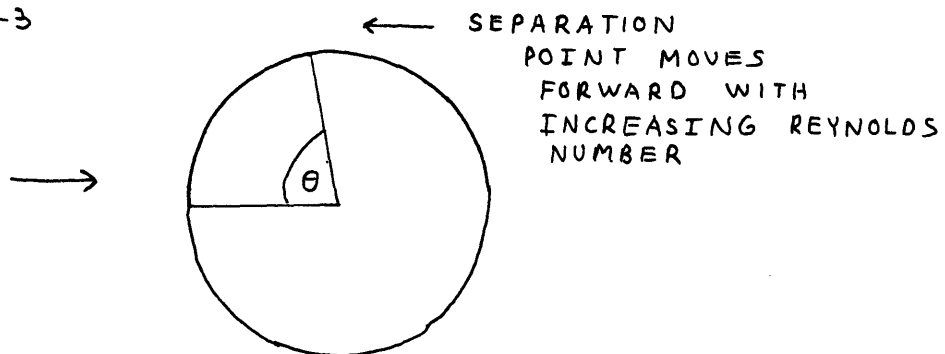
from the Navier-Stokes equation when written in terms of vorticity, $\bar{w}$, transport and a stream function, ψ, (Schlichting, 1968). Let

$$\nabla \times \bar{w} = w = 1/2\left(\frac{\partial Vy}{\partial x} - \frac{\partial Vx}{\partial y}\right) \qquad \text{(B-1)}$$

Then for two dimensional, steady flow equation (33c) becomes

$$Vx \frac{\partial w}{\partial x} + Vy \frac{\partial w}{\partial y} = v\left(\frac{\partial^2 w}{\partial x^2} + \frac{\partial^2 w}{\partial y^2}\right) \qquad \text{(B-2)}$$

Introducing the stream function defined by equations (39a) and (39b), the vorticity in (B-1) may be written as

$$w = -1/2\nabla^2\psi \qquad \text{(B-3)}$$

Then (B-2) becomes

$$\frac{\partial\psi}{\partial y} \frac{\partial\nabla^2\psi}{\partial x} - \frac{\partial\psi}{\partial x} \frac{\partial\nabla^2\psi}{\partial y} = v\nabla^4\psi \qquad \text{(B-4)}$$

The proper boundary conditions at the body surface are

$$\frac{\partial\psi}{\partial x} = \frac{\partial\psi}{\partial y} = 0 \qquad \text{(B-5)}$$

The other boundary condition depends on the free stream conditions.

This procedure was first introduced by Thom (1933) who calculated vortex patterns numerically using finite difference equations to form a grid network. With the advent of computers, the calculations have become much quicker allowing for more detailed grids. A recent compilation of numerical solutions may be found in Physics of Fluids, 12, supplement II.

APPENDIX C

Listing of Computer Programs

```
C     SINGLE CYLINDER MODEL
C
C     VARIABLES LISTED IN ORDER OF APPEARANCE
C     STARTING WITH MAIN PROGRAM
C     H IS THE APPLIED FIELD MAGNITUDE
C     CHI IS THE MOLAR SUSCEPTIBILITY
C     PERM IS THE PERMEABILITY
C     DENS IS THE DENSITY OF THE PARTICLE
C     GMW IS THE MOLECULAR WEIGHT OF THE PARTCLE MATERIAL
C     XLIM AND YLIM ARE TERMINATION LIMITS ON X AND Y POSITION
C     TPRIN IS THE PRINTING INTERVAL, T=1 FOR PRINTING AT EVERY STEP
C     A IS THE CYLINDER RADIUS
C     R IS THE PARTICLE RADIUS
C     VINF IS THE FREESTREAM VELOCITY
C     XO AND YO ARE THE INITIAL COORDINATES OF THE PARTICLE
C     VXO AND VYO ARE THE INITIAL X AND Y VELOCITIES
C     STEP IS THE STEP SIZE FOR THE RUNGE-KUTTA METHOD
C     HS IS THE APPLIED FIELD NECESSARY FOR SATURATION
C     RMASS IS THE MASS OF THE PARTICLE
C     TSTOP IS A MAXIMUM TIME LIMIT
C     DVX AND DVY ARE DERIVATIVE VALUES CALCULATED IN SUBROUTINE DODAH
C     VARIABLES IN SUBROUTINE DODAH
C     RAD IS RADIAL DISTANCE
C     THETA IS ANGLE MEASURED FROM SECOND QUADRANT IN RADIANS
C     WTHET IS THETA IN DEGREES
C     VY IS THE VELOCITY IN THE Y DIRECTION
C     DIFVY IS THE RELATIVE Y VELOCITY
C     REY IS THE FLUID REYNOLDS NUMBER FOR THE Y DIRECTION
C     FDY IS THE DRAG FORCE IN THE Y DIRECTION
C     FMY IS THE MAGNETIC FORCE IN THE Y DIRECTION
C     DVY IS THE DERIVATIVE OF VY W.R.T. TIME
C   VARIABLES SUFFIXED WITH X ARE THE SAME AS THOSE SUFFIXED WITH Y
C    EXCEPT THEY APPLY FOR THE X DIRECTION
C
      SUBROUTINE DODAH
C
C     CALCULATION OF DERIVATIVE FUNCTIONS
C
      COMMON DVX,DVY,X,Y,DENS,RMASS, BETA,CONST,VPX,VPY,VINF,A,R ,THETA
     2  ,HS,H,HCHEK
      RAD=SQRT(X*X+Y*Y)
      PI=3.1415926536
      BEET=BETA*HS/H
C
C     CALCULATION OF ANGLE FROM RECTANGULAR COORDINATES, ANGLE MEASURED
C     FROM SECOND QUADRANT
C
      IF (X) 18,15,18
15     IF (Y) 16,17,17
16    THETA=1.5000*PI
      GO TO 25
17    THETA=.5000*PI
      GO TO 25
18    XX=-X
```

```
       IF(XX) 22,22,19
19     IF(Y) 21,21,20
20     THETA=ATAN(Y/XX)
       GO TO 25
21     THETA=ATAN(Y/XX) + 2.00*PI
       GO TO 25
22     THETA=ATAN(Y/XX) +PI
25     WTHET=THETA/2./ PI     *360.
C
C   CALCULATION OF DRAG FORCE IN Y DIRECTION
C
26     VY=VINF*A*A/RAD/RAD*SIN(2.*THETA)
       DIFVY=ABS(VY-VPY)
31     REY=DIFVY*2.*R/.01
       IF(REY-1.92) 32,33,33
32     FDY=6. *PI     *.01*R*(VY-VPY)
       GO TO 34
33     FDY=18.5*PI*R**2 *ABS(VY-VPY)*(VY-VPY)/REY**.6/2.
C
C   CALCULATION OF MAGNETIC FORCE AND DERIVATIVE IN Y DIRECTION
C
34     IF(HCHEK) 341,341,342
341    FMY=-CONST*2.*BETA/RAD**3*((BETA/RAD/RAD+COS(2.*THETA))*SIN(THETA)
      2  +SIN(2.*THETA)*COS(THETA))
       GO TO 343
342    FMY=-CONST*2.*BETA/RAD**3*((BEET/RAD/RAD+COS(2.*THETA))*SIN(THETA)
      2  +SIN(2.*THETA)*COS(THETA))
343    DVY=FMY/DENS+FDY/RMASS-980.*1.333*3.14159*R**3*(DENS-1.)/RMASS
C
C      CALCULATION OF DRAG FORCE IN X DIRECTION
C
30     VX=VINF*(1.-A*A/RAD/RAD*COS(2.*THETA))
       REX=ABS(VX-VPX)*2.*R/.01
       IF(REX-1.92) 35,40,40
35     FDX=6.* PI     *.01*R*(VX-VPX)
       GO TO 43
40     FDX=18.5*PI*R**2*ABS(VX-VPX)*(VX-VPX)/REX**.6/2.
C
C   CALCULATION OF MAGNETIC FORCE AND DERIVATIVE IN X DIRECTION
C
43     IF(HCHEK) 44,44,45
44     FMX=CONST*2.*BETA/RAD**3*((BETA/RAD/RAD+COS(2.*THETA))*COS(THETA)-
      2  SIN(2.*THETA)*SIN(THETA))
       GO TO 46
45     FMX=CONST*2.*BETA/RAD**3*((BEET/RAD/RAD+COS(2.*THETA))*COS(THETA)-
      2  SIN(2.*THETA)*SIN(THETA))
46     DVX=FMX/DENS+FDX/RMASS
       RETURN
       END
C
C   MAIN PROGRAM
C
       REAL K1X,K2X,K3X,K4X,K1Y,K2Y,K3Y,K4Y
       COMMON DVX,DVY,X,Y,DENS,RMASS, BETA,CONST,VPX,VPY,VINF,A,R,THETA
```

```
   2   ,HS,H,HCHEK
C
C     INITIALIZATION OF VARIABLES
C
1       READ(5,1000) H,CHI,PERM,DENS,GMW,XLIM,YLIM,TPRIN
1000    FORMAT(8F10.5)
        IF(H) 100,100,3
 3      READ(5,1000) A,R,VINF,XO,YO,VXO,VYO,STEP
        WRITE(6,1001) H,CHI,PERM,DENS,GMW,A,R,VINF
        READ(5,1000) HS
        WRITE(6,1009) HS
        WRITE(6,1002) XO,YO,VXO,VYO,STEP
        IF ( H-HS) 305,306,306
305     CONST=H*H*CHI*DENS/GMW
        HCHEK=0.0
        GO TO 4
306     CONST=H*HS*CHI*DENS/GMW
        HCHEK=1.0
4       X=XO
        Y=YO
        PMASS=4./3.*3.1415926536*R**3*DENS
        BETA=(PERM-1.)/(PERM+1.)*A*A
        TSTOP=(XLIM-XO)/VINF
        TIME=0.0
        PRIN=0.0
        CHECK=0.0
        VPX=VXO
        VPY=VYO
5       VPXO=VPX
        VPYO=VPY
C
C     FIRST R-K STEP
C
        XO=X
        YO=Y
        CALL DODAH
        K1X=STEP*DVX
        K1Y=STEP*DVY
C
C     SECOND R-K STEP
C
        VPX=VPXO+K1X/2.
        VPY=VPYO+K1Y/2.
        TIME=TIME+STEP/2.
        X=XO+VPX*STEP/2. + DVX*(STEP/2.)**2/2.
        Y=YO+VPY*STEP/2. + DVY*(STEP/2.)**2/2.
        CALL DODAH
        K2X=STEP*DVX
        K2Y=STEP*DVY
C
C     THIRD R-K STEP
C
        VPX=VPXO+K2X/2.
        VPY=VPYO+K2Y/2.
```

```
      X=XO+VPX*STEP/2. + DVX*(STEP/2.)**2/2.
      Y=YO+VPY*STEP/2. + DVY*(STEP/2.)**2/2.
      CALL DODAH
      K3X=STEP*DVX
      K3Y=STEP*DVY
C
C     FOURTH R-K STEP
C
      VPX=VPXO+K3X
      VPY=VPYO+K3Y
      TIME=TIME+STEP/2.
      PRIN=PRIN+1.
      X=XO+VPX*STEP+.5*DVX*STEP**2
      Y=YO+VPY*STEP+.5*DVY*STEP**2
      CALL DODAH
      K4X=STEP*DVX
      K4Y=DVY*STEP
      VPX=VPXO+(K1X+2.*K2X+2.*K3X+K4X)/6.
      VPY=VPYO+(K1Y+2.*K2Y+2.*K3Y+K4Y)/6.
      X=XO+VPX*STEP*1.5
      Y=YO+VPY*STEP*1.5
C
C     CHECK FOR COLLISION WITH CYLINDER
C
      IF((SQRT(X*X+Y*Y)-A)- R) 90,90,14
C
C     RESET OF Y TO AVOID UNDERFLOW
C
14    IF( ABS(Y) -1.0E-20 ) 141,141,15
141    Y=0.0
15    IF(TPRIN-PRIN) 20,20,205
20    WRITE(6,1003) X,Y,VPX,VPY,TIME
      PRIN=0.0
C
C     CHECK AGAINST REGION LIMITS
C
205   IF(XLIM-X) 25,25,21
21     IF(YLIM-ABS(Y)) 25,25,35
25    WRITE(6,1005) X,Y,VPX,VPY,TIME
      GO TO 1
C
C     CHECK AGAINST MAXIMUM TIME ALLOWED
C
35    IF(TIME-TSTOP) 5,5,45
45    WRITE(6,1006) X,Y,VPX,VPY,TIME
      GO TO 1
90    IF (CHECK) 91,91,92
91    WRITE(6,1004) X,Y,VPX,VPY,TIME
      CHECK=1.0
92    IF( THETA-.5*3.14159) 93,96,96
93    IF(VPY) 94,95,95
94    WRITE(6,1008) X,Y,VPX,VPY,TIME
      GO TO 1
95    X=-(A+R)*COS(THETA)
```

```
       Y=(A+R)*SIN(THETA)
       PRIN=0.0
       GO TO 5
96     IF(VPX) 97,95,95
97     WRITE(6,1007) X,Y,VPX,VPY,TIME
       GO TO 1
1001   FORMAT(1H1,6X,'H          CHI',8X,'PERM',8X,'DENS',8X,'GMW',8X,
      2 'A',7X,'R',9X,'VINF'// E10.2,E12.4,E10.2,2E12.3,3E10.3//)
1002    FORMAT(6X,'XO',8X,'YO',8X,'VXO',8X,'VYO',8X,'STEP'// 2F10.5,
      2  2F11.5,F12.6 ////6X,'X',9X,'Y',9X,'VX',9X,'VY',9X,'TIME',
      3  9X,'X',14X,'Y',14X,'VX',13X,'VY' //)
1003   FORMAT(2F10.5,2F11.5,F12.6,4E15.5)
1004    FORMAT(' PARTICLE AT CYLINDER' / 2F10.5,2F11.5,F12.6)
1005   FORMAT(' PARTCLE PAST CYLINDER'/ 2F10.5,2F11.5,F12.6)
1006    FORMAT(' TIME LIMIT EXCEEDED' / 2F10.5,2F11.5,F12.6)
1007   FORMAT(' BACKSIDE CAPTURE'/ 2F10.5,2F11.5,F12.6)
1008    FORMAT(' FRONTSIDE CAPTURE'/ 2F10.5,2F11.5,F12.6)
1009   FORMAT(' SATURATION MAGNETIZATION=',E10.2 //)
100    CALL EXIT
       END
```

```
C                                                                   154
C      LISTING OF TWO CYLINDER PROGRAM
C
C      ADDITIONAL VARIABLES ARE
C      D= DISTANCE BETWWEN THE ACTUAL CYLINDER AND IMAGINARY CYLINDER
C      THE SUFFIX ONE INDICATES THE VARIABLE IS BEING MEASURED FROM THE
C      ACTUAL CYLINDER
C      THE SUFFIX 2 INDICATES THE VARIABLE IS MEASURED FROM THE ADDITIONAL
C      MAGNETIC SOURCE
C      PROGRAM IS ESSENTIALLY THE SAME AS THE SINGLE CYLINDER MODEL
C      DIFFERENCES IN THE MAIN PROGRAM ARE INDICATED BY ***
C
C      SUBROUTINE DEDAH IS TO FIND ANGLE THETA
C
       SUBROUTINE DEDAH
       COMMON DVX,DVY,X,Y,DENS,RMASS, BETA,CONST,VPX,VPY,VINF,A,R ,THETA
      2  ,HS,H,HCHEK,D,PI
       IF (X) 18,15,18
15      IF (Y) 16,17,17
16     THETA=1.5000*PI
       GO TO 25
17     THETA=.5000*PI
       GO TO 25
18     XX=-X
       IF(XX) 22,22,19
19      IF(Y) 21,21,20
20     THETA=ATAN(Y/XX)
       GO TO 25
21     THETA=ATAN(Y/XX) + 2.00*PI
       GO TO 25
22     THETA=ATAN(Y/XX) +PI
25     WTHET=THETA/2./ PI      *360.
       RETURN
       END
C
       SUBROUTINE DODAH
C
       COMMON DVX,DVY,X,Y,DENS,RMASS, BETA,CONST,VPX,VPY,VINF,A,R ,THETA
      2  ,HS,H,HCHEK,D,PI
       RAD1=SQRT(X*X+Y*Y)
       RAD=RAD1
       RAD2=SQRT(X*X+(D-Y)**2)
       PI=3.14159
       REFT=BETA*HS/H
       CALL DEDAH
       THET1=THETA
       YKEEP=Y
       Y=Y-D
       CALL DEDAH
       THET2=THETA
       Y=YKEEP
       THETA=THET1
       VY=VINF*A*A/RAD/RAD*SIN(2.*THET1)
       DIFVY=ABS(VY-VPY)
```

```
31      REY=DIFVY*2.*R/.01
        IF(REY-1.92) 32,33,33
32      FDY=6. *PI      *.01*R*(VY-VPY)
        GO TO 34
33      FDY=18.5*PI*R**2 *ABS(VY-VPY)*(VY-VPY)/REY**.6/2.
34      IF(HCHEK) 341,341,342
341     FMY1=-CONST*2.*BETA/RAD1**3*((BETA/RAD1/RAD1+COS(2.*THET1))*
       2 SIN(THET1) + SIN(2.*THET1)*COS(THET1))
        FMY2=-CONST*2.*BETA/RAD2**3*((BETA/RAD2/RAD2+COS(2.*THET2))*
       2 SIN(THET2) + SIN(2.*THET2)*COS(THET2))
        GO TO 343
342     FMY1=-CONST*2.*BETA/RAD1**3*((BEET/RAD1/RAD1+COS(2.*THET1))*
       2 SIN(THET1) + SIN(2.*THET1)*COS(THET1))
        FMY2=-CONST*2.*BETA/RAD2**3*((BEET/RAD2/RAD2+COS(2.*THET2))*
       2 SIN(THET2) + SIN(2.*THET2)*COS(THET2))
343     DVY=FMY1/DENS+FMY2/DENS+FDY/RMASS-980.*1.333*PI*R**3*(DENS-1.)
       2 /RMASS
30      VX=VINF*(1.-A*A/RAD/RAD*COS(2.*THET1))
        REX=ABS(VX-VPX)*2.*R/.01
        IF(REX-1.92) 35,40,40
35      FDX=6.* PI      *.01*R*(VX-VPX)
        GO TO 43
40      FDX=18.5*PI*R**2*ABS(VX-VPX)*(VX-VPX)/REX**.6/2.
43      IF(HCHEK) 44,44,45
44      FMX1=CONST*2.*BETA/RAD1**3*((BETA/RAD1/RAD1+COS(2.*THET1))*
       2 COS(THET1)-SIN(2.*THET1)*SIN(THET1))
        FMX2=CONST*2.*BETA/RAD2**3*((BETA/RAD2/RAD2+COS(2.*THET2))*
       2 COS(THET2)-SIN(2.*THET2)*SIN(THET2))
        GO TO 46
45      FMX1=CONST*2.*BETA/RAD1**3*((BEET/RAD1/RAD1+COS(2.*THET1))*
       2 COS(THET1)-SIN(2.*THET1)*SIN(THET1))
        FMX2=CONST*2.*BETA/RAD2**3*((BEET/RAD2/RAD2+COS(2.*THET2))*
       2 COS(THET2)-SIN(2.*THET2)*SIN(THET2))
46      DVX=FMX1/DENS+FMX2/DENS+FDX/RMASS
        RETURN
        END
C
C    MAIN PROGRAM
C
        REAL K1X,K2X,K3X,K4X,K1Y,K2Y,K3Y,K4Y
        COMMON DVX,DVY,X,Y,DENS,RMASS, BETA,CONST,VPX,VPY,VINF,A,R,THETA
       2 ,HS,H,HCHEK,D,PI
1       READ(5,1000) H,CHI,PERM,DENS,GMW,XLIM,YLIM,TPRIN
1000    FORMAT(8F10.5)
        IF(H) 100,100,3
3       READ(5,1000) A,R,VINF,XO,YO,VXO,VYO,STEP
        WRITE(6,1001) H,CHI,PERM,DENS,GMW,A,R,VINF
C    ***
        READ(5,1000) HS,D
C    ***
        WRITE(6,1009) HS
C    ***
        WRITE(6,1010) D
C    ***
```

```
         WRITE(6,1002) XO,YO,VXO,VYO,STEP
C    ***
         IF ( H-HS) 305,306,306
305      CONST=H*H*CHI*DENS/GMW
         HCHEK=0.0
         GO TO 4
306      CONST=H*HS*CHI*DENS/GMW
         HCHEK=1.0
C    ***
4        X=XO
         Y=YO
         RMASS=4./3.*3.1415926536*R**3*DENS
         BETA=(PERM-1.)/(PERM+1.)*A*A
         TSTOP=(XLIM-XO)/VINF
         TIME=0.0
         PRIN=0.0
         CHECK=0.0
         VPX=VXO
         VPY=VYO
5        VPXO=VPX
         VPYO=VPY
         XO=X
         YO=Y
         CALL DODAH
         K1X=STEP*DVX
         K1Y=STEP*DVY
         VPX=VPXO+K1X/2.
         VPY=VPYO+K1Y/2.
         TIME=TIME+STEP/2.
         X=XO+VPX*STEP/2. + DVX*(STEP/2.)**2/2.
         Y=YO+VPY*STEP/2. + DVY*(STEP/2.)**2/2.
         CALL DODAH
         K2X=STEP*DVX
         K2Y=STEP*DVY
         VPX=VPXO+K2X/2.
         VPY=VPYO+K2Y/2.
         X=XO+VPX*STEP/2. + DVX*(STEP/2.)**2/2.
         Y=YO+VPY*STEP/2. + DVY*(STEP/2.)**2/2.
         CALL DODAH
         K3X=STEP*DVX
         K3Y=STEP*DVY
         VPX=VPXO+K3X
         VPY=VPYO+K3Y
         TIME=TIME+STEP/2.
         PRIN=PRIN+1.
         X=XO+VPX*STEP+.5*DVX*STEP**2
         Y=YO+VPY*STEP+.5*DVY*STEP**2
         CALL DODAH
         K4X=STEP*DVX
         K4Y=DVY*STEP
         VPX=VPXO+(K1X+2.*K2X+2.*K3X+K4X)/6.
         VPY=VPYO+(K1Y+2.*K2Y+2.*K3Y+K4Y)/6.
         X=XO+VPX*STEP*1.5
         Y=YO+VPY*STEP*1.5
```

```
        IF((SQRT(X*X+Y*Y)-A)- R) 90,90,14
14      IF( ABS(Y) -1.0E-20 ) 141,141,15
141      Y=0.0
15      IF(TPRIN-PRIN) 20,20,205
20      WRITE(6,1003) X,Y,VPX,VPY,TIME
        PRIN=0.0
205     IF(XLIM-X) 25,25,21
21       IF(YLIM-ABS(Y)) 25,25,35
25      WRITE(6,1005) X,Y,VPX,VPY,TIME
        GO TO 1
35      IF(TIME-TSTOP) 5,5,45
45      WRITE(6,1006) X,Y,VPX,VPY,TIME
        GO TO 1
90      IF (CHECK) 91,91,92
91      WRITE(6,1004) X,Y,VPX,VPY,TIME
        CHECK=1.0
92      IF( THETA-.5*3.14159) 93,96,96
93      IF(VPY) 94,95,95
94      WRITE(6,1008) X,Y,VPX,VPY,TIME
        GO TO 1
95      X=-(A+R)*COS(THETA)
        Y=(A+R)*SIN(THETA)
        PRIN=0.0
        GO TO 5
96      IF(VPX) 97,95,95
97      WRITE(6,1007) X,Y,VPX,VPY,TIME
        GO TO 1
1001    FORMAT(1H1,6X,'H         CHI',8X,'PERM',8X,'DENS',8X,'GMW',8X,
     2  'A',7X,'R',9X,'VINF'// E10.2,E12.4,E10.2,2E12.3,3E10.3//)
1002     FORMAT(6X,'XO',8X,'YO',8X,'VXO',8X,'VYO',8X,'STEP'// 2F10.5,
     2   2F11.5,F12.6 ////6X,'X',9X,'Y',9X,'VX',9X,'VY',9X,'TIME',
     3   9X,'X',14X,'Y',14X,'VX',13X,'VY' //)
1003    FORMAT(2F10.5,2F11.5,F12.6,4E15.5)
1004     FORMAT(' PARTICLE AT CYLINDER' / 2F10.5,2F11.5,F12.6)
1005    FORMAT(' PARTCLE PAST CYLINDER'/ 2F10.5,2F11.5,F12.6)
1006     FORMAT(' TIME LIMIT EXCEEDED' / 2F10.5,2F11.5,F12.6)
1007    FORMAT(' BACKSIDE CAPTURE'/ 2F10.5,2F11.5,F12.6)
1008     FORMAT(' FRONTSIDE CAPTURE'/ 2F10.5,2F11.5,F12.6)
1009    FORMAT(' SATURATION MAGNETIZATION=',E10.2 //)
1010     FORMAT(' SEPARATION DISTANCE BETWEEN CYLINDERS=',E12.4 //)
100     CALL EXIT
        END
```

APPENDIX D

Results of Computer Cases

For all cases μ_S = 10., ρ^* = 3.0 gm/ cm^3 (except case 9),

and H_S = 10,000 gauss (except case 5 where H_S = 20,000 gauss).

If parameters are not indicated, they remain the same as last listed.

Case	H(gauss)	K x10^6	a (cm)	R (cm)	V_∞ (cm/sec)	y (cm) ± 2.5%
5A	5000	60	.005	.0005	4	.003075
5B	15,000					.0098
5C	10,000					.00675
5D	20,000					.01275
5E	30,000					.01125
5F	45,000					.01325
5G	70,000					.01575
5H	100,000					.0177
5I	25,000					.01
5J	35,000					.012
8A	10,000	60	.005	.0005	4	.00675
8B	15,000					.00815
8C	20,000					.00915
8D	12,500					.00745
8E	17,500					.00867
8F	30,000					.011
8G	45,000					.01325

Case	H(gauss)	K x10^6	a (cm)	R (cm)	V$_\infty$ (cm/sec)	y (cm) ± 2.5%
11A	12,000	60	.005	.0005	8	.0047
11B	15,000					.0053
11C	20,000					.00625
11D	30,000					.008
11E	60,000					.01125
11F	100,000					.01375
11G	8,000					.003375
12A	15,000	30	.005	.0005	2	.0083
12B	20,000					.0093
12C	30,000					.01125
12D	5,000					.00308
12E	10,000					.00665
13B	10,000	60	.005	.0005	12	.00312
13C	20,000					.0049
13D	30,000					.00615
13E	45,000					.00782
13F	70,000					.00975
13G	100,000					.01175
14A	10,000	40	.005	.0005	4	.00538
14B	15,000					.00645
14C	20,000					.0075
14D	30,000					.0091

Case	H(gauss)	$K \times 10^6$	a (cm)	R (cm)	V_∞ (cm/sec)	y (cm) ± 2.5%
14E	10,000	20	.005	.0005	4	.00371
14F	15,000					.0042
14G	20,000					.00492
14H	30,000					.00635
14I	40,000					.00732
15A	5,000	60	.005	.00025	4	none
15B	10,000					.00307
15C	20,000					.004
15D	30,000					.00518
16A	5,000	60	.0025	.0005	4	.00225
16B	10,000					.00487
16C	20,000					.00645
16D	30,000					.00748
16E	50,000					.00932
17A	4,000	60	.01	.0005	4	.00322
17B	10,000					.00925
17C	20,000					.0129
17D	30,000					.01612

Case	H(gauss)	K x10^6	a (cm)	R (cm)	V$_\infty$ (cm/sec)	y (cm) ± 2.5%
18A	10,000	60	.01	.00025	4	.0042
18B	20,000					.00377
18C	30,000					.00587
19A	10,000	60	.0025	.00025	4	.00225
19B	20,000					.00322
19C	30,000					.00391
20A	10,000	60	.005	.00015	4	.00172
20B	20,000					none
20C	30,000					.00158
20D	10,000	60	.01	.00015	4	.00215
20E	20,000					.00215
20F	30,000					none
20G	10,000	60	.0025	.00015	4	.00125
20H	20,000					.00145
20I	30,000					.00195
21A	3,000	15	.005	.0005	1	none
21B	5,000					.00368
21C	7,000					.0049
21D	10,000					.00705
21E	15,000					.0085

CASE 9

H = 10,000 gauss   R = .0005 cm

K = 60 x 10^{-6} V_∞ = 4 cm/sec

a = .005 cm

Case	$\rho*$ gm/cm^3	y ± 2.5%	Case	$\rho*$ gm/cm^3	y ± 2.5%
9A	6.0	.00705	9E	4.0	.00685
9B	3.0	.00685	9F	12.0	.00735
9C	2.0	.00685	9G	8.0	.00705
9D	1.0	.00685			

CASE 22

H = 10,000 gauss   R = .0005 cm

K = 60 x 10^{-6} V_∞ = 4 cm/sec

a = .005 cm

Case	d (cm)	y (cm) ± 2.5%
--	∞	.00685
22A	.03	.00685
22B	.02	.00615

CASE 23

H = 20,000 gauss   R = .0005 cm

K = 60 x 10^{-6} V_∞ = 4 cm/sec

a = .005 cm

Case	d (cm)	y (cm) ± 2.5 %	Case	d (cm)	y (cm) ± 2.5%
--	∞	.0092	23B	.03	.0092
23A	.04	.0092	23C	.02	to other

CASE 24   H = 45,000 gauss   R = .0005 cm

K = 60 x 10^{-6} V_∞ = 4 cm/sec

a = .005 cm

Case	d (cm)	y (cm) ± 2.5%	Case	d (cm)	y (cm) ± 2.5%
--	∞	.01325	24C	.03	.01267
24A	.06	.01325	24D	.02	to other cylinder
24B	.04	.01325			

CASE 25   H = 100,000 gauss   R = .0005 cm

K = 60 x 10^{-6} V_∞ = 4 cm/sec

a = .005 cm

Case	d (cm)	y (cm) ± 2.5%	Case	d (cm)	y (cm) ± 2.5%
--	∞	.01825	25E	.04	.01755
25C	.1	.01825	25F	.03	to other cylinder
25 D	.06	.01825			

Appendix E - Recognition of Dimensionless Groups

Buckingham's Pi theorem states "the functional relationship among q quantities,whose units may be given in terms of u fundamental units, may be written as a function of q - u dimensionless groups (the Π's)." Given 8 quantities (fluid velocity V_∞, particle radius R, cylinder radius a, particle susceptibility K, applied field H, fluid density ρ_f, trapping length y, and fluid viscosity η; μ_s is assumed constant but a function of H, and the dependence of ρ^*, the particle density, is incorporated in K), and four fundamental units (the generalized cgs 4 dimensional system) mass (M), length (L), time (T), and electromagnetic unit of charge (B), one needs four dimensionless groups. One can identify possible groupings by the dimensions of the individual variables:

V_∞ (LT^{-1}) ρ_f (ML^{-3})

K $(MLT^{-2}B^{-2})$ η $(ML^{-1}T^{-1})$

a (L)   y (L)

H (BL^{-1}) R (L)

Since KH^2 (or KHH_s for $H > H_s$) is an obvious couple, one needs to find a group with similar dimensions, $\rho_f V_\infty^2$. Another group should be a length ratio, either y/R or y/a. There should also be two Reynolds numbers $2L\rho_f/\eta$ where L is a characteristic length, either R or a. The actual groupings are not predictable from Buckingham's Pi theorem. They must be deduced from the governing equations or the data.

APPENDIX F

Averaged Experimental Data for $Co_3(PO_4)_2 \cdot 2H_2O$

Flow Rate cm/sec	Trapping Thickness cm	Wire Diameter cm	Applied Field Amperes	Applied Field Gauss
.55	.0135	.01	10	5000
.55	.0124	.01	7	3500
.55	.0097	.01	4	2000
.55	.035	.052	10	5000
2.9	.0116	.01	10	5000
2.9	.008	.01	7	3500
2.9	.0075	.01	4	2000
2.9	.0283	.052	10	5000
5.2	.0083	.01	10	5000
5.2	.0072	.01	7	3500
5.2	.0033	.01	4	2000
5.2	.020	.052	10	5000